

## Noncovalent Interactions in Density-Functional Theory<sup>a)</sup>

Gino A. DiLabio<sup>1,2</sup> and Alberto Otero-de-la-Roza<sup>2</sup>

<sup>1)</sup>*Department of Chemistry, University of British Columbia, Okanagan,  
3333 University Way, Kelowna, British Columbia V1V 1V7,  
Canada*

<sup>2)</sup>*National Institute for Nanotechnology, National Research Council of Canada,  
11421 Saskatchewan Drive, Edmonton, Alberta T6G 2M9,  
Canada*

(Dated: 30 December 2014)

---

<sup>a)</sup>This chapter will appear in volume 29 of Reviews in Computational Chemistry.

## CONTENTS

<b>Introduction</b>	2
Overview of Non-Covalent Interactions	4
<b>Theory Background</b>	9
Density-Functional Theory	9
Failure of Conventional DFT for Non-Covalent Interactions	16
<b>Non-Covalent Interactions in DFT</b>	19
Pairwise Dispersion Corrections	19
The Exchange-Hole Dipole Moment (XDM) Model	24
The DFT-D Functionals	29
Other Approaches	34
Potential-Based Methods	38
Dispersion-Correcting Potentials (DCP)	39
Dispersion-Corrected Atom-Centered Potentials (DCACP)	42
Minnesota Functionals	43
Non-Local Functionals	50
<b>Performance of Density-Functionals for Non-Covalent Interactions</b>	54
Description of Non-Covalent Interactions Benchmarks	54
Performance of Dispersion-Corrected Methods	60
<b>Non-Covalent Interactions in Perspective</b>	68
<b>References</b>	71

## INTRODUCTION

Density-functional theory<sup>1-10</sup> (DFT) is arguably the most successful approach to the calculation of the electronic structure of matter. The success of the theory is largely based on the fact that many DFT approximations can predict properties such as thermochemistry, kinetics parameters, spectroscopic constants, and a large range of properties with an accuracy rivaling those obtained by high-level *ab initio* wavefunction theory methods in terms of agreement with experimental quantities. The computational cost of DFT scales formally as  $N^3$ , where  $N$  is the number of electrons in the system, as compared to the  $N^5 - N^7$  scaling (or even higher) of correlated wavefunction methods, indicating that DFT can be applied to much larger systems than wavefunction methods, and to the same systems at a much lower computational cost. Furthermore, DFT can be applied to molecular systems using atom-centered basis sets and to molecular and solid state systems through periodic, plane wave approaches, thus allowing for the prediction of the properties of molecular and condensed matter systems on the same theoretical footing.

Despite their broad success in predicting many chemical and physical properties, conventional density-functional approximations have well-known shortcomings.<sup>12-14</sup> In recent years, a great deal of attention has been paid to the inability of conventional DFT methods to predict dispersion interactions accurately. This particular failing of DFT was first illustrated<sup>11</sup>

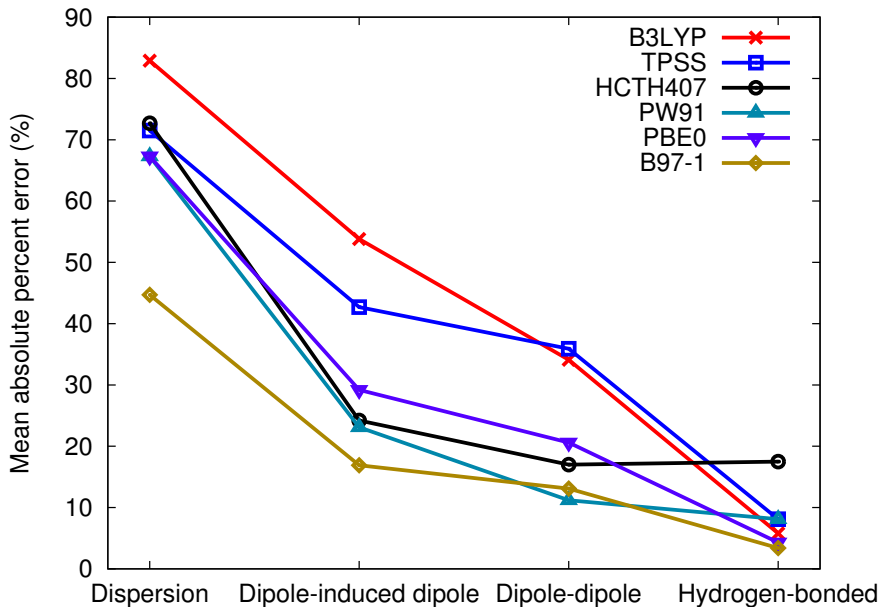


Figure 1. Mean absolute percent errors in the predicted binding energies of noncovalently-interacting dimers using various DFT methods for different types on interactions (adapted from ref. 22).

in the 1990s.<sup>15–21</sup> An early work by Kristyán and Pulay<sup>16</sup> demonstrated that the local density approximation of DFT significantly overbinds the noble-gas dimers  $\text{He}_2$ ,  $\text{Ne}_2$ , and  $\text{Ar}_2$ , while “improved” DFT methods based on generalized gradient approximations significantly underbind or predict their interactions to be completely repulsive. This work serves as one of the early descriptions of the “dispersion problem” of DFT that underpinned two decades of effort to understand and correct DFT in this capacity.

The absence of explicit dispersion physics in common approximations to DFT naturally focussed the attention of researchers on this problem. Current understanding amongst some members of the DFT community is that, of the van der Waals forces in general, only dispersion is poorly treated. The prevailing opinion is that DFT can treat electrostatics and other effects accurately.<sup>5,23</sup> Considering the percent errors in the binding energies of noncovalently-interacting dimers predicted by various DFT methods, as shown in Figure 1, this view may seem justified. The figure indicates that DFT methods tend to offer poor predictions of binding energies in predominantly dispersion-bound systems but work well for hydrogen-bonded systems. But is this true?

Applying the very popular B3LYP method to a set of 23 predominantly dispersion-bound dimers yields a mean error of 5.1 kcal/mol, which supports the notion that approximate DFT methods underbinds in the case of dispersion. However, for a set of 23 dimers in which hydrogen-bonding is the dominant interaction, B3LYP underbinds by an average of 1.7 kcal/mol, an error that is large enough to contradict the notion that hydrogen-bonding is well-treated by DFT methods. Some of the 1.7 kcal/mol error in binding may come from the absence of dispersion in B3LYP but this, as we shall see, is not likely the only deficiency.

The shortcomings of B3LYP are not unique and there is evidence in the literature that other DFT methods are likewise deficient with respect to predicting the strength of hydrogen bonding interactions. For instance, Xu and Goddard studied a range of conventional DFT methods for their ability to reproduce a number of properties in water dimer.<sup>24</sup> Based on

their design principles, there is no *a priori* reason to believe that the DFT methods used in their study have any particular deficiencies or advantages when it comes to modeling hydrogen bonding. And yet, Xu and Goddard found that different DFT methods gave errors in binding energies ranging from overbinding by 0.41 kcal/mol (PWPW functional) to underbinding by 1.42 kcal/mol (BPW91 functional), with the latter result being worse than uncorrelated wavefunction theory. If all of these functionals are missing dispersion to a similar extent, the broad range of error in the DFT-predicted binding energies offers evidence that DFT-based methods do not accurately reproduce electrostatic interactions in general, and point to broader difficulties in predicting noncovalent interactions.

On the basis of the foregoing discussion, we consider the “dispersion problem” a “non-covalent interaction problem”. This distinction is important because the nomenclature that is used directs one’s thinking, and the term “dispersion-corrected DFT” leads to the notion that the shortcomings in common DFT approximations are related to dispersion alone. We are not advocating a change in the nomenclature of “dispersion”-corrected DFT methods at this point because it has been in wide-spread use for nearly a decade; however, it is important to understand the breadth of the problems DFT methods have in modeling noncovalent interactions. Part of the motivation for this chapter is to underscore, where appropriate, the limitations of dispersion-corrected DFT methods. The flurry of activity associated with the development of new dispersion-correcting methods may obfuscate that these methods cannot correct all of the underlying deficiencies of the functional to which they are applied.

We begin this chapter by providing an overview of the different categories of noncovalent interactions, as generally described in chemistry. This is accompanied by some recent examples of noncovalent interactions that focus on dispersion. We then provide some background on general density-functional theory, which is structured so that a reader who is familiar with this material can skip to the remainder of the chapter without loss of continuity. We then introduce some modern DFT methods that are capable of treating dispersion and other noncovalent interactions. The chapter closes with a comparison of methods using standard benchmark data sets and some perspectives on the general applicability of the methods and outlook.

## Overview of Non-Covalent Interactions

Dispersion is the weakest of the van der Waals forces that arises from instantaneous charge fluctuations (e.g. induced dipoles) that occur in otherwise non-polar systems. In chemistry, dispersion forces (or interactions) are often called “London” forces. In the physics community, Casimir forces<sup>25</sup> are described as arising from quantum fluctuations in a quantized field that polarizes nearby systems to induce the formation of dipoles. Both have their origins in the same physical phenomenon.<sup>26</sup>

Dispersion forces play a critical role at the molecular scale. As a simple example, dispersion (and other van der Waals) interactions are responsible for the deviation from the ideal gas behavior of most real gases. Friction and wetting phenomena are also influenced by dispersion forces. Dispersion can lead to the attraction of molecules to a surface, often referred to as “physisorption”. The measurement of the physisorption of gases on solids is used to determine, among other properties, the porosity and surface area of materials,<sup>27</sup> and it may precede important chemical events like catalytic steps of chemical reactions, or surface modifications.

An interesting demonstration of surface physisorption is provided by the formation of

one-dimensional organic nanostructures on silicon surfaces. Under ultrahigh vacuum conditions, it was demonstrated that styrene ( $C_6H_5CHCH_2$ ) is capable of undergoing a radical-mediated line growth process by reacting with rare silicon surface dangling bonds on an otherwise hydrogen-terminated silicon surface. The reaction produces lines through a successive addition-abstraction reaction mechanism that connects individual molecules to the silicon surface such that they are juxtaposed. While styrene can undergo line-growth, efforts to grow lines derived from propylene ( $H_3CCHCH_2$ ) failed.<sup>28</sup> The rationale at the time was that styrene could undergo the line-growth process because when its alkene moiety added to the silicon surface dangling bond, the resulting carbon-centered radical was significantly stabilized by radical delocalization of the unpaired electron into the phenyl moiety. The propylene addition product does not benefit from delocalization stabilization and so it undergoes desorption rather than line growth and it was speculated that all linear alkenes could not be made to undergo line growth for this reason. However, it was later hypothesized that dispersion interaction between a longer chain alkene, like 1-undecene ( $C_9H_{19}CHCH_2$ ), could stabilize the addition intermediate long enough to enable the growth of molecular lines on the silicon surface. This hypothesis was verified by scanning tunneling microscopy studies, which showed “caterpillar”-like molecular structures derived from 1-undecene with styrene-derived lines nearby (see Figure 2).<sup>29</sup>

The macroscale action of dispersion was nicely demonstrated by the work by Autumn et al.<sup>30</sup> They showed that geckos use dispersion as the primary means of adhesion between their feet (specifically small structures on their feet called setae) and hydrophobic surfaces. This example illustrates that, although dispersion tends to be the weakest of the noncovalent interactions, it can result in significant interaction strengths when integrated over large areas and/or over many atoms.

The macroscopic nature of the dispersion force is dependent upon the media separating objects. From the Casimir force perspective, the electromagnetic vacuum fluctuations give rise to polarization in nearby atoms or molecules almost instantaneously at small (nanometer) distances. However, the finite speed of light results in a retardation in polarization when objects are far apart. Munday et al.<sup>31</sup> demonstrated experimentally that this retardation can lead to repulsive interactions between objects immersed in a solvent when the materials have particular relative dielectric functions. In other words, the dispersion/Casimir force can be exploited at large distances to levitate objects!

When two molecules interact, the noncovalent attraction between them contains other forces along with dispersion. Dipole-induced dipole forces are somewhat stronger than dispersion forces when compared on a per atom basis. This force is created when the permanent electric dipole in one molecule induces an electric dipole in an otherwise non-polar molecule. The dipole arises from the redistribution of electrons between bonded atoms having different electronegativities. The strength of the interaction that results depends on the magnitude of the permanent dipole moment and the polarizability of the molecule with which the dipole interacts.

The dipole-dipole force tends to be stronger than the dipole-induced dipole force and arises through the interaction between two (or more) permanent electric dipoles. The most energetically favorable alignment between dipoles is such that the positive “head” of one dipole is arranged in space to be as close as possible to the negative “tail” of a second dipole. Dipoles arranged in this fashion and oriented in a line interact most strongly. “Head-to-tail” dipole arrangements where the dipoles reside in a plane interact less strongly.

Hydrogen bonding, which tends to be much stronger than the other noncovalent interac-

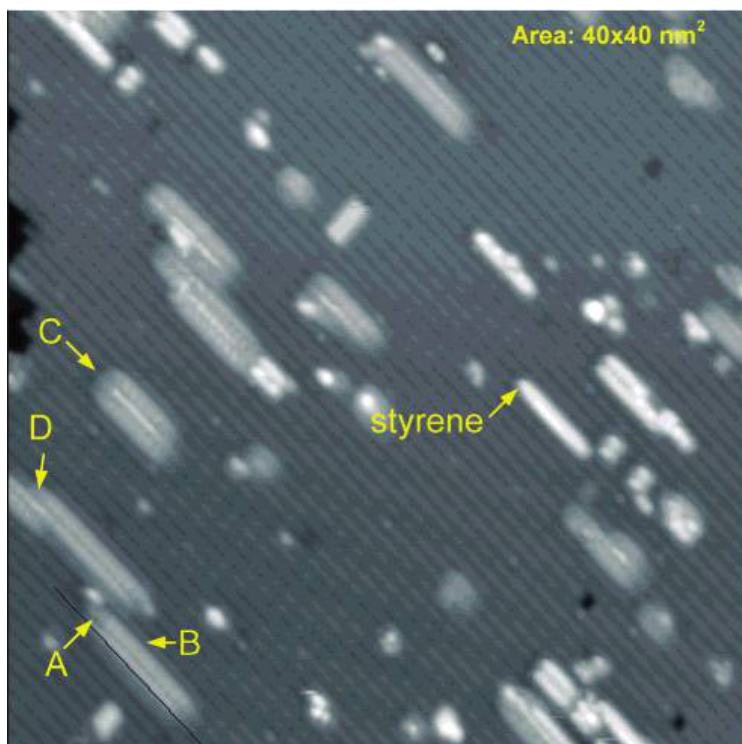
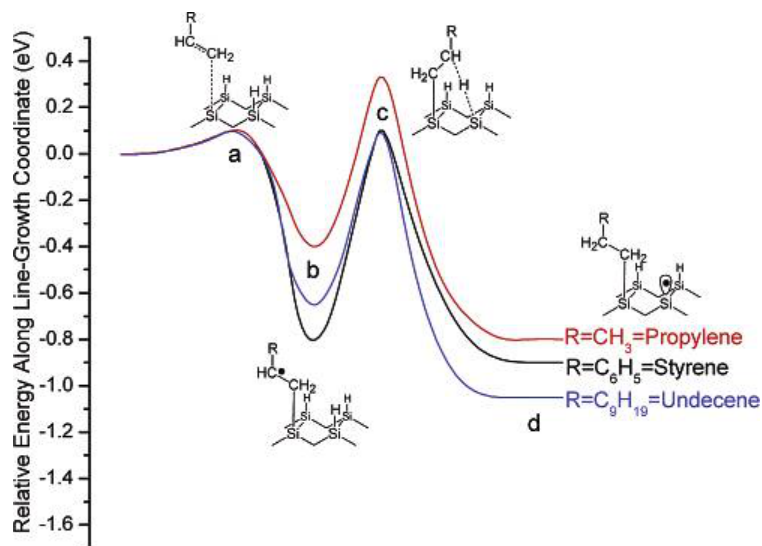


Figure 2. Top panel: Potential energy curves showing the relative energetics associated with one-dimensional organic nanostructure formation on hydrogen-terminated silicon surfaces. Following the chemisorption of a molecule another molecule may add at a neighbouring silicon surface site that holds a radical and this continues the line growth process. Bottom panel: Scanning tunneling microscope image showing 1-undecene (labeled "B", "C", and "D") and styrene-derived lines on the silicon surface (taken with permission from reference 29).

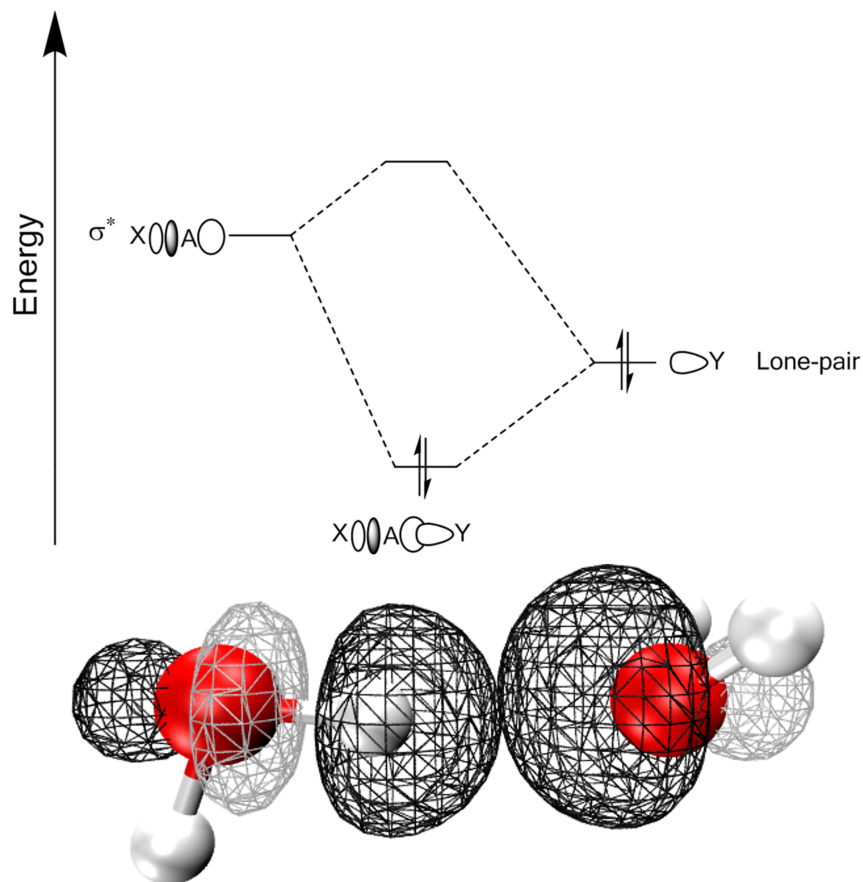


Figure 3. Diagram illustrating the stabilization that occurs between the  $\sigma$  antibonding orbital associated with an X-A bond and a lone-pair orbital of Y in hydrogen-bonded water dimer. Opposite molecular orbital phases are shown in different shades.

tions on a per atom basis, is often considered to be a special case of dipole-dipole interaction, as is suggested by the IUPAC definition.<sup>32</sup> This definition may be due to the importance that hydrogen bonding has in the determination of the structure of biological molecules such as proteins<sup>33</sup> and deoxyribonucleic acid (DNA),<sup>34</sup> and the central role that water plays in life. Hydrogen bonding is also important in materials chemistry and provides a valuable design motif for the production of industrially relevant polymers like nylon and kevlar.

While the nature of the atoms involved in dipole-dipole forces are generally not specified, hydrogen bonds are usually described as occurring between a donor species having a bond of the type X-H, where X is an electronegative atom like oxygen or nitrogen, and an acceptor atom that has a lone-pair of electrons. In this case, the donor has a dipole resulting from the electronegativity difference in the X-H bond and the acceptor has a dipole that exists between the center of the negative charge distribution of the lone-pair of electrons and the positive nucleus of the atom to which it belongs. There is also a secondary orbital interaction associated with hydrogen bonding. The donor lone-pair orbital overlaps to some extent with the antibonding  $\sigma_{XH}^*$  orbital of the X-H moiety, which contributes to the overall stability of the hydrogen bond. A diagram illustrating this is given in Figure 3, where the atom A represents a hydrogen atom. The molecular orbitals involved in the hydrogen bonding in the

water dimer are shown in the bottom panel of Figure 3. The stability comes at the expense of a weakening of the X-H bond because of the extra electron density in its antibonding orbital as a result of the overlap with a lone-pair. The weakening is manifested by the lengthening of the X-H bond and is often, but not always,<sup>35</sup> accompanied by the reduction of the frequency of the X-H vibration.<sup>36</sup> There are many excellent books and reviews on the different facets and the impacts of hydrogen bonding to which the interested reader is directed.<sup>37-39</sup>

In some cases, C-H groups can also be donors to strong hydrogen bonds. Experimental and theoretical work by Salamone and collaborators showed that the benzyloxy radical (BnO,  $C_6H_5CH_2O$ ) is capable of forming strongly bound pre-reaction complexes with amines.<sup>40,41</sup> Calculations indicate that the strength of binding in dimers of this kind in vacuum is ca. 7 kcal/mol, which is stronger than that of the water dimer. The large binding energy is attributed to the strong electron withdrawing effects of the oxygen-centered radical that is  $\alpha$  to the C-H hydrogen bond donor group. The experimental outcome is that the reactivity of BnO with amine substrates is more than a factor of 3300 larger than the cumyloxy radical ( $C_6H_5C(CH_3)_2O$ ), which cannot engage in hydrogen bonding.

In general, the interactions of higher-order multipoles with each other or with non-polar species are not allocated a separate category of noncovalent interaction, despite the fact that their effects can sometimes be significant. For example, the complementary quadrupole-quadrupole interactions that arise between benzene and hexafluorobenzene, which are both liquids at room temperature, results in the formation of a crystal.<sup>42</sup> In its unperturbed state, benzene has no dipole moment but it does have a substantial quadrupole moment arising from the electron density above and below the ring plane which is composed of the relatively positive carbon nuclei. In most cases, however, as the order of the multipole increases the forces that arise from them diminish in magnitude.

A number of new nomenclatures associated with noncovalent interactions have emerged over the last few decades that contrast with the preceding classification. For instance, the interactions of dipoles with the  $\pi$  face of aromatic molecules, like benzene, may be considered a special case of dipole-induced interactions.

Cation- $\pi$  interactions,<sup>43</sup> which describe the attraction between a cation and the negative electron cloud above the plane of an aromatic system such as benzene, may be considered a monopole-induced dipole interaction. The charge associated with the cationic center polarizes the “fluffy” cloud of the aromatic moiety, resulting in moderately strong interactions. Work by Dougherty<sup>43</sup> and others has characterized the strengths of interaction in various cation- $\pi$  systems using various quantum mechanical tools. It is generally believed that these interactions are operative in biological systems where salt cations, such as  $Na^+$ , interact with aromatic moieties in proteins (e.g. tryptophan, phenylalanine, and tyrosine). Cation- $\pi$  interactions, however, will be strongly attenuated, or eliminated, by solvation effects.

Related to cation- $\pi$  interactions, but weaker and perhaps less well-known, are anion- $\pi$  interactions.<sup>44</sup> It may be counterintuitive at first that a negatively charged atom could interact attractively with the  $\pi$  cloud of an aromatic system; indeed, beyond a critical distance the interactions between an anion and the  $\pi$ -face are repulsive. However, when the two components are within a certain distance, charge-induced polarization provides attraction between the two moieties. Anion- $\pi$  interactions have been shown to exist in inorganic crystals<sup>45</sup> and may be utilized for anion sensing applications.<sup>46</sup>

Halogen-bonding (XB) is another type of noncovalent interaction that has gathered a great deal of attention recently, although some have argued that XB effects were reported



more than 100 years ago.<sup>47</sup> This interaction occurs between a halogen bond acceptor in the form of X-X or X-Y (X = halogen; Y = H, C, N, O) and a donor, which is usually a Lewis base (e.g. acetonitrile and formaldehyde). For a set of 51 small neutral species used for theoretical methods benchmarking purposes, gas-phase interaction strengths were predicted to be as large as ca. 34 kcal/mol, depending on the nature of the donor and acceptor species.<sup>48</sup> Interestingly, there does not appear to be a need to incorporate dispersion corrections into DFT methods in order to accurately predict the halogen bonding interaction strengths. In fact, dispersion corrections were found to be detrimental for this purpose in most cases. The consensus amongst those that study halogen bonding is that it arises largely from the interaction between the lone-pair of electrons on the Lewis base with the so-called  $\sigma$ -hole on the halogen bond acceptor. The  $\sigma$ -hole is the area of relatively positive charge on the otherwise electronegative halogen on the acceptor that arises from the antibonding orbital associated with the X-halide  $\sigma$ -bond. Halogen bonds, like hydrogen bonds, have a directionality that corresponds to maximum overlap between the Y-X  $\sigma^*$  and the acceptor lone-pair, which is 180°, and are derived from electrostatic and orbital overlap effects<sup>49</sup> (see Figure 3) with A the halogen atom.

Finally, we mention here pnictogen and chalcogen bonding, which are similar in nature to hydrogen and halogen bonding in that they derive from electrostatic and orbital overlap effects. Pnictogen bonding involves the lone-pair orbitals of group 15 (N to Bi) donor atoms and chalcogen bonding involves the lone-pair orbitals of group 16 atoms (O to Po). In this respect the pnictogen/chalcogen atoms behave as a Lewis base, while the acceptors can be any empty anti-bonding orbital, and can be depicted using the same orbital diagram of Figure 3 that was used to illustrate hydrogen and halogen bonding. From this perspective, halogen, pnictogen and chalcogen bonding may all be considered variations of Lewis acid-base interactions and one may question the need to provide them with different names. Indeed, hyperconjugation, which is the name given to the overlap between the bonding (i.e. doubly-occupied) orbital on one center and an anti-bonding (i.e. empty) orbital on an adjacent center covalently bonded to the first,<sup>50</sup> strongly parallels the concepts behind pnictogen, chalcogen, halogen and hydrogen bonding. It seems reasonable to focus on the notion of secondary orbital interactions as being broadly operative in all of these noncovalent interactions.

## THEORY BACKGROUND

### Density-Functional Theory

Density-functional theory<sup>1-10</sup> (DFT) is at present the most popular method to study the electronic structure of chemical systems. DFT approximates the solution of the time-independent Schrödinger equation under the Born-Oppenheimer approximation, which is the foundation of most of quantum chemistry and materials physics:

$$\hat{H}\Psi = E\Psi \tag{1}$$

The non-relativistic many-electron Hamiltonian (atomic units are used throughout this chapter) that describes the problem is:

$$\hat{H} = -\frac{1}{2} \sum_i \nabla_i^2 - \sum_{i,A} \frac{Z_A}{R_{iA}} + \sum_{i>j} \frac{1}{r_{ij}} \tag{2}$$

where  $i$  runs over electrons,  $A$  runs over atoms,  $Z_A$  are the atomic numbers,  $r_{ij}$  are electron-electron distances, and  $R_{iA}$  are electron-nucleus distances. The many-electron wavefunction ( $\Psi$ ) contains all the information about the system. Because of the electron-electron interaction (the last term in the Hamiltonian), the electronic structure of a system with more than one electron is a complicated many-body problem, and impossible to solve analytically.

Traditional approaches in quantum chemistry are based on the orbital approximation. Under it, a single Slater determinant is proposed as an ansatz for the eigenfunctions of the many-body Hamiltonian. The determinant is composed of one-electron functions (orbitals), which are in turn expressed as linear combinations of basis functions. Application of the variational principle, which states that the correct ground-state wavefunction minimizes the expectation value of the Hamiltonian, leads to a set of one-electron equations that must be solved iteratively in what is called the self-consistent field (SCF) method. This procedure is the Hartree-Fock (HF) method, and the difference between the exact ground-state and the HF energy is called the correlation energy (not to be confused with the DFT correlation energy, see below).

Many approaches have been developed to improve the accuracy of the HF results and calculate the missing correlation energy by working with the HF solution. We collectively refer to these as wavefunction methods, which have been described extensively elsewhere.<sup>51,52</sup> In the wavefunction approach, the exact many-electron wavefunction is written as a linear combination of Slater determinants, that correspond to excitations of one or more reference configurations. If enough computing power were available, the exact solution of the Schrödinger equation could be found by employing enough determinants in the wavefunction expansion. Hence, there is a systematic recipe to improve the calculation level in wavefunction theory, but the scaling of the computational cost prevents the application of higher-level wavefunction theory in all but the simplest systems. Two popular wavefunction methods are Møller-Plesset perturbation theory (specifically, to second-order, MP2) and coupled cluster (CC). The coupled-cluster singles doubles and perturbative triples (CCSD(T)) variant of the latter is the preferred method in the literature to obtain accurate reference data for the binding energies of small noncovalently-bound dimers (see the section below titled “Description of Non-covalent Interaction Benchmarks”).

In contrast to wavefunction theory, the essential quantity in DFT is not the wavefunction but the electron density ( $\rho(\mathbf{r})$ ), a three-dimensional scalar function that describes the probability of finding electrons in real space. DFT, in general, reduces the computational cost compared to wavefunction theory, but there is no systematic recipe to approach the exact solution for a given system. The idea of using the electron density instead of the many-electron wavefunction as the central quantity first appeared in the Thomas-Fermi theory,<sup>3,53,54</sup> an early version of DFT from the computerless days when even the simplest wavefunction calculation was impossible to carry out. However, Thomas-Fermi theory predicts no molecular binding<sup>3,55,56</sup> rendering the method useless in practical applications.

The foundation of modern-day DFT was laid by two theorems proven by Hohenberg and Kohn<sup>1</sup> (HK) in 1964. The first HK theorem establishes that there is a one-to-one correspondence between the external potential (the electrostatic potential created by the nuclei at the chosen molecular geometry) and the ground-state electron density. Since the external potential is the only non-universal (i.e. system-dependent) part of equation 2, the first theorem establishes a one-to-one correspondence between density and the many-electron wavefunction. Hence, any observable can be obtained as a functional of the electron density, including the energy  $E[\rho]$ . The second HK theorem establishes that the ground state electron

density is a minimum of the exact energy functional. This theorem enables the use of the variational principle, which is a very powerful tool in the search for the ground-state electron density.

The energy functional  $E[\rho]$  is unknown and the HK theorems provide no indication as to how to obtain it. However, large contributions to the energy, like the classical electron-electron repulsion ( $J[\rho]$ ) or the electron-nuclei attraction ( $E_{ne}[\rho]$ ), depend directly on the density and can be calculated in a straightforward manner. The energy functional can be expressed as a sum of component functionals and written as:

$$E[\rho] = T[\rho] + J[\rho] + E_{ne}[\rho] + E_{xc}[\rho] \quad [3]$$

$$J[\rho] = \int \frac{\rho(\mathbf{r})\rho(\mathbf{r}')}{|\mathbf{r} - \mathbf{r}'|} d\mathbf{r}d\mathbf{r}' \quad [4]$$

$$E_{ne}[\rho] = - \sum_A \int \frac{Z_A \rho(\mathbf{r})}{|\mathbf{R}_A - \mathbf{r}|} d\mathbf{r} \quad [5]$$

where  $T[\rho]$  is the kinetic energy functional and  $E_{xc}[\rho]$  is the exchange-correlation functional, which encapsulates the missing energy contributions not contained in the other functionals. The exchange-correlation functional is usually partitioned into a exchange part and a correlation functional:

$$E_{xc} = E_x + E_c \quad [6]$$

The exchange functional is defined as the difference between the classical electron-electron repulsion and the expectation value of the many-body electron-electron energy term:

$$E_x = \langle \sum_{i>j} r_{ij}^{-1} \rangle - J[\rho] \quad [7]$$

For a one-electron system, the exchange term would cancel exactly the spurious self-interaction of the electron with itself coming from  $J[\rho]$ , a role that is fulfilled by the exchange term in HF theory. Hence,  $E_x$  contains the energetic contribution coming from the antisymmetry requirement imposed on the many-body wavefunction and corrects for double-counting of electrons in  $J[\rho]$ . The correlation energy ( $E_c$ ) is defined as the missing energy necessary to make  $E_{xc}$  exact. Note that in equation 3, only the  $E_{ne}$  term depends on the geometry of the system. The rest is a *universal* functional, that is, it is the same regardless of the details of the system under calculation.

The second seminal paper in DFT was published by Kohn and Sham<sup>2</sup> a year after the HK theorems were proposed. The Kohn-Sham (KS) formulation of DFT gives a practical recipe to the calculation of the ground-state energy and electron density, and uses much of the same technology (programs, algorithms) as does HF theory. In KS-DFT, one assumes there is a collection of non-interacting quasi-particles, similar to electrons and equal in number, that has the same particle density as the actual electron density for the system of interest. By doing so, the electron density of a system has the same expression as if it were derived from a Slater determinant:

$$\rho(\mathbf{r}) = \sum_i |\psi_i(\mathbf{r})|^2 \quad [8]$$

where the  $\psi_i$  are the occupied orbitals (called the *Kohn-Sham orbitals*). The KS scheme provides a simple kinetic energy functional expression:

$$T[\rho] \approx T_{KS} = -\frac{1}{2} \sum_i |\nabla \psi_i(\mathbf{r})|^2 \quad [9]$$

$T_{KS}$  is the Kohn-Sham kinetic energy, which is only an approximation to the true kinetic energy functional. In the KS scheme, the difference between the exact kinetic energy and  $T_{KS}$  is incorporated into the correlation energy  $E_c$ . It is important to note that the theory is formally exact even for systems that traditionally can not be treated accurately with a single Slater determinant (e.g. low-energy excited states, bond breaking, biradicals, etc.).

Minimization of the energy functional within the KS scheme with respect to variations in the electron density leads to the one-electron Kohn-Sham operator:

$$H_{KS} = T + V_H + V_{\text{ext}} + V_{xc} \quad [10]$$

with:

$$T = -\frac{1}{2}\nabla^2 \quad ; \quad V_H = \int \frac{\rho(\mathbf{r}')}{|\mathbf{r} - \mathbf{r}'|} d\mathbf{r}' \quad ; \quad V_{\text{ext}} = -\sum_A \frac{Z_A}{|\mathbf{R}_A - \mathbf{r}|} \quad [11]$$

and the exchange-correlation potential being defined as the functional derivative of  $E_{xc}$  with respect to the electron density:

$$V_{xc} = \frac{\delta E_{xc}}{\delta \rho(\mathbf{r})} \quad [12]$$

Equation 10, when combined with orbitals expressed as linear combinations of basis functions, yields matrix equations similar to those in HF theory, which simplified (and still does) the implementation of DFT in preexisting quantum chemistry software.

The advantage of DFT with respect to traditional wavefunction methods is that, at a computational cost similar to or even less than HF, it is possible to obtain electronic properties that in many cases rival correlated wavefunction approaches in accuracy. The downside is, in contrast to wavefunction theory where increasingly complex methods yield better results, there is no systematic approach to improve the approximations to the exact exchange-correlation functional  $E_{xc}$ , which, recall, is unknown in the formalism. The design of exchange-correlation functionals is, consequently, the cornerstone of development in DFT and users should be aware of the strong and weak points of the functionals being used.

The earliest and simplest method to approximate the exchange correlation functional is the local-density approximation<sup>1,2</sup> (LDA). In LDA, the  $E_{xc}$  is calculated by assuming the system behaves locally as a uniform electron gas. That is:

$$E_{xc} = \int \rho(\mathbf{r}) \varepsilon_{xc}^{LDA}(\rho(\mathbf{r})) d\mathbf{r} \quad [13]$$

where  $\varepsilon_{xc}^{LDA}(\rho)$  is the exchange-correlation energy density per electron of a uniform electron gas with density  $\rho$ . The exchange contribution to  $\varepsilon_{xc}^{LDA}$  is analytical ( $\varepsilon_x^{LDA} = -3/4(3/\pi)^{1/3}\rho^{1/3}$ ), while the correlation energy was obtained from accurate quantum Monte Carlo calculations<sup>57</sup> and is parametrized.<sup>58,59</sup>

The performance of LDA in actual calculations is surprisingly good for such a crude model. Unlike Thomas-Fermi theory, LDA binds molecules and, while there are hundreds of more modern functionals, it is still occasionally used in the materials science community. However, gross overestimation of bond energies and poor thermochemistry have ruled out its use to solve problems of interest in chemistry.

The most basic class of functionals that improve upon LDA rely on the generalized gradient approximation (GGA). Here which the exchange-correlation functional depends on both the value and the gradient of the electron density:

$$E_{xc} = \int \rho(\mathbf{r}) \varepsilon_{xc}^{GGA}(\rho(\mathbf{r}), \nabla \rho(\mathbf{r})) d\mathbf{r} \quad [14]$$

By making the energy density depend on the density gradient, it is possible to account for local inhomogeneity in the electron density. Unlike LDA, there is not a single GGA, that is, the expression for  $\varepsilon_{xc}^{\text{GGA}}$  is not unique. The existing GGA functionals (there are tens of them) vary in the exact constraints that they fulfill, as well as in the amount of empiricism in their construction and in the number of adjustable parameters they contain. Popular exchange GGA functionals include the Perdew-Burke-Erzenhof<sup>60</sup> (PBE) and subsequently revised versions (revPBE,<sup>61</sup> PBEsol,<sup>62</sup>), Perdew-Wang 1986 (PW86),<sup>63</sup> Becke 1986b,<sup>64</sup> (B86b), and Becke 1988<sup>65</sup> (B88). Standalone gradient-corrected correlation functionals include the popular Lee-Yang-Parr functional<sup>66</sup> (LYP) as well as the correlation part of the PBE functional.<sup>60</sup> Exchange and correlation functionals are usually combined to give composite functionals, such as PW86PBE and B88LYP (often simply BLYP). PBE is the most popular functional in solid-state calculations, and it is non-empirical (its parameters are not determined by resorting to fits to reference data). B86b and B88 and the correlation functional LYP contain fitted parameters, but their performance in the calculation of thermochemical quantities is notably better than PBE. In general, GGA functionals provide much better results for the calculation of most properties, although not enough to be useful in the calculation of chemical reaction energies. GGA functionals are also very popular in the solid-state field because they yield accurate geometries, elastic properties of periodic solids and qualitatively correct electronic band structures. However, they severely underestimate the electronic band gaps.

Meta-GGA functionals increase the flexibility in the functional definition by using, in addition to the density and its derivatives, the Kohn-Sham kinetic energy density ( $\tau_{KS}$ ):

$$E_{xc} = \int \rho(\mathbf{r}) \varepsilon_{xc}^{\text{GGA}}(\rho(\mathbf{r}), \nabla\rho(\mathbf{r}), \nabla^2\rho(\mathbf{r}), \tau_{KS}(\mathbf{r})) d\mathbf{r} \quad [15]$$

where:

$$\tau_{KS}(\mathbf{r}) = -\frac{1}{2} \sum_i |\nabla_i(\mathbf{r})| \quad [16]$$

The development of accurate meta-GGAs is still an active area of research.<sup>67-73</sup> Popular meta-GGA approximations to exchange include the Tao-Perdew-Staroverov-Scuseria<sup>67</sup> functional (TPSS, there is also a meta-GGA correlation functional proposed in the same work), its revised version revTPSS<sup>68</sup> and the Minnesota functionals reviewed later in the section titled “Minnesota Functionals”. With an increased degree of freedom, meta-GGAs usually improve upon GGAs in the accuracy of calculated properties.

LDA, GGAs, and meta-GGAs are *semilocal* or *pure* functionals, for which the exchange-correlation energy density at a point depends solely on the properties at that point. In a seminal article,<sup>74</sup> Becke showed that the calculation of molecular thermochemistry (particularly, atomization energies, ionization potentials and electron affinities) can be greatly improved by using an admixture of a GGA and a fraction of exact exchange, which is calculated as the exchange energy in HF theory but obtained using the KS orbitals. The use of exact exchange in a functional is justified by invoking the adiabatic connection formula.<sup>75-77</sup>

The adiabatic connection is a rigorous formula for the calculation of the exact exchange-correlation functional. It says:

$$E_{xc}[\rho] = \int_0^1 \left( \langle \sum_{i>j} r_{ij}^{-1} \rangle_\lambda - J[\rho^\lambda] \right) d\lambda = \int_0^1 U_{xc}^\lambda d\lambda \quad [17]$$

where  $\lambda$  is a parameter that turns on the electron-electron interaction (the  $r_{ij}^{-1}$  term in Eq. 2).  $\lambda = 0$  is the non-interacting Kohn-Sham system and  $\lambda = 1$  is the fully-interacting real system. The integrand ( $U_{xc}$ ) is defined as in equation 17, and is called the potential exchange-correlation energy. Equation 17 represents an interpolation with the  $\lambda = 0$  endpoint being the exact exchange energy calculated using the Kohn-Sham orbitals:

$$U_{xc}^0 = -\frac{1}{2} \sum_{ij}^{\text{occ}} \int \frac{\psi_i^*(\mathbf{r}_1)\psi_j^*(\mathbf{r}_2)\psi_j(\mathbf{r}_1)\psi_i(\mathbf{r}_2)}{r_{12}} d\mathbf{r}_1 d\mathbf{r}_2 \quad [18]$$

where the sum runs over all pairs of occupied Kohn-Sham states. Hence, it makes sense to define the exchange-correlation functional approximation as an interpolation between the known  $\lambda = 0$  limit (exact exchange) and  $\lambda = 1$ , represented by the semilocal functional:<sup>74</sup>

$$E_{xc}[\rho] = a_x U_{xc}^0 + (1 - a_x) E_{xc}^{\text{semilocal}}[\rho] \quad [19]$$

where  $a_x$  is the parameter controlling the amount of exact exchange in the approximate functional.

The functionals that use a fraction of exact exchange in their definition are called *hybrids* and, of those, the most popular by far is B3LYP, a combination of Becke’s 1993 exchange hybrid<sup>78</sup> and LYP correlation.<sup>66</sup> In B3LYP, 20% exact exchange is used, a number that was obtained by fitting to a set of reference thermochemical values (atomization energies, ionization potentials, and proton affinities) and total energies. Subsequently, a 25% fraction of exact exchange was justified on theoretical grounds by Perdew et al.,<sup>79</sup> resulting in the definition of PBE0,<sup>80</sup> the non-empirical hybrid extension of PBE. Another popular hybrid is B3P86 (same exchange as B3LYP but using Perdew 1986 correlation<sup>81</sup>).

By including exact exchange, hybrid functionals are no longer semilocal: the exact exchange energy involves a double integration over real-space. Thus, they are computationally more expensive than semilocal functionals. This is particularly true in periodic solids with plane wave basis sets, for which they are feasible only in very simple systems. For this reason, and also because of unphysical features in the HF description of metals,<sup>82</sup> hybrids are not much used in materials studies,<sup>83</sup> but they are very popular in quantum chemistry, where B3LYP is the most used functional by number of citations. The improved thermochemistry with respect to GGAs enable accurate studies of reaction energetics, justifying their continued popularity.

Even though hybrids provide improved accuracy in many chemically-relevant properties, they still face problems. One of these is “self-interaction” error. Because the antisymmetry of the wavefunction is not enforced as in HF, there can be overcounting (or undercounting) of electron-electron interactions, which results in electrons interacting with themselves. The simplest instance of self-interaction error happens in the hydrogen atom, for which most functionals fail to find the correct ground state energy ( $-1/2$  Hartree) because the  $E_{xc}[\rho]$  does not cancel  $J[\rho]$  exactly.

A popular approach to deal with this problem is to use range-separated or (also called long-range corrected) functionals.<sup>84–86</sup> Similar to hybrids, range-separated hybrids combine exact exchange with a semilocal functional, but they do so by partitioning the electron-electron interaction kernel ( $1/r_{ij}$ ) into long-range ( $\text{erf}(\omega r_{ij})/r_{ij}$ ) and short-range parts ( $(1 - \text{erf}(\omega r_{ij}))/r_{ij}$ ), where  $\text{erf}$  is the standard error function. The range-separation parameter ( $\omega$ ) controls the relative extent of the short-range and long-range electron interactions. The idea behind range-separated hybrid functionals is to recover the correct long-range behavior

of the exchange-correlation potential. For semilocal functionals,  $V_{xc}$  decays exponentially when moving away from the system, but the correct tail goes as  $-1/r$ . This behavior is recovered by using exact exchange as the limit when  $r \rightarrow \infty$ . This does *not* mean, however, that long-range corrected functionals model dispersion, but it does mean that the treatment of non-dispersive intermolecular electron-electron interactions are, in general, improved.

In most range-separated hybrids, the short-range part corresponds to the semilocal functional, while exact exchange is the long-range part. Common functionals in this category are LC- $\omega$ PBE,<sup>87,88</sup> CAM-B3LYP,<sup>89</sup> and  $\omega$ B97,<sup>90</sup> (and also its reparametrized  $\omega$ B97X version<sup>90</sup>). Range-separated functionals give improved charge transfer excitation energies, reaction barriers and, in general, minimize self-interaction error. Their behavior for thermochemistry is good, outperforming, in general, their hybrid counterparts. Some range-separated functionals, most notably the Heyd-Scuseria-Ernzerhof (HSE) functional,<sup>91,92</sup> use a short-range exact exchange and a long-range semilocal functional. The reason is that these functionals are designed to recover some of the good properties of the hybrids in periodic solid-state calculations. At a cost of 2–4 times over semilocal functionals, HSE delivers increased accuracy in the calculation of geometries and bulk moduli (by about 50%), and, particularly, band gaps (errors from 1.3 eV to 0.2 eV on average).<sup>93</sup>

A major application of range-separated functionals, and a very active area of research is time-dependent density functional theory<sup>94</sup> (TDDFT). TDDFT is based on the extension of the Hohenberg-Kohn theorems to time-dependent electron densities put forward by Runge and Gross.<sup>95</sup> It is mostly used in the calculation of excited-state transition energies and probabilities (optical spectra), as well as properties of the excited states, and ground-state properties related to the excitations (e.g. polarizabilities and hyperpolarizabilities). Range-separated functionals are essential in alleviating some of the problems in TDDFT, including the modelling of excitations involving long-range charge transfer.

Table I shows the comparative performance of several functionals from different approximations. The benchmark sets chosen are the same as in ref. 99: the G3/99 set comprising 222 atomization energies,<sup>100</sup> the bond dissociation energy database of Johnson et al.<sup>101</sup> (BDE), the hydrogen-transfer reaction set by Lynch and Truhlar<sup>102</sup> (BH), the set of linear alkane isodesmic reactions (Isod) used by Wodrich et al.<sup>103</sup> (with the geometries from the G3X set<sup>104</sup>), the isomerization of organic molecules set by Grimme et al.<sup>105</sup> (Isom), the charge-transfer complex set of Zhao and Truhlar<sup>106</sup> (CT) and the database of mean ligand-removal enthalpies in transition-metal complexes (TM) by Johnson and Becke.<sup>107</sup> The results can be used as an estimate of the performance of different functionals for those common chemical problems.

As mentioned earlier, functionals, in general, perform better in the order: range-separated > hybrids > meta-GGAs > GGAs. Range-separated hybrids partially address the problem with self-interaction error, that is particularly relevant in the barrier height set (BH). LC- $\omega$ PBE achieves an excellent result, and so does BHandHLYP at the hybrid level. However, the good performance of BHandHLYP for self-interaction error problems comes at a cost. It fails spectacularly for atomization energies (G3) and ligand-removal energies in transition metal complexes. The latter failure is caused by the multideterminant character of these systems, whose correlation is roughly approximated by semilocal density functionals.

TABLE I. Comparative Assessment of Several Functionals in Standard Thermochemical Tests. The Side Column Labels the Type of Functional Approximation (mGGA=meta-GGA, RS hybrids=range-separated hybrids). The Calculations were Run Using aug-cc-pVTZ Basis Sets. The Entries are Mean Absolute Deviations (MAD) in kcal/mol.

	Functional	G3/99	BDE	Isod	Isom	BH	TM	CT
GGA	LDA <sup>1,2,58,96</sup>	117.5	11.9	0.2	2.5	18.1	34.2	6.4
	PBE <sup>60</sup>	18.9	4.9	3.4	1.9	9.6	10.4	2.6
	PW86PBE <sup>60,63</sup>	9.4	7.2	3.8	2.3	8.0	7.8	2.5
mGGA	BLYP <sup>65,66</sup>	11.4	7.6	4.8	3.3	7.9	5.8	1.4
	TPSS <sup>67</sup>	4.7	5.9	4.9	2.5	8.1	10.0	1.9
Hybrids	M06-L <sup>97</sup>	5.1	3.9	3.2	2.0	4.6	31.8	1.7
	B3LYP <sup>66,78</sup>	7.8	5.7	4.4	2.3	4.6	4.5	0.5
	BHandHLYP <sup>66,78</sup>	32.3	7.2	4.1	1.6	2.4	18.2	0.7
	PBE0 <sup>80</sup>	5.5	4.6	3.5	2.0	4.6	2.8	0.8
	B97-1 <sup>98</sup>	6.1	3.8	3.9	1.5	4.6	3.2	0.9
RS hybrids	B3P86 <sup>78,81</sup>	23.4	2.9	3.9	1.8	6.0	3.3	0.8
	CAM-B3LYP <sup>89</sup>	4.2	4.0	3.4	1.7	3.4	4.2	0.3
	LC- $\omega$ PBE <sup>87,88</sup>	5.1	4.4	3.4	2.4	1.3	3.0	1.2
	HSE06 <sup>91,92</sup>	5.1	5.0	3.5	1.8	4.6	2.9	1.0

## Failure of Conventional DFT for Non-Covalent Interactions

The last twenty years have been a bright story of success for density-functional theory.<sup>14</sup> DFT can, at a relatively modest computational cost, give a reliable picture of such diverse properties as structures of molecules and solids, excitation energies, spectroscopic properties, reaction energies, and so on. DFT is nowadays used widely in the physics and chemistry communities, with the most popular density functionals (B3LYP in gas-phase chemistry and PBE in condensed matter) having more than three thousand citations every year and growing.<sup>14</sup> Despite its popularity, current density-functional approximations have well-known shortcomings,<sup>12-14</sup> including the inability to calculate noncovalent interactions accurately.

The first studies of the applicability of common density-functionals to noncovalent interactions were carried out in the 1990s.<sup>15-21</sup> Among the first works were the articles by Lacks and Gordon<sup>15</sup> and Kristyán and Pulay,<sup>16</sup> which serve as an illustration of the state of the DFT field at the time as well as of some of the problems dispersion functionals face today. Lacks and Gordon<sup>15</sup> showed that common exchange functionals reproduce the exact exchange energy of noble gases to within 1%. However, these variations in the exchange contributions stand out against the very small binding energies in the noble gas dimers. This results in exchange contributions to the binding energies that can range from 0 to more than 100 % of the exact exchange.<sup>108</sup> Kristyán and Pulay<sup>16</sup> tried to reproduce the binding energy curves of the noble-gas dimers He<sub>2</sub>, Ne<sub>2</sub>, and Ar<sub>2</sub>, only to find that all GGAs and B3LYP are repulsive, to a varying extent, whereas LDA overbinds these systems significantly.

The picture is equally dismal for other types of noncovalent interactions as well. Figure 4 shows the performance of several common density-functional approximations in the calculation of three kinds of intermolecular interactions. Ne dimer, because of its closed-



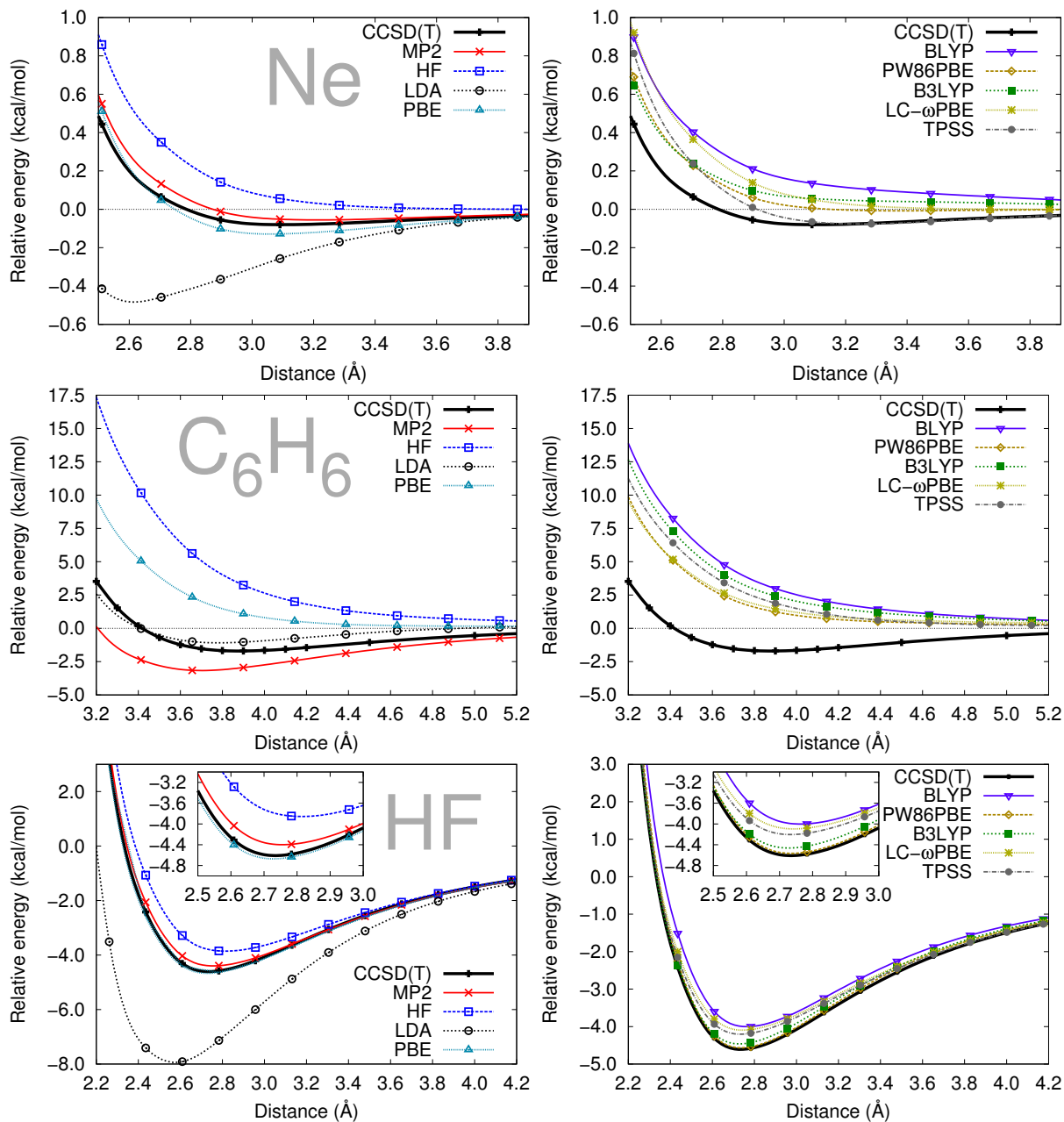


Figure 4. Binding energy curves of neon (top), benzene (middle), and hydrogen fluoride (bottom) dimers, calculated using wavefunction theory methods, LDA, and PBE (left), and other common density functionals (right). Note the different energy scales in the three dimers. For benzene dimers, all DFT calculations were run at aug-cc-pVTZ level, MP2 calculations used counterpoise-corrected aug-cc-pVQZ, and the CCSD(T) results come from ref. 109. For the HF dimer, DFT and HF calculations used aug-cc-pVTZ, MP2 and CCSD(T) used counterpoise-corrected aug-cc-pVQZ. Ne dimer was run using aug-cc-pV5Z in all cases (counterpoise-corrected in MP2 and CCSD(T)).

shell electron configuration, serves as the prototypical example of binding coming exclusively from dispersion. Hartree-Fock (HF), which contains no correlation at all (dispersion or otherwise), predicts a purely repulsive curve, while MP2 and CCSD(T) predict roughly the correct binding. The CCSD(T) minimum (our accurate reference) is at 3.09Å interatomic distance. The binding energy at equilibrium is small (0.084 kcal/mol) but enough to crystallize neon into a closed-packed face-centered cubic structure at low temperature (24.56 K<sup>110</sup>) and zero pressure.

All density functionals fail to correctly describe the dispersion binding behavior in Ne dimer. LDA is spuriously attractive while GGAs show a range of behaviors from overly attractive (PBE) to more repulsive than HF (BLYP). The accuracy does not improve by using more sophisticated functionals: meta-GGA functionals, hybrids, and range-separated hybrids all fail to describe the binding in neon dimer. This result is hardly surprising.<sup>15,16</sup> LDAs and GGAs are semilocal approximations—it is not in their design to account for dispersion interactions, which are long-range correlation effects. Incorporating HF exchange in one form or another does not help either.

The results are equally disappointing for  $\pi$ - $\pi$  interactions. Figure 4 shows the binding energy curve for the stacked configuration of the benzene dimer. Most of the stabilization comes from dispersion, and CCSD(T) predicts a binding energy of 1.681 kcal/mol (this configuration of benzene dimer is not the most stable, but  $\pi$ - $\pi$  stacks are a particularly important motif in biological systems<sup>111</sup>). Again, all functionals except LDA are purely repulsive to varying degrees. LDA gives an answer close to the correct result, which explains its popularity in modelling graphene-based systems in the past.<sup>112</sup> Interestingly, MP2 grossly overbinds the  $\pi$ - $\pi$  interaction—an effect that is found whenever the monomers have low-lying excited states, for known reasons.<sup>113,114</sup> The attractive or repulsive character of the functionals follows the same trend as in the Ne dimer, with PBE giving the most binding and BLYP the most repulsive.

The third interaction type are hydrogen bonds, represented by the hydrogen fluoride dimer in Figure 4. Because of their strength relative to the rest of the van der Waals interactions, hydrogen bonds usually dominate molecular aggregation and, as a consequence, they are prevalent in supramolecular (e.g. molecular crystal packing, crystal engineering) and biological systems (protein folding, DNA structure and function), making their accurate representation extremely important. The performance of various density functionals for the hydrogen fluoride dimer, with a binding energy of 4.57 kcal/mol at equilibrium, is not as bad as for dispersion-dominated dimers. Except for LDA, all density functionals perform relatively well in absence of dispersion. This is reasonable because hydrogen bonding is dominated by electrostatic and orbital interactions, and HF alone obtains almost 4 kcal/mol of the binding energy. A closer look reveals that all functionals are underbinding except for PBE by an amount of up to 0.7 kcal/mol, which points to the missing dispersion attraction.

Despite the reasonable performance for hydrogen bonding, common density functionals have serious difficulties in bonding hydrogen-bonded systems accurately. These problems surface in the modeling of more complex systems, as, for instance, the overstructuring and overly small diffusion coefficient in molecular dynamics simulations of liquid water,<sup>115</sup> the incorrect relative energies of the phases of ice,<sup>116</sup> and the incorrect energy ranking of water hexamer structures.<sup>99,117</sup> Up to a point, dispersion has been proven able to correct, at least partially, some of these problems,<sup>99,116</sup> but the accurate modelling of extended hydrogen-bonded networks is still a challenge in DFT.

In summary, traditional density-functionals perform reasonably well for thermochem-

istry or reaction barriers but, as we have just shown, are unreliable when it comes to the calculation of noncovalent interaction energies. These difficulties are partially caused by noncovalent binding being significantly weaker than covalent binding. Errors from approximate functionals are much more significant relative to a noncovalent bond energy than to a covalent bond. The simplest way to account for the missing dispersion energy is to assume that the density functional (in the following called the *base* functional) is approximately accounting for the other noncovalent interactions and to simply add the dispersion term separately:

$$E = E_{\text{base}} + E_{\text{disp}} \quad [20]$$

The quantity  $E_{\text{disp}}$  is the *dispersion correction* to the base functional, and has to account for the missing dispersion energy as well correct the behavior and uncontrolled effects on the binding energies coming from the base functional.

The erratic behavior of various functionals for different types of interactions is exemplified in Figure 1. The performance of different functionals improves, and the spread in the average errors decreases, with the amount of binding that is accounted for by the interaction of the ground-state charge distributions. In this way, hydrogen bonds, which are dominated by electrostatic interactions, are relatively well modeled. On the other hand, dispersion interactions, which arise from instantaneous dipoles on both molecules, present the largest average errors and spread.

Many dispersion corrections have been proposed over the last 15 years,<sup>26,111</sup> some of which we consider in the following sections. The simplest of those corrections is to use the asymptotic form of the dispersion energy, with a leading  $R^{-6}$  term, to capture the long-range interaction between atoms and molecules. This approximation is the basis of the pairwise dispersion corrections, and works surprisingly well considering the simplicity of the premise. We review this approach next.

## NON-COVALENT INTERACTIONS IN DFT

### Pairwise Dispersion Corrections

The accurate and efficient calculation of the dispersion energy ( $E_{\text{disp}}$  in Eq. 20) is a complex problem in the context of density-functional theory. The physical origin of dispersion is the interaction between instantaneous dipoles in two different molecules or fragments of the same molecule. These instantaneous dipoles are created by short-lived molecular excitations. As a consequence, dispersion is strictly a long-range electron correlation effect, meaning it arises from the correlated movement of electrons in two different molecules (or distant parts of the same molecule). Common correlation functionals are based on local approximations (i.e. the energy density at a point in space depends on local properties such as the density or the gradient at that point) and are, consequently, unable to model dispersion by design.

For two sufficiently-separated interacting neutral atoms, the dispersion energy is always attractive, and decays as the sixth power of the intermolecular distance:

$$E_{\text{disp}} = -\frac{C_6^{AB}}{R_{AB}^6} \quad [21]$$

The asymptotic behavior can be proven using simple arguments like, for instance, the interaction of two coupled harmonic oscillators,<sup>110</sup> or second-order perturbation theory.<sup>118</sup> In

Eq. 21, the  $C_6^{AB}$  are the dispersion coefficients (or simply the interaction coefficients), and can be estimated using London’s formula:<sup>118</sup>

$$C_6^{AB} = \frac{3}{2} \left( \frac{I_A I_B}{I_A + I_B} \right) \alpha_A \alpha_B \quad [22]$$

where  $I$  are the atomic ionization potentials and  $\alpha_A$  are the atomic polarizabilities.

The values calculated using London’s formula are approximate estimates with little practical value. The formula contains qualitative information, namely, the interaction coefficient depends directly on the polarizabilities of both atoms, which in turn are proportional to the atomic size and the number of valence electrons.<sup>118</sup> A more accurate value for the interaction coefficients can be obtained from second-order perturbation theory.<sup>118</sup>

$$C_6^{AB} = \frac{2}{3} \sum'_{n_A n_B} \frac{(\boldsymbol{\mu}_{A,0n_A} \cdot \boldsymbol{\mu}_{A,n_A0})(\boldsymbol{\mu}_{B,0n_B} \cdot \boldsymbol{\mu}_{B,n_B0})}{\varepsilon_{n_A} + \varepsilon_{n_B}} \quad [23]$$

where the sum runs over the excited states of atoms A and B,  $\boldsymbol{\mu}_{A,0n_A} = \langle 0 | \boldsymbol{\mu}_A | n_A \rangle$  is the transition dipole moment, and  $\varepsilon_{n_A} = E_{n_A} - E_0$  is the excitation energy for the  $n_A$  state of molecule A. The  $C_6^{AB}$  coefficients can be calculated more rigorously, using the Casimir-Polder formula:<sup>25</sup>

$$C_6^{AB} = \frac{3}{\pi} \int_0^\infty \alpha_{1,A}(i\omega) \alpha_{1,B}(i\omega) \quad [24]$$

that involves the atomic frequency-dependent polarizabilities  $\alpha(i\omega)$ . This formula is consistent with the familiar picture of dispersion arising from induced-dipole interactions on A and B. These quantities model the response of the atom under frequency-dependent electric fields, and are not directly available in time-independent DFT, although models exist for their calculation (e.g. ref. 119). The Casimir-Polder formula can be generalized to the calculation of higher-order dispersion contributions:

$$C_{2n}^{AB} = \sum_{l=1}^{n-2} \frac{(2n-2)!}{2\pi(2l)!(2n-2l-2)!} \int_0^\infty \alpha_l^A(i\omega) \alpha_{n-l-1}^B(i\omega) d\omega \quad [25]$$

that involves the higher order ( $2^l$ -polar) dynamic polarizabilities.

Equation 21 can be generalized to the interaction between molecules, or distant fragments of the same molecule, by considering that all atoms in the system interact with one another in a pairwise fashion:

$$E_{\text{disp}} = - \sum_{A>B} C_6^{AB} R_{AB}^{-6} f_6(R_{AB}) - \dots \quad [26]$$

The atom-based calculation of the dispersion energy has proven to be an excellent approximation, even possibly accounting for the missing anisotropy in the dispersion interaction coefficients<sup>26,120</sup> (i.e., the dependence of the dispersion interaction coefficients on the relative orientation of the interacting molecules). Equation 26 contains not only the  $R^{-6}$  contribution but also less important terms involving interactions of order higher than the dipole-dipole (dipole-quadrupole, quadrupole-quadrupole,...). These terms are important,<sup>121</sup> and involve the coefficients in equation 25 for  $n > 3$ , but for simplicity we will momentarily consider only the leading term. The higher-order terms are considered in a forthcoming section titled “The Exchange-Hole Dipole Moment (XDM) Model”.

The  $f_6$  factor is called the *damping function* and is a one-dimensional function of the interatomic distance that goes to zero when  $R_{AB} \rightarrow 0$  and to one when  $R_{AB} \rightarrow \infty$ . This function has two roles in dispersion-corrected DFT: one is to correct for the error introduced by the approximations leading up to equation 26, an important one being that the interacting atoms are not infinitely separated. The other is to deactivate the dispersion contribution at very short range to avoid the singularity at  $R_{AB} = 0$ . As will be shown, the damping function also performs the role of fixing the problems the base functional has in reproducing other terms in the intermolecular interaction energy (e.g. electrostatics) through its adjustable parameters. Figure 4 illustrates how different functionals treat the non-dispersion part of the binding energy. Taking, for instance, the example of the Ne dimer, the behavior of the functional can range from spuriously attractive (PBE) to extremely repulsive (BLYP) compared to the HF repulsive wall. The same effects are observed in the benzene dimer and, to a lesser extent, in the HF dimer.

The energy correction in equation 26 coupled with first-principles simulations at the HF level was used for the first time by Scoles et al. in the 1970s.<sup>108,122</sup> In parallel, pairwise dispersion corrections were also applied as additions to the Gordon-Kim model<sup>123</sup>—an approximate model applied to the sum of frozen molecular electron densities that uses the uniform electron gas exchange, correlation and kinetic energy expressions in order to calculate intermolecular potentials. The dispersion-corrected Gordon-Kim model was first proposed by Rae,<sup>124</sup> and subsequently refined by Cohen and Pack.<sup>125</sup> The objective of these early studies was simply to model the repulsive wall in noble gas dimers (and the triplet of H<sub>2</sub>) using the HF or the Gordon-Kim energies, and the attractive part using the dispersion correction. It is also important to note that a van der Waals term in the form of a Lennard-Jones potential, which uses equation 26 for the attractive part, is also used in practically all classical molecular force fields,<sup>126</sup> such as CHARMM<sup>127</sup> and AMBER.<sup>128</sup>

Because HF is missing all electron correlation it is not suitable for the treatment of general intermolecular interactions, regardless of the presence or absence of a dispersion correction, and this has limited the applicability of the Hartree-Fock-Dispersion (HFD) methods. As a consequence, in later years, the modelling of dispersion was replaced by post-HF wavefunction calculations (e.g. MP2, coupled-cluster, etc.). When the inability of DFT to model noncovalent interactions became apparent in the 1990s, pairwise energy corrections became popular as a straightforward and reasonably accurate way of correcting for the missing dispersion. Among the first studies to include these terms are those by Gianturco et al.<sup>129</sup> on the potential energy surface of the Ar-CO dimer, and Elstner et al.<sup>130</sup> and Wu and Yang<sup>131</sup> on small molecules (rare gas dimers, DNA base pairs, etc.), and Wu et al.<sup>132</sup>

At the heart of all pairwise dispersion corrections is the calculation of the interatomic interaction coefficients  $C_6^{AB}$ . The interaction coefficients traditionally used in classical force fields are not adequate because they are treated as fitted parameters, rather than physical quantities, so they account for other effects in addition to dispersion<sup>131</sup> and therefore are widely variable across different classical force fields.<sup>126</sup>

Early pairwise-dispersion-corrected DFT studies adapted a method proposed by Halgren<sup>126</sup> employing the Slater-Kirkwood formula:<sup>133</sup>

$$C_6^{AB} = \frac{3}{2} \frac{\alpha_A \alpha_B}{(\alpha_A/N_A)^{1/2} + (\alpha_B/N_B)^{1/2}} \quad [27]$$

in which  $N_A$  is the effective number of valence electrons ( $N_A$  is smaller than the actual number of valence electrons and not directly calculable). Halgren proposed using empirical

formulas for  $N_A$ , together with accurate atomic polarizability data and the combination rule derived from equation 27 for the mixed coefficients:

$$C_6^{AB} = \frac{2\alpha_A\alpha_B C_6^{AA} C_6^{BB}}{\alpha_A C_6^{BB} + \alpha_B C_6^{AA}} \quad [28]$$

In their seminal work, Wu and Yang obtained the interaction coefficients by fitting the atomic  $C_6^{AA}$  to molecular interaction coefficients (that can be obtained as sums of the atomic  $C_6^{126}$ ), which in turn had been calculated from experimental dipole-oscillator strength distribution measurements by Meath et al.<sup>134-146</sup> By using least-square fitting, the authors obtained molecular  $C_6$  in excellent agreement with experimental data (1% mean absolute errors for hydrocarbons) and binding energies with an accuracy comparable to MP2. This method is similar to the procedure followed in classical force field calculations and, although not generalizable, the early articles proved that the idea of adding a simple pairwise dispersion correction to an unrelated density functional is not only valid, but gives intermolecular interaction energies with an accuracy that is at least as good as MP2.

In the last ten years, a number of approximations have been proposed for the  $C_6$  and higher-order coefficients with varying degrees of accuracy and empiricism. Some of these have been turned into full-fledged dispersion corrections by parametrization of an associated damping function to routinely-used functionals. We will review some of the most popular in the following sections. The list includes:

- The exchange-hole dipole moment (XDM) model of dispersion, which calculates the  $C_6$ , as well as higher-order coefficients, without any empirical parameters.
- Grimme’s DFT-D<sup>147</sup> and DFT-D2,<sup>148</sup> with empirical fixed  $C_6$  coefficients, and DFT-D3<sup>149</sup> with a model that introduces the dependence of the coefficients on the molecular geometry. The approach by Ortman,<sup>112</sup> which was popular in condensed-matter, and similar in spirit to DFT-D2.
- The Tkatchenko-Scheffler approach in its first version<sup>150</sup> (2009): the  $C_6$  coefficients are obtained from reference data but they are made geometry-dependent by using the direct relation between polarizability and atomic volume.
- The method by Tao, Perdew and Ruzsinszky<sup>119</sup> that calculates the frequency-dependent polarizabilities non-empirically using a model consisting of a metallic sphere of uniform density. The frequencies yield the coefficients through equation 24.

The pairwise dispersion correction in equation 26 can be generalized by considering the complete multipolar expansion of the intermolecular interaction. The generalized dispersion energy is written as a sum of 2-body, 3-body, etc. terms:

$$E_{\text{disp}} = E_{\text{disp}}^{(2)} + E_{\text{disp}}^{(3)} + \dots \quad [29]$$

The leading term in this expansion is the pairwise interaction, which contains terms of order higher than the dipole-dipole:

$$\begin{aligned} E_{\text{disp}}^{(2)} &= E_6^{(2)} + E_8^{(2)} + E_{10}^{(2)} + \dots \\ &= - \sum_{n=6,8,10,\dots} \sum_{A>B} C_n^{AB} R_{AB}^{-n} f_n(R_{AB}) \end{aligned} \quad [30]$$

The simple damping is replaced by a family of functions  $f_n$  that, again, account for the approximate nature of the multipolar expansion at short range.

Dispersion corrections with fixed interaction coefficients benefit from the simplicity in the implementation. Indeed, taking the derivatives of the energy (up to any order) is trivial and the programming is equally easy, which has undoubtedly contributed to the popularity of these methods. In addition, the dispersion contribution is relatively minor in “thermochemical” cases, where there is breaking or formation of covalent bonds. In those cases, the good performance of the base functional is retained, which allows for the treatment a wide range of chemical problems on equal footing. Despite the simplicity of the approximation, the results are surprisingly accurate and methods where the parameters in the base functional are optimized together with dispersion such as B97D<sup>148</sup> and  $\omega$ B97XD<sup>151</sup> see a widespread use nowadays.

A further advantage of pairwise dispersion corrections is that the asymptotic  $R^{-6}$  tail of the interaction energy is captured by design. This is in contrast with methods based on modifications of the existing base functionals (like the Minnesota functionals). The correct  $R^{-6}$  dependence is important in large condensed systems, such as molecular crystals or biological macromolecules, but has little or no consequence in small systems. A related limitation is that  $R^{-6}$  is, for particular systems, not the correct asymptotic limit of the dispersion interaction. This happens in polarizable extended systems, particularly in metal surfaces<sup>152</sup> because of the collective motion of the extensively delocalized electrons. The pairwise-correction results for the binding in graphite at equilibrium, however, are rather accurate.<sup>153,154</sup>

Another possible advantage of pairwise approaches is that the relative values of the dispersion contribution to binding might give “insight”<sup>26</sup> into the nature of noncovalent bonding, although the extent to which this insight is significant is arguable since at equilibrium distances the base functional also contributes to binding and might contain spurious contributions that are absorbed by the damping function. The dispersion contribution to the binding energy is always attractive. In particular cases involving hydrogen-bonded systems, the base functional may already overestimate the binding energy, in which case the dispersion correction will only lead to poorer agreement with the reference binding energies, regardless of the shape of the damping function (see Figure 4 and the last section of this chapter).

Some aspects to consider regarding pairwise dispersion corrections are: i) the interaction coefficients are known to depend upon the chemical environment, as already noted by Wu and Yang<sup>131</sup> and others,<sup>155</sup> ii) higher-order two-body interactions involving the  $C_8$ ,  $C_{10}$ , etc. coefficients are known to give a non-negligible contribution to the energy as well,<sup>26,121</sup> and iii) depending on how the interaction coefficients are calculated, there may be no simple way to include the dispersion effects back into the density in the self-consistent procedure. For a self-consistent implementation of the dispersion functional in equation 20, it is necessary to add a dispersion potential to the one-electron Hamiltonian (Eq. 10), corresponding to the functional derivative of  $E_{\text{disp}}$  with respect to the density:

$$V_{\text{disp}} = \frac{\delta E_{\text{disp}}}{\delta \rho(\mathbf{r})} \quad [31]$$

Because the dispersion forces are relatively small, the effect of the dispersion potential on the self-consistent electron density is relatively minor,<sup>156–159</sup> justifying the calculation of the dispersion energy after the self-consistent field procedure (post-SCF), which is far simpler.

In the following sections, we review the most popular approaches to calculate the dispersion energy using pairwise energy expressions (equations 29 and 30). These methods comprise two components: i) a way of calculating or estimating the interaction coefficients  $C_n$ , and ii) an expression for the damping function that depends upon a number of adjustable coefficients, which are empirical and must be fitted to a training set of reference data (usually small dimers calculated using accurate wavefunction methods). Normally, the training sets for the damping function parametrization are small, in accordance with the likewise small number of parameters in the models. The empirical parameters for the damping function transfer relatively well to other noncovalently bound dimers not in the parametrization set, making the pairwise approach fairly easy to generalize to all atoms in the periodic table.

### *The Exchange-Hole Dipole Moment (XDM) Model*

The exchange-hole dipole-moment (XDM) model of dispersion<sup>121,154,160–169</sup> was proposed in 2005 by Becke and Johnson<sup>160,161</sup> and developed in subsequent papers into a practical approach to correct density functionals for dispersion effects. The XDM model in its current formulation is a semilocal functional (a meta-GGA) that gives the interaction coefficients  $C_n$  strictly from first principles, without intervening empirical parameters.

An essential component of the XDM model is the exchange or Fermi hole:

$$h_{X\sigma}(\mathbf{r}_1, \mathbf{r}_2) = -\frac{|\rho_{1\sigma}(\mathbf{r}_1, \mathbf{r}_2)|^2}{\rho_\sigma(\mathbf{r}_1)} \quad [32]$$

where  $\rho_{1\sigma}$  is the one-electron spin density matrix, and  $\rho_\sigma$  is the  $\sigma$ -spin electron density. In the usual one-determinant representation used in Kohn-Sham DFT,

$$h_{X\sigma}(\mathbf{r}_1, \mathbf{r}_2) = -\frac{1}{\rho_\sigma(\mathbf{r}_1)} \sum_{ij} \psi_{i\sigma}(\mathbf{r}_1)\psi_{j\sigma}(\mathbf{r}_1)\psi_{i\sigma}(\mathbf{r}_2)\psi_{j\sigma}(\mathbf{r}_2) \quad [33]$$

which involves a double sum over the occupied spin-orbitals ( $\psi_{i\sigma}$ ).

Given an electron of spin  $\sigma$  at the reference point  $\mathbf{r}_1$ , the exchange-hole represents the probability depletion of finding a same-spin electron at  $\mathbf{r}_2$ . The exchange-hole is always negative, and has well-known properties:

1. The on-top depth condition:

$$h_{X\sigma}(\mathbf{r}, \mathbf{r}) = -\rho_\sigma(\mathbf{r}) \quad [34]$$

establishes that, at the reference point, the hole excludes exactly the amount of electron density at that point. This is a local version of the Pauli exclusion principle.

2. The hole depletes exactly one electron:

$$\int h_{X\sigma}(\mathbf{r}_1, \mathbf{r}_2) d\mathbf{r}_2 = -1 \text{ for all } \mathbf{r}_1 \quad [35]$$

3. The associated exchange energy is:

$$E_x = \frac{1}{2} \sum_{\sigma} \int \rho_\sigma(\mathbf{r}_1) \frac{h_{X\sigma}(\mathbf{r}_1, \mathbf{r}_2)}{r_{12}} d\mathbf{r}_1 d\mathbf{r}_2 \quad [36]$$

with  $r_{12}$  the interelectronic distance.



Let us assume two neutral non-overlapping atoms A and B. The key idea in XDM is that the dispersion energy originates from the interaction of the real-space electrostatic distributions generated by the electrons and their associated exchange holes. At any point  $\mathbf{r}$ , there is a negative charge equal to  $\rho_\sigma(\mathbf{r})$ , and an associated positive distribution represented by the exchange-hole at that reference point equal to  $\rho_\sigma(\mathbf{r})h_{X\sigma}(\mathbf{r}, \mathbf{r}')$ . The hole integrates to -1, so the leading contribution to the electrostatic potential from that point is the dipole formed by the hole and the electron:

$$\mathbf{d}_{X\sigma}(\mathbf{r}) = \int \mathbf{r}' h_{X\sigma}(\mathbf{r}, \mathbf{r}') d\mathbf{r}' - \mathbf{r} \quad [37]$$

Hence, the dispersion interaction in XDM originates from the asymmetry of the exchange-hole.<sup>160</sup>

With the definitions above, and under the assumption that the exchange-hole dipole is directed towards the closest nucleus, it is relatively straightforward to apply classical electrostatic arguments<sup>166</sup> to calculate the square of the  $l$ -pole operator:

$$\langle M_l^2 \rangle_A = \sum_\sigma \int \rho_\sigma(\mathbf{r}) [r_A^l - (r_A - d_{X\sigma})^l]^2 d\mathbf{r} \quad [38]$$

In this way, the multipoles can be calculated up to any order using only the norm of the exchange-hole dipole. The squared moments are then used to obtain the dispersion interaction coefficients:<sup>166</sup>

$$C_6^{AB} = \frac{\alpha_A \alpha_B \langle M_1^2 \rangle_A \langle M_1^2 \rangle_B}{\langle M_1^2 \rangle_A \alpha_B + \langle M_1^2 \rangle_B \alpha_A} \quad [39]$$

$$C_8^{AB} = \frac{3 \alpha_A \alpha_B (\langle M_1^2 \rangle_A \langle M_2^2 \rangle_B + \langle M_2^2 \rangle_A \langle M_1^2 \rangle_B)}{2 (\langle M_1^2 \rangle_A \alpha_B + \langle M_1^2 \rangle_B \alpha_A)} \quad [40]$$

$$C_{10}^{AB} = 2 \frac{\alpha_A \alpha_B (\langle M_1^2 \rangle_A \langle M_3^2 \rangle_B + \langle M_3^2 \rangle_A \langle M_1^2 \rangle_B)}{\langle M_1^2 \rangle_A \alpha_B + \langle M_1^2 \rangle_B \alpha_A} + \frac{21}{5} \frac{\alpha_A \alpha_B \langle M_2^2 \rangle_A \langle M_2^2 \rangle_B}{\langle M_1^2 \rangle_A \alpha_B + \langle M_1^2 \rangle_B \alpha_A} \quad [41]$$

where  $\alpha$  are the atomic polarizabilities (see below). By using a model of dispersion based on the electrostatic interaction of electrons and holes, the dispersion interaction in XDM can be calculated without recourse to time-dependent or excited state calculations.

The scheme above depends upon the definition of fragments A and B, but it is far more practical to assign interaction coefficients to atoms instead of molecules. To do this, Johnson and Becke<sup>162</sup> proposed to make use of the Hirshfeld partitioning scheme:<sup>170</sup>

$$\omega_A(\mathbf{r}) = \frac{\rho_A^{\text{at}}(\mathbf{r})}{\sum_B \rho_B^{\text{at}}(\mathbf{r})} \quad [42]$$

where  $A$  is an atom in a molecule,  $\omega_A$  is the Hirshfeld weight,  $\rho_A^{\text{at}}$  is the *in vacuo* atomic density of A and the denominator is the promolecular density (the sum of the *in vacuo* atomic densities at the molecular geometry). The Hirshfeld weights enter the moment equations:

$$\langle M_l^2 \rangle_A = \sum_\sigma \int \omega_A(\mathbf{r}) \rho_\sigma(\mathbf{r}) [r_A^l - (r_A - d_{X\sigma}(\mathbf{r}))^l]^2 d\mathbf{r} \quad [43]$$

and these are subsequently used to calculate atomic dispersion coefficients using equations 39 through 41.

The atom-in-molecule polarizabilities are obtained in a similar way by using the known direct proportionality between polarizability and volume<sup>162</sup> (see ref. 171 and references therein for details):

$$\alpha_A = \frac{V_A}{V_A^{\text{at}}} \alpha_A^{\text{at}} \quad [44]$$

$$V_A = \int r^3 \omega_A(\mathbf{r}) \rho(\mathbf{r}) d\mathbf{r} \quad [45]$$

$$V_A^{\text{at}} = \int r^3 \rho_A^{\text{at}}(\mathbf{r}) d\mathbf{r} \quad [46]$$

where  $\alpha_A^{\text{at}}$  is the free-atom polarizability and the fraction measures the volume occupied by atom A in the molecular environment ( $V_A$ ) in relation to the same atom in the vacuum ( $V_A^{\text{at}}$ ).

The computation of the  $C_n$  coefficients using the exchange hole in equation 33 involves a double sum over occupied orbitals, which is computationally expensive, particularly in periodic plane wave approaches that are used in condensed-matter calculations. As a consequence, recent implementations of XDM do not use the exact exchange hole but an approximation to it: the Becke-Roussel (BR) model.<sup>172</sup> BR is a model of the spherically-averaged exchange hole,  $h_{X\sigma}(\mathbf{r}, s)$ . In it,  $h_{X\sigma}(\mathbf{r}, s)$  is represented as an exponential  $Ae^{-ar}$  located at a distance  $b$  from the reference point  $\mathbf{r}$ . The three parameters  $A$ ,  $a$ , and  $b$  are determined by imposing the on-top depth condition (Eq. 34), the hole normalization (Eq. 35) and the exact curvature at the reference point, which is:

$$Q_\sigma = \frac{1}{6} (\nabla^2 \rho_\sigma - 2D_\sigma) \quad [47]$$

where

$$D_\sigma = \tau_\sigma - \frac{1}{4} \frac{(\nabla \rho_\sigma)^2}{\rho_\sigma} \quad [48]$$

$$\tau_\sigma = \sum_i (\nabla \psi_{i\sigma})^2 \quad [49]$$

with  $\nabla^2 \rho_\sigma$  the Laplacian of the electron density and  $\tau_\sigma$  the Kohn-Sham kinetic energy density.

By using the BR model, and under the constraints above, the exchange-hole dipole ( $d_{X\sigma}$ ) reduces to the value of the parameter  $b$ , which is calculated by solving for  $x$  in:

$$\frac{x e^{-2x/3}}{x-2} = \frac{2}{3} \pi^{2/3} \frac{\rho_\sigma^{5/3}}{Q_\sigma} \quad [50]$$

and then substituting in:

$$b^3 = \frac{x^3 e^{-x}}{8\pi \rho_\sigma} \quad [51]$$

See ref. 161 for details on the derivation.

The BR model has the computational advantage with respect to the exact exchange-hole that determining the dipole depends only on local quantities: the density and its derivatives and the kinetic energy density. Hence, by using BR, XDM is formally a meta-GGA model

of dispersion, and the computational cost becomes negligible compared to the base DFT calculation. In addition, the interaction coefficients using the BR model give significantly better results in the calculation of binding energies of small noncovalently bonded dimers.<sup>168</sup>

In the canonical implementation of XDM, the pairwise terms involving  $C_6$ ,  $C_8$ , and  $C_{10}$  are used in the energy expression:

$$E_{\text{disp}} = - \sum_{A>B} \sum_{n=6,8,10} \frac{C_n^{\text{AB}} f_n(R_{AB})}{R_{AB}^n} \quad [52]$$

Generalized expressions for the pairwise coefficients up to any order and for the coefficients involving more than two atoms have been formulated.<sup>169</sup> However, using pairwise terms of order higher than  $n = 10$  gives, at first, a negligible contribution to the energy and, ultimately, makes the dispersion series diverge. The leading three-body term has the well-known Axilrod-Teller-Muto expression<sup>173-175</sup> that decays globally as  $R^{-9}$  and involves a  $C_9$  coefficient:

$$E_{\text{disp}}^{(3)} = C_9 \frac{3 \cos \theta_A \cos \theta_B \cos \theta_C + 1}{R_{AB}^3 R_{AC}^3 R_{BC}^3} \quad [53]$$

In XDM, the three-body dispersion coefficient is:<sup>169</sup>

$$C_9 = \langle M_1^2 \rangle_A \langle M_1^2 \rangle_B \langle M_1^2 \rangle_C \times \frac{Q_A Q_B Q_C}{(Q_A + Q_B)(Q_A + Q_C)(Q_B + Q_C)} \quad [54]$$

with  $Q_X = \langle M_1^2 \rangle_X / \alpha_X$ . Despite the  $C_9$  calculated with an accuracy similar to the  $C_6$ , no simple way of conciliating this term with the pairwise correction (Eq. 52) has been found,<sup>169</sup> mainly because of uncertainties as to the shape of the damping function  $f_9$  (see below).

To turn the dispersion coefficients into a practical energy correction, an expression for the damping function in equation 52 is needed. The damping function traditionally used in XDM is the Becke-Johnson damping function,<sup>121</sup> that is defined as:

$$f_n(R) = \frac{R^n}{R^n + R_{\text{vdw}}^n} \quad [55]$$

This damping function depends naturally on the order of the interaction, and the whole  $f_n$  family has only two adjustable parameters ( $a_1$  and  $a_2$ ) inside the van der Waals radii:

$$R_{\text{vdw}} = a_1 R_c + a_2 \quad [56]$$

$R_{\text{vdw}}$  is related to the size of the associated atom.  $R_c$  is the critical radius, which is defined as the arithmetic average of the distances where the  $C_6$ ,  $C_8$  and  $C_{10}$  terms acquire the same magnitude:

$$R_c = \frac{1}{3} \left[ \left( \frac{C_8}{C_6} \right)^{1/2} + \left( \frac{C_{10}}{C_6} \right)^{1/4} + \left( \frac{C_{10}}{C_8} \right)^{1/2} \right] \quad [57]$$

The damping function parameters  $a_1$  and  $a_2$  are the only two adjustable parameters in the XDM model. As mentioned before, these are determined by fitting to a set of high-quality reference data (usually at the CCSD(T) level extrapolated to the complete basis set limit). In XDM it is customary to use the Kannemann-Becke (KB) set.<sup>167,168</sup> The dimers in the KB set are made of small molecules with a mixture of interaction types (hydrogen bonding, dipole-dipole, dispersion) and include the noble-gas dimers. The latter have very small binding

TABLE II.  $C_6$  Dispersion Coefficients for the Carbon Atom in Different Bonding Situations Calculated with Different Dispersion Corrections. The XDM Values Were Computed using the LC- $\omega$ PBE Functional at the aug-cc-pVTZ level. The remaining values are from Johnson.<sup>155</sup>

Molecule	WY <sup>a</sup>	TS <sup>b</sup>	B97D <sup>c</sup>	D3 <sup>d</sup>	XDM <sup>e</sup>
C free	—	46.6	24.6	49.10	48.84
C sp	29.71	30.6	24.6	29.36	31.31
C sp <sup>2</sup>	27.32	30.3	24.6	25.78	25.68
C sp <sup>3</sup>	22.05	24.1	24.6	18.21	23.89

<sup>a</sup> Wu and Yang.<sup>131</sup>

<sup>b</sup> Tkatchenko-Scheffler.<sup>150</sup>

<sup>c</sup> DFT-D2-adapted functional by Grimme (B97D).<sup>148</sup>

<sup>d</sup> Grimme’s DFT-D3.<sup>149</sup>

<sup>e</sup> XDM.

energies and many functionals overbind, even in absence of a dispersion correction. Because the parametrization is performed by minimizing the mean absolute percent error (MAPE), for certain functionals the determination of  $a_1$  and  $a_2$  is done on a smaller subset of KB that does not contain noble-gas dimers (with 49 dimers instead of the original 65). The dimers and the corresponding binding energies in the KB set have been adapted from previous works, and subsequently reviewed in later articles.<sup>176</sup> The reader is pointed to ref. 177 for the most recent energies, molecular geometries, and the original literature references.

XDM has been implemented for use in molecular quantum chemistry programs<sup>99,168</sup> as well as in condensed-matter plane-wave-based codes.<sup>154</sup> It has been extensively parametrized for common density-functionals in both scenarios<sup>99</sup> (the  $a_1$  and  $a_2$  parameters are sensitive to the implementation, see ref. 177 for the latest values), presents excellent performance in molecular<sup>99</sup> and solid-state<sup>178</sup> applications (see the section titled “Performance of Dispersion-Corrected Methods” for detailed statistics), and has been used in a number of real-life applications,<sup>179–183</sup> although to a lesser extent than other functionals like those in the DFT-D family.

The advantages and disadvantages of the XDM model follow those mentioned in earlier for pairwise dispersion corrections. In addition, the interaction coefficients depend naturally on the chemical environment, the importance of which was already recognized in the early days of the DFT dispersion corrections<sup>131</sup> and in the classical-force-field community.<sup>126</sup> A study of the variation of the coefficients on the chemical environment for selected examples has been presented by Johnson.<sup>155</sup> As an illustration, the  $C_6$  values for carbon in different hybridization states are shown in Table II. All variable-coefficient methods predict the same trend, and roughly agree in the values. The coefficients become smaller because they are proportional to the square of the polarizability (Eq. 22), which in turn is proportional to the atomic volume (Eq. 44), which becomes smaller as more hydrogens sit around the carbon. B97D, which is based on Grimme’s DFT-D2 (see below), uses a fixed  $C_6$  with an average value.

The use of variable coefficients introduces the question of whether the proper calculation of the nuclear forces is being done in the course of a geometry optimization calculation. Since the  $C_n$  depend on the geometry, the differentiation of Eq. 52 may no longer be an easy task, particularly for XDM. Because the term coming from the  $C_n$  nuclear derivatives is relatively

small in the canonical implementation of XDM,<sup>99,154,168</sup> the pragmatic assumption is made that the  $C_n$  are fixed. This approximation works if the optimization algorithm is robust enough to handle small mismatches between energies and forces (as is the case, for instance, for the Gaussian<sup>184</sup> program), whereas in other cases (e.g., Quantum ESPRESSO<sup>185</sup>) the geometry optimization is carried out with fixed  $C_n$ , and then needs to be repeated after completion.

The atomic  $C_n^{\text{AB}}$  in XDM are completely non-empirical, and the model to obtain them is physically motivated. Although it may look like a philosophical—rather than practical—advantage, the plus in practice is that dispersion from atoms in the whole periodic table can be treated on the same footing, without concerns about the reliability of the empirical interaction coefficients for “exotic” atoms.

The Hellmann-Feynman theorem establishes that atomic forces are calculated using the nuclear positions and the electron density in the classical electrostatics fashion. As a consequence, dispersion forces must have an impact (albeit small) on the electron density distribution. Dispersion functionals like XDM, where the dispersion correction depends on the electron density, can be incorporated back into the density by solving the self-consistent problem in the presence of the dispersion potential contribution. This has been done in the past by Kong et al.<sup>157</sup> though the implementation in other software packages is still work in progress.

The XDM dispersion correction is available in the latest version of Quantum ESPRESSO<sup>185</sup> (post-SCF) and in Q-chem<sup>186</sup> (self-consistent). It is also provided as an external program<sup>177</sup> (postg) that calculates the dispersion energy and its derivatives and can be used with quantum chemistry codes, particularly Gaussian.<sup>184</sup> The code can be used to drive a geometry optimization coupled with Gaussian’s “external” keyword. A collaboration aimed to achieve a robust self-consistent implementation of the XDM dispersion energy functional and its derivatives in the Gaussian program is underway.

### ***The DFT-D Functionals***

The functionals in the DFT-D family, designed by Grimme and collaborators, are the most widely-used dispersion corrections today thanks to their relative accuracy, simplicity, and, particularly, to its widespread implementation in popular software packages. The DFT-D family consists of three generations: DFT-D itself<sup>147</sup> (proposed in 2004), which is seldom used today, the very popular DFT-D2<sup>148</sup> (2006), and the last and “final” development, DFT-D3<sup>149</sup> (2010), which is replacing DFT-D2 in modern usage. The DFT-Dx functionals are all based on the pairwise dispersion energy correction (equation 30) with increasing levels of complexity and accuracy in later generations of the family. The design philosophy in DFT-Dx sacrifices strong adherence to theoretical principles (many design decisions in the DFT-D3 functional are *ad hoc*) in exchange for improved accuracy, flexibility, and simplicity in the implementation.

The DFT-Dx functionals are extensively parametrized—they have been combined with tens of different functionals from all levels<sup>149</sup>—and benchmarked.<sup>187</sup> DFT-D2 has been implemented in most software packages for quantum chemistry and solid-state, including Gaussian,<sup>184</sup> GAMESS,<sup>188,189</sup> NWChem,<sup>190</sup> Quantum ESPRESSO,<sup>185</sup> VASP,<sup>191,192</sup> and abinit.<sup>193,194</sup> DFT-D3 has been implemented in most quantum chemistry packages as well, although it is not available in the mainstream solid-state codes yet.

The original DFT-D method<sup>147</sup> uses a pairwise dispersion energy correction involving

only the  $C_6$  coefficient and a global scaling factor ( $s_6$ ):

$$E_{\text{DFT-D}} = -s_6 \sum_{i>j} \frac{C_6^{AB}}{R_{AB}^6} f_{\text{damp}}(R_{AB}) \quad [58]$$

where the damping function is:

$$f_{\text{damp}}(R) = \frac{1}{1 + \exp(-\alpha(R/R_0 - 1))} \quad [59]$$

In this equation,  $R_0$  is a quantity representing the atomic size (akin to the sum of the van der Waals radii). For a particular pair of atoms,  $R_0$  is determined by assigning atomic radii to those atomic species. These radii are calculated using the distance to the 0.01 a.u. isodensity envelopes of the *in vacuo* atoms, scaled by an *ad hoc* factor of 1.22. The value of the  $\alpha$  parameter is set to 23, as in the previous article by Wu and Yang.<sup>131</sup>

The homoatomic interaction coefficients were replicated from the previous work of Wu and Yang,<sup>131</sup> but averaged over different hybridization states in order to avoid the need to define atomic types, which would be impractical. The heteroatomic coefficients are calculated using the combination rule:

$$C_6^{AB} = 2 \frac{C_6^{AA} C_6^{BB}}{C_6^{AA} + C_6^{BB}} \quad [60]$$

The global scaling coefficient  $s_6$  is a fitted functional-dependent parameter in the DFT-D method, with several values for different functionals. The method is parametrized<sup>147</sup> using a collection of 18 gas-phase dimers for BLYP ( $s_6 = 1.4$ ), B986 ( $s_6 = 1.4$ ), and PBE ( $s_6 = 0.7$ ). These values of the global scaling factor conform to the overrepulsive behavior of the B88 exchange functional and the overattractive behavior of PBE (see Figure 4). The results presented in the original paper for a collection of molecules improved upon MP2 for  $\pi$ - $\pi$  stacked interactions, although the results for hydrogen bonds were somewhat unsatisfactory.

DFT-D was an early attempt at turning the work of Wu and Yang<sup>131</sup> into a practical and general dispersion correction. Although the success was limited, it showed that a practical correction based on a pairwise expression of the energy coupled with a common functional and parameterized appropriately gives reasonably accurate results, fit for real-life applications. However, DFT-D was limited by lack of  $C_6$  data for general atomic pairs, by systematic errors in molecules involving heavy elements (third row or below), and by errors in the treatment of normal thermochemistry.<sup>148</sup>

The next development in the series, DFT-D2,<sup>148</sup> was a vast improvement and greatly popularized the whole approach. Two things were proposed in the DFT-D2 paper: the standalone dispersion correction itself, reviewed below, and a modification of the B97 semilocal functional proposed by Becke<sup>195</sup> but refitted at the same time as the dispersion correction to a molecular set containing noncovalent interaction energies as well as thermochemistry reference data. The resulting functional, B97-D, proved to yield accurate noncovalent interactions while, at the same time, improving the thermochemistry of plain B97. Being a semilocal functional, B97-D was also proposed as an efficient functional, coupled with the resolution of the identity (RI) technique<sup>196,197</sup> to the computation of the Coulomb energy (already in the TURBOMOLE<sup>198</sup> program at the time).

The DFT-D2 dispersion correction uses the same expression as DFT-D (equation 58), with a number of minor differences: i) the scaling factor in the van der Waals radius is

reduced from 1.22 to 1.10, and ii) the value of the  $\alpha$  parameter is reduced from 23 to 20. The combination rule for obtaining the heteroatomic coefficients is also replaced by:

$$C_6^{AB} = \sqrt{C_6^{AA}C_6^{BB}} \quad [61]$$

and an *ad hoc* formula based on London’s (Eq. 22) is used to calculate the homoatomic coefficients:

$$C_6^{AA} = 0.05NI_p^A\alpha^A \quad [62]$$

where the 0.05 coefficient is selected to adjust previous  $C_6$  values,  $N$  is the atomic number of the noble gas on the same period as A,  $I_p^A$  are the atomic ionization potentials, and  $\alpha^A$  are the *in vacuo* atomic static polarizabilities.

Grimme argues that DFT-D2 is less empirical than DFT-D, and that there are fewer parameters than in other contemporaneous methods.<sup>148</sup> It is also claimed that DFT-D2 has CCSD(T) accuracy on average which, following years of testing, seems not to be the case. However, DFT-D2 does improve greatly upon the accuracy of DFT-D and provides a functional that is in principle valid for the whole periodic table.

The refitted functional B97-D performs better in thermochemical tests than both uncorrected B97 and the DFT-D2 dispersion-corrected version of B97, but without re-fitting the base functional. For instance, B97-D gives 3.8 kcal/mol average error on the G97/2 set of atomization energies<sup>199</sup> as compared to the 3.6 kcal/mol for B3LYP. This result is not surprising (and is observed for other dispersion corrections<sup>99</sup>) since GGAs, in general, slightly underbind molecules and solids. Addition of a dispersion correction, which stabilizes molecules with respect to atoms, tends to correct for those systematic deviations. In other cases, such as reaction barriers affected by self-interaction error, the incorporation of a dispersion correction can be detrimental.<sup>99,148</sup> The improvement upon B97 is argued to be associated with the “avoidance of double counting effect” and the balance in the description of “long-range” and “medium-range” correlation effects in the original article.<sup>148</sup>

Subsequent works inspired by the performance of B97-D explored the idea of refitting different functionals in combination with the dispersion correction for noncovalent interactions as well as for thermochemistry. For instance, the DFT-D2 scheme was used with minor changes by Chai and Head-Gordon<sup>151</sup> in combination with a refitted version of the long-range corrected B97 functional.<sup>90</sup> The resulting functional, called  $\omega$ B97X-D, goes to 100% exact-exchange in the long-range electron-electron interaction limit, while the amount of short-range exchange is treated as an adjustable parameter. The parameters in the dispersion correction as well as in the functional are fit to a set that contains both thermochemical and noncovalent interaction reference energies. The fitted parameters include the range-separation parameter, as well as the coefficients in the enhancement factor and the damping function. Unlike in plain DFT-D2, there is no global scaling parameter in the  $\omega$ B97X-D approach.

Despite the good performance of DFT-D2, there are several notorious disadvantages. The  $C_6$  dispersion coefficients are fixed and independent of the environment, which limits the accuracy of the method (see Table II), although, as shown in ref. 148, the damping function is flexible enough to account for this shortcoming to some degree. DFT-D2 is also lacking higher-order dispersion coefficients, which are known to give a non-negligible contribution to the dispersion energy.<sup>26,121,149</sup> Also, DFT-D2 is not properly defined for metals because of the diversity in their bonding environments,<sup>149</sup> which precludes the use of a single  $C_6$  in all bonding situations.

In parallel to DFT-D2, a similar approach was presented by Ortmann,<sup>112</sup> that became relatively popular in the condensed-matter community. In this approach, the PW91 GGA was combined with London’s formula (Eq. 22), and experimental polarizabilities and ionization potentials. A simple Fermi function was used for damping:

$$f_{AB}(R) = 1 - \exp(-\lambda x_{AB}) \quad [63]$$

$$x_{AB} = \frac{R}{R_{\text{cov}}^A + R_{\text{cov}}^B} \quad [64]$$

where  $\lambda = 7.5 \times 10^{-4}$ , set to match the  $c$  cell parameter of graphite. The correction gives excellent results for graphite, and corrects systematic deviations of GGAs in the structures and elastic properties (bulk moduli) of hard solids such as diamond and NaCl, for a reason similar to why DFT-D2 improves results for thermochemistry, that is, because GGAs are underbinding. The lattice parameters of noble gas crystals are, however, overestimated because PW91 is much more attractive than PBE.

The most recent development in the DFT-D family is DFT-D3, proposed by Grimme and collaborators in 2010.<sup>149</sup> DFT-D3 is more complex than DFT-D2, and the interaction coefficients are dependent upon the geometry, though not on the electron density. The formulation of DFT-D3 is extensively based on pre-computed quantities using TDDFT and *ad hoc* recipes in order to determine the basic components entering the model. In DFT-D3, the dispersion energy is written as a sum of the  $C_6$  term and the  $C_8$  term:

$$E_{\text{disp}} = - \sum_{A>B} \frac{C_6^{AB}}{R_{AB}^6} f_6(R_{AB}) + s_8 \frac{C_8^{AB}}{R_{AB}^8} f_8(R_{AB}) \quad [65]$$

In this case, and contrary to DFT-D2, there is no  $s_6$  scaling parameter, and  $s_8$  is an adjustable parameter. The higher-order contributions ( $C_{10}$ , etc.) are omitted because the correction becomes unstable.

The damping functions are the same as proposed in the previous work by Chai and Head-Gordon:<sup>151</sup>

$$f_n(R_{AB}) = \frac{1}{1 + 6(R_{AB}/(s_{r,n}R_0^{AB}))^{-\alpha_n}} \quad [66]$$

In this equation, the  $s_{r,8}$  is set to 1 and the  $s_{r,6}$  is treated as an adjustable parameter. The other parameters are set to  $\alpha_6 = 14$  and  $\alpha_8 = 16$ . This choice is made so that the dispersion energy contribution is less than 1% of the maximum total dispersion energy for interatomic interactions at covalent distances.

The dispersion coefficients do not use the empirical formula of the previous generation in equation 62. Instead, they are obtained by considering the hydrides of all the elements in the periodic table, and by calculating their frequency-dependent polarizabilities using TDDFT with PBE38 (the same as PBE0 but with 37.5% of exact exchange instead of the physically-motivated 25%; this has been shown to give improved excitation energies). The calculated frequency-dependent polarizabilities enter a Casimir-Polder-like equation in the calculation of the atomic interaction coefficients:

$$C_6^{AB} = \frac{3}{\pi} \int_0^\infty \frac{1}{m} \left[ \alpha^{A_m H_n}(i\omega) - \frac{n}{2} \alpha^{H_2}(i\omega) \right] \times \frac{1}{k} \left[ \alpha^{B_k H_l}(i\omega) - \frac{l}{2} \alpha^{H_2}(i\omega) \right] d\omega \quad [67]$$

where  $m$ ,  $n$ ,  $k$ , and  $l$  are the stoichiometric numbers of the corresponding hydrides. The formula involves the frequency-dependent polarizability of the hydrogen molecule.



Calculation of the higher-order coefficients makes use of recurrence formulas. In particular,

$$C_8^{AB} = 3C_6^{AB} \sqrt{Q^A Q^B} \quad [68]$$

$$Q^A = s_{42} \sqrt{Z^A} \frac{\langle r^4 \rangle^A}{\langle r^2 \rangle^A} \quad [69]$$

where  $\langle r^2 \rangle$  and  $\langle r^4 \rangle$  are moments of the electron density,  $s_{42}$  is chosen so that the  $C_8^{AA}$  for He, Ne, and Ar are reproduced and the  $\sqrt{Z^A}$  is an *ad hoc* term introduced to get consistent interaction energies for heavier elements. Coefficients of order higher than  $C_8$  can be calculated as well, using other recurrence relations but they are not used in the energy expression. The three-body interaction coefficient  $C_9$ , that enters the Axilrod-Teller-Muto term (Eq. 53) is calculated in DFT-D3 using another approximate formula:

$$C_9^{ABC} = -\sqrt{C_6^{AB} C_6^{AC} C_6^{BC}} \quad [70]$$

However, the DFT-D3 authors recommend that the three-body term should not be used.

The cutoff radii ( $R_0^{AB}$ ) in the damping function (Eq. 66) are pre-computed for all pairs of atoms independently rather than as the sum of radii for single atoms. As in previous generations, the approach for obtaining  $R_0^{AB}$  involves obtaining the interatomic distance for which the first-order DFT interaction energy (that is, the DFT energy obtained using the frozen electron density distribution resulting from the sum of the two *in vacuo* atoms) is less than a certain cutoff value. The value of this cutoff energy is chosen so that the  $R_0$  of the carbon-carbon interaction is the same as in DFT-D2.

The dependence of the interaction coefficients on the chemical environment is obtained by an *ad hoc* geometry dependence term that is independent of the electron density distribution, and is based on a recipe for calculating the coordination number (CN) of an atom:

$$\text{CN}^A = \sum_{A \neq B} \frac{1}{1 + \exp -k_1 (k_2 (R_{\text{cov}}^A + R_{\text{cov}}^B) / R_{AB} - 1)} \quad [71]$$

The  $k_2$  parameter is set to 4/3, but the covalent radii of all metals are decreased by 10%, the  $k_1$  parameters is set to 16, and the covalent radii are taken from a previous paper by Pyykkö and Atsumi.<sup>200</sup> The CN recovers the “chemically intuitive” coordination numbers for normal molecules.

The CN formula is used in the calculation of dispersion coefficients by formulating a 2-dimensional space  $C_6^{AB}(\text{CN}^A, \text{CN}^B)$  where the  $C_6$  coefficients are calculated for a certain number of reference molecules (and incorporated as fixed quantities within the model), and the  $C_6$  for unknown coordination numbers are interpolated. The parameters in the interpolation scheme are also given. There is one more parameter in the interpolation scheme ( $k_3$ ), which is chosen to get smooth interpolation and plateaus for the integer CN values.

DFT-D3 is widely implemented in popular software packages, and is replacing DFT-D2. DFT-D3 provides a parametrization (on the same footing) for all elements up to Pu, in principle solving the shortcomings in DFT-D2 for heavy elements. The dependence on the geometry and not on the electron density provides an energy expression that is easier to differentiate, but the interatomic coefficients also depend on the oxidation state, which is not directly addressed by DFT-D3. It has also been extensively benchmarked (for instance, see ref. 187) and used in many applications to good effect.

## Other Approaches

*Tkatchenko-Scheffler model.* The method proposed by Tkatchenko and Scheffler<sup>150</sup> (TS) in 2009 is based on a pairwise dispersion energy correction. In TS, the London formula (Eq. 22) is rewritten in order to calculate the heteroatomic interaction coefficients from the homoatomic  $C_6^{AA}$ :

$$C_6^{AB} = \frac{2C_6^{AA}C_6^{BB}}{\frac{\alpha_B}{\alpha_A}C_6^{AA} + \frac{\alpha_A}{\alpha_B}C_6^{BB}} \quad [72]$$

where  $\alpha_A$  are the atomic static polarizabilities in the molecular environment (atom-in-molecule polarizabilities). The static polarizabilities are calculated using the same approach as XDM, proposed by Johnson and Becke.<sup>162</sup> The atom-in-molecule polarizabilities are scaled according to equation 44, with the *in vacuo* atomic polarizabilities taken from the accurate TDDFT results of Chu and Dalgarno.<sup>201</sup> Contrary to XDM, the homoatomic interaction coefficients are scaled from reference atomic data. The scaling is defined using the same atomic partitioning scheme (Hirshfeld) as the polarizabilities:

$$C_6^{AA} = \left( \frac{\int r^3 \omega_A(\mathbf{r}) \rho(\mathbf{r}) d\mathbf{r}}{\int r^3 \rho_A^{\text{at}}(\mathbf{r}) d\mathbf{r}} \right)^2 C_6^{AA,\text{at}} \quad [73]$$

The atomic reference values ( $C_6^{AA,\text{at}}$ ) are taken from the same database as the polarizabilities.<sup>201</sup> The intermolecular interaction coefficients computed in this way have an average error of 5.5% for the intermolecular  $C_6$  coefficients tested on the dipole oscillator strength distribution (DOSD) experimental data of Meath et al.<sup>134-146</sup> The coefficients are sensitive to the chemical environment (see Table II).

The damping function in TS is a Fermi function, similar to the original used in Wu and Yang<sup>131</sup> and in DFT-D.<sup>147</sup> It is defined as:

$$f_{\text{damp}} = \frac{1}{1 + \exp -d(R_{AB}/(s_R R_{AB}^0 - 1))} \quad [74]$$

where  $R_{AB}^0$  is the sum of atomic van der Waals radii. The atomic radius is defined as:

$$R_A^0 = \left( \frac{V_A}{V_A^{\text{at}}} \right)^{1/3} R_A^{0,\text{at}} \quad [75]$$

where  $R_A^{0,\text{at}}$  is defined as the iso-density contour radius corresponding to the density where the noble gas on the same period equals the values by Bondi.<sup>202</sup> The value of the parameter  $d$  is set to 20, and the  $s_R$  is fitted to the S22 database of Jurecka et al.<sup>203</sup> The mean absolute error of the fit is 0.30 kcal/mol when the dispersion correction is coupled with the PBE functional.

The TS model of dispersion has been further revised to include screening and anisotropy effects on the atomic polarizabilities as well as many-body dipole-dipole dispersion effects.<sup>23,204-206</sup> Screening effects are important in systems with extensive electron delocalization,<sup>207</sup> for instance, on metal surfaces. The revisions are based on a random-phase approximation (RPA) approach to a model of interacting quantum harmonic oscillators located at the atomic positions. The harmonic oscillators vibrate with a characteristic frequency related to the effective atomic excitation energy in London's formula and interact via a screened (range-separated) Coulomb potential that is attenuated at short distances using an adjustable parameter.

The atomic polarizabilities calculated using the volume scaling in equation 44 enter a self-consistent equation derived from the RPA treatment of the model system of coupled harmonic oscillators. In this simplified system, the adiabatic connection formula can be integrated analytically to yield a coupled set of self-consistent equations that can be solved for the anisotropic polarizabilities using matrix operations. The anisotropic static polarizabilities present an improved agreement with experimental reference data.<sup>23</sup>

A drawback of the TS method, and subsequent revisions, is that it is limited to dipole-dipole interactions and, therefore, does not take into account the higher-order  $C_8$  and  $C_{10}$  pairwise terms. Nevertheless, the energetics obtained by fitting the damping and the range-separation parameters to standard datasets are promising,<sup>23,150,205</sup> particularly in the formalism that includes many-body interactions. The TS method with has been implemented in the FHI-AIMS<sup>208</sup> program and in the latest version of Quantum ESPRESSO.<sup>185</sup>

*Density-dependent energy correction.* The density-dependent energy correction (dDsC) proposed by Steinmann and Corminboeuf<sup>209–212</sup> is a dispersion correction based on XDM, but with modifications pertaining to the calculation of the exchange-hole as well as a density-dependent damping function that achieves excellent performance in standard thermochemical and noncovalent interactions tests at a low computational cost.

The dispersion energy and the calculation of the interaction coefficients in dDsC is the same as in XDM (equations 52 and 39 to 41). The exchange-hole, unlike the Becke-Roussel model, is based on a GGA approximation and contains adjustable parameters:

$$b = Asr_s e^{-Bs} \quad [76]$$

where  $s$  is the reduced density gradient ( $s = \nabla\rho/[2(3\pi^2)^{1/3}\rho^{4/3}]$ ), and  $r_s = [3/(4\pi\rho)]^{1/3}$  is the Wigner-Seitz radius. The adjustable parameters  $A$  and  $B$  are obtained by fitting to reference data for the noble gas dimers.

The second major difference of dDsC with respect to XDM is the density dependence in the damping function. dDsC uses the Tang-Toennies damping function,<sup>213</sup> which gives excellent results in describing the potential energy curve of the noble gases. Its expression is:

$$f_n(x) = 1 - \exp(-x) \sum_{k=0}^n \frac{x^k}{k!} \quad [77]$$

The damping function enters the energy dispersion expression with a scaling parameter:  $f_n(bR_{AB})$  with  $R_{AB}$  the interatomic distance. The  $b$  parameter depends on the system electron density and contains two adjustable parameters  $a_0$  and  $b_0$ . A further minor change from XDM is that dDsC uses the Hirshfeld-dominant scheme: the atomic weights  $\omega_A(\mathbf{r})$  for atom  $A$  assigned to a point  $\mathbf{r}$  are either 1 if in the normal Hirshfeld partition the weight is greater for atom  $A$  than for any other atom or 0 otherwise.

The dDsC model has been parametrized for a number of popular base functionals<sup>212</sup> using noncovalent interactions as well as thermochemical reference data. The method presents good accuracy in the calculation of intermolecular coefficients<sup>211</sup> (errors of slightly less than 10%) as well as in the energetics of noncovalent dimers,<sup>212</sup> slightly improving upon B2PLYP-D3 (described earlier) and M06-2X (described later) for the tests presented in ref. 212. The dDsC method is implemented in recent versions of ADF,<sup>214–216</sup> Q-Chem<sup>186</sup> and there is a patch for GAMESS<sup>188,189</sup> on the authors’ webpage.<sup>217</sup>

*Local-response dispersion model.* The local-response dispersion (LRD) model proposed by Sato and Nakai<sup>218,219</sup> is based on the second-order perturbation-theory intermolecular

interaction. In the latest version, the dispersion energy is written as a generalized multicenter approach, obtained from the Casimir-Polder equation (Eq. 25) by expanding the Coulomb interaction operator in a multicenter atomic partition:<sup>220</sup>

$$E_{\text{disp}}^{AB} = - \sum_{aa'bb'} \sum_{tt'uu'} T_{tu}^{ab} T_{t'u'}^{a'b'} \int_0^\infty \alpha_{tt'}^{aa'}(i\omega) \alpha_{uu'}^{bb'}(i\omega) d\omega \quad [78]$$

where  $t$  and  $u$  are indices corresponding to different angular momentum contributions ( $t = lm$ ),  $T$  is a damped interaction tensor that depends only upon the relative position of the atoms,<sup>220</sup> and  $\alpha_{tt'}^{aa'}(i\omega)$  are the generalized atom-pair dynamic polarizabilities. These are calculated in the local-response approximation proposed by Dobson and Dinte.<sup>221</sup>

$$\alpha_{tt'}^{aa'}(iu) = \int w_a(\mathbf{r}) w_{a'}(\mathbf{r}) \bar{\alpha}(\mathbf{r}, i\omega) \nabla R_t(\mathbf{r} - \mathbf{R}_a) \nabla R_{t'}(\mathbf{r} - \mathbf{R}_{a'}) \quad [79]$$

with  $R_t$  a solid harmonic,  $w_a$  an atomic partition function (in this case, the Becke integration weights<sup>222</sup>) and  $\bar{\alpha}$  is the polarization density. For the latter, Sato and Nakai use the approximation proposed by Vydrov and van Voorhis.<sup>223</sup>

$$\bar{\alpha}(\mathbf{r}, i\omega) = \frac{\rho(\mathbf{r})}{\omega_0^2(\mathbf{r}) + \omega^2} \quad [80]$$

$$\omega_0(\mathbf{r}) = \frac{q_0^2(\mathbf{r})}{3} \quad [81]$$

$$q_0(\mathbf{r}) = k_F(1 + \lambda s^2) \quad [82]$$

with  $k_F = (3\pi^2\rho)^{1/3}$  being the Fermi wave-vector and  $s = \nabla\rho/(2k_F\rho)$  being the reduced density gradient.  $\lambda$  is an adjustable parameter that is fit to a training set. The damping of the dispersion interaction occurs via the interaction tensor  $T_{t'u'}^{a'b'}$ , which corresponds to the usual geometric function<sup>220</sup> times a damping factor that depends on the atoms and the angular momenta in  $t$  and  $u$  (the compound  $t$  and  $u$  indices contain  $l_1$  and  $l_2$  respectively):

$$f_{l_1 l_2}^{ab} = \exp \left[ -\frac{l_1 + l_2 - 1}{2} \left( \frac{R_{ab}}{\bar{R}} \right)^{-6} \right] \quad [83]$$

with  $R_{ab}$  the interatomic distance and  $\bar{R}$  is an atomic radius that contains the adjustable parameters.

The method described above is equivalent to calculating the interatomic interaction coefficients as:

$$C_n^{ab} = \frac{1}{2\pi} \sum_{tt'uu'} S_{tu}^{ab} S_{t'u'}^{ab} \int_0^\infty \alpha_{tt'}^{aa'}(i\omega) \alpha_{uu'}^{bb'}(i\omega) d\omega \quad [84]$$

with  $S_{tu}^{ab}$  a geometric factor that depends on the positions of  $a$  and  $b$  and the angular momenta of the interaction. The order  $n$  is determined as the sum of the angular momenta in  $t$ ,  $t'$ ,  $u$ , and  $u'$  plus 2. The atom-atom interaction coefficients and the closely-related intermolecular dispersion coefficients are relatively accurate with errors averaging 6.0% in a test of more than a thousand interaction coefficients.<sup>219</sup>

The LRD functional has been combined with long-range-corrected B88<sup>65</sup> plus the one-parameter progressive (OP) correlation functional<sup>224</sup> (LC-BOP), and variants thereof.<sup>225</sup>

The self-consistent implementation has been developed,<sup>158</sup> and the energies and general performance of the method are essentially unaffected by the relatively minor changes in the electron density distribution caused by the dispersion potential. The three parameters in the LC-BOP-LRD functional were obtained first by fitting to rare-gas atoms,<sup>218,219</sup> then to the S66 database of dimer binding energies.<sup>226</sup> Tests on the S22 give an accuracy of 0.22 kcal/mol (4.6%), where the interactions corresponding to higher-order coefficients are relatively important. The functional has been tested in other benchmark datasets<sup>225</sup> with relative success. To our knowledge, the only software package implementing the LRD dispersion model is GAMESS.<sup>188,189</sup>

*Solid-sphere model.* The solid-sphere model (SSM) by Tao, Perdew and Ruzsinszky<sup>119,227,228</sup> relies on calculating the dynamic polarizabilities (including those of higher-order) using a uniform-density metallic sphere model. The dynamic polarizabilities, and the dispersion coefficients through the Casimir-Polder formula, are non-empirical.

The SSM model was first proposed in the context of correcting the overbinding behavior of GGAs for alkali metals.<sup>227</sup> The authors argue that alkali metals are “soft matter”, and that an adequately-screened dispersion correction is necessary to correct for the incorrect behavior of the GGAs, in agreement with previous work by Rehr, Zaremba and Kohn.<sup>207</sup> The SSM model was subsequently extended to the calculation of the  $C_8$  and  $C_{10}$  coefficients as well.<sup>119,228</sup> Although it has not been transformed into a general-purpose dispersion energy functional, the SSM model has been used successfully in the calculation of fullerene interaction coefficients.<sup>229</sup>

The SSM model is based on the calculation of the  $2^l$ -pole dynamic polarizabilities  $\alpha_l(i\omega)$ . For a metallic sphere of uniform density and radius  $R$ , and assuming a uniform electron gas expression for the dielectric function ( $\varepsilon = 1 + \frac{\omega_p^2}{\omega^2}$ ), this gives:

$$\alpha_l(i\omega) = \left( \frac{\omega_l^2}{\omega_l^2 + \omega^2} \right) R^{2l+1} \quad [85]$$

where  $\omega_l$  is the multipole resonance frequency of the sphere, equal to:

$$\omega_l = \omega_p \sqrt{\frac{l}{2l+1}} \quad [86]$$

with  $\omega_p = \sqrt{4\pi\rho}$  being the plasmon frequency.

Three constraints are imposed on the model: having the correct static polarizability ( $\alpha_l(0)$ ), reproducing the correct high frequency limit ( $\alpha_l(iu) \rightarrow l \int_0^\infty 4\pi r^2 n(r) r^{2l-2} / u^2 dr$ ) and the model must be exact for a metallic sphere of uniform density and radius  $R$ . Under these constraints, the model dynamic polarizability is:

$$\alpha_l(i\omega) = \frac{1}{4\pi a_l} \left( \frac{2l+1}{l} \int \Theta(R_l - r) \frac{lr^{2l-2} a_l^4 \omega_l^2}{a_l^4 \omega_l^2 + \omega^2} dr \right) \quad [87]$$

where  $\Theta$  is a step function and the  $a_l$  and  $R_l$  are obtained by self-consistently solving the equations:

$$R_l = (a_l \alpha_l(0))^{1/(2l+1)} \quad [88]$$

$$a_l = \left[ \frac{\int_0^\infty 4\pi r^2 r^{2l-2} \rho(r) dr}{\int_0^\infty 4\pi r^2 r^{2l-2} \rho(r) dr} \right]^{1/3} \quad [89]$$

with  $\rho(r)$  being the electron density of the system. Interatomic interaction coefficients are reproduced with an accuracy of 3%, similar to XDM for the  $C_6$  coefficients, but significantly better for the higher-order coefficients. The SSM model has been used to calculate the interaction coefficients of nanoparticles and large systems,<sup>228,229</sup> but it has not been coupled with functionals in order to obtain a dispersion energy correction.

*Miscellaneous approaches.* The dispersion correction proposed by Alves de Lima<sup>230</sup> is based on a local approximation to the density response function. The calculation of the dispersion coefficients is based on the generalized Casimir-Polder formula (Eq. 25), with the dynamic polarizabilities calculated as:

$$\alpha_l^A(i\omega) = \int_{V_A} \chi_l^A(i\omega, n) d\mathbf{r}_A \quad [90]$$

where  $V_A$  symbolizes an atomic partitioning (in this model, Hirshfeld), and  $\chi_l$  is the dynamic  $2^l$ -polar susceptibility, which is calculated using a Padé approximant. The model gives good results for the interatomic coefficients of noble gases and alkali metals. We are not aware of any software package that implements this dispersion correction.

In the spherical atom model (SAM) correction, proposed by Austin et al.,<sup>231</sup> the dispersion energy is calculated by assuming that every atomic site has a shell attached that contributes to the dispersion interaction. The SAM is reminiscent of the Drude shell model used to capture polarization in force-field calculations. In the SAM model, the energy is calculated using a modified pairwise contribution:

$$E_{\text{disp}} = - \sum_{A>B} \frac{C_6^{AB} f(R_{AB})g(R_{AB})}{(R_{AB}^2 - R_{s,AB}^2)^3} \quad [91]$$

where  $f$  and  $g$  are two different damping functions and  $C_6^{AB}$  are obtained using London’s formula. The dispersion energy is nullified if the interatomic distance is less than  $R_{s,AB}$ . The functional describes accurately noble gas dimers and small dispersion-bound complexes, although the results are less satisfactory for  $\pi$ - $\pi$  interactions. It is implemented in the Gaussian package.<sup>184</sup>

## Potential-Based Methods

Another approach to tackling the dispersion problem in DFT that differs from pairwise corrections is through the use of atom-centered potentials. The philosophy behind methods of this kind is that the densities in the intermolecular regions associated with noncovalently-interacting systems predicted by conventional DFT methods are not correct, and applying potentials to some or all of the atoms in a system can adjust the density in such a way that noncovalent interactions are better reproduced. The potentials are completely empirical in the sense that they are generated through a fitting procedure for which the goal is to minimize the error in DFT-calculated noncovalent properties relative to a set of reference data. In the next two subsections, we review two atom-centered potential approaches that have been described in the literature. We first discuss the dispersion-correcting potential (DCP) approach, which has been developed for use with computational chemistry programs that employ atom-centered basis sets. The second is the dispersion-corrected atom-centered potential (DCACP) approach, which is a plane-wave-based method.

## Dispersion-Correcting Potentials (DCP)

The notion that the success in modeling noncovalent interactions with DFT methods significantly improves when the leading contribution to the binding energy goes from dispersion to electrostatics<sup>22</sup> drove the initial development of dispersion-correcting potentials (DCPs). These were first developed for the carbon atom with the motivation that most of the problems with dispersion in DFT methods are made obvious in the interactions between hydrocarbon molecules, which interact mainly via dispersion.<sup>232,233</sup> Later efforts extended the library of DCPs to include the H, N, and O atoms,<sup>234,235</sup> and an on-line tool is available to help users build input files containing DCPs.<sup>236</sup> The DCP approach itself is based on a philosophy associated with earlier efforts to develop new approaches to bridging quantum and classical regions in quantum mechanics/molecular mechanics (QM/MM) simulations.<sup>237,238</sup>

DCPs are composed of atom-centered Gaussian-type functions having the same form as effective core potentials (equation 92 below). Effective core potentials are atom centered potentials that are normally used to replace the core electrons during simulations of heavy elements. An example is provided in ref. 239. To efficiently model systems containing atoms with many electrons (such as, for instance, lead), computational advantages are obtained by modeling such atoms using only their valence electrons. Core electrons do not participate directly in chemical bonding, but if the core electrons of an atom were removed, the remaining electrons in the valence space would collapse into the core owing to the strongly attractive Coulomb attraction between the positive nucleus and the negatively-charged electrons. By including a potential in place of the core electrons, the collapse can be prevented and the atoms can be made to behave as though the core electrons were present. This approach not only reduces the computational expense associated with simulating these systems but also has the added advantage of introducing the effects of relativity in the simulation, which is important for obtaining reasonably accurate atomic and molecular properties.<sup>240,241</sup> The effective core potentials are thus developed to reproduce some of the valence properties of the atoms for which they are designed and modify the energy landscape in which valence electrons move through a direct modification of the Hamiltonian of the system.

DCP functions are the same as those used for effective core potentials but they do not replace core electrons. Instead, DCPs modify the potential in which all of the electrons move so that noncovalent interactions are reproduced, as manifested by binding energies and structural properties. The functional form of an effective core potential is:

$$U^{\text{ECP}} = U_{l_{\text{max}}+1}(r) + \sum_{l=0}^{l_{\text{max}}} \sum_{m=-l}^l |Y_{lm}\rangle U_l(r) \langle Y_{lm}| \quad [92]$$

where  $Y_{lm}$  are spherical harmonics that allow for applying potentials to the electron density associated with different angular momenta  $l$  (viz., s-, p-, d-density). In the case of DCPs, there are no limits or requirements associated with equation 92 in terms of the number of functions utilized to build a set of DCPs.

Each  $U_l(r)$  in equation 92 is built from Gaussian-type functions of the form:

$$U_l(r) = r^{-2} \sum_i^{N_l} c_{li} r^{n_{li}} e^{-\zeta_{li} r^2} \quad [93]$$

where  $N_l$  is the number of Gaussian functions,  $n_{li}$  is an integer power of  $r$ ,  $c_{li}$  is the coefficient of the Gaussian and  $\zeta_{li}$  is its exponent.

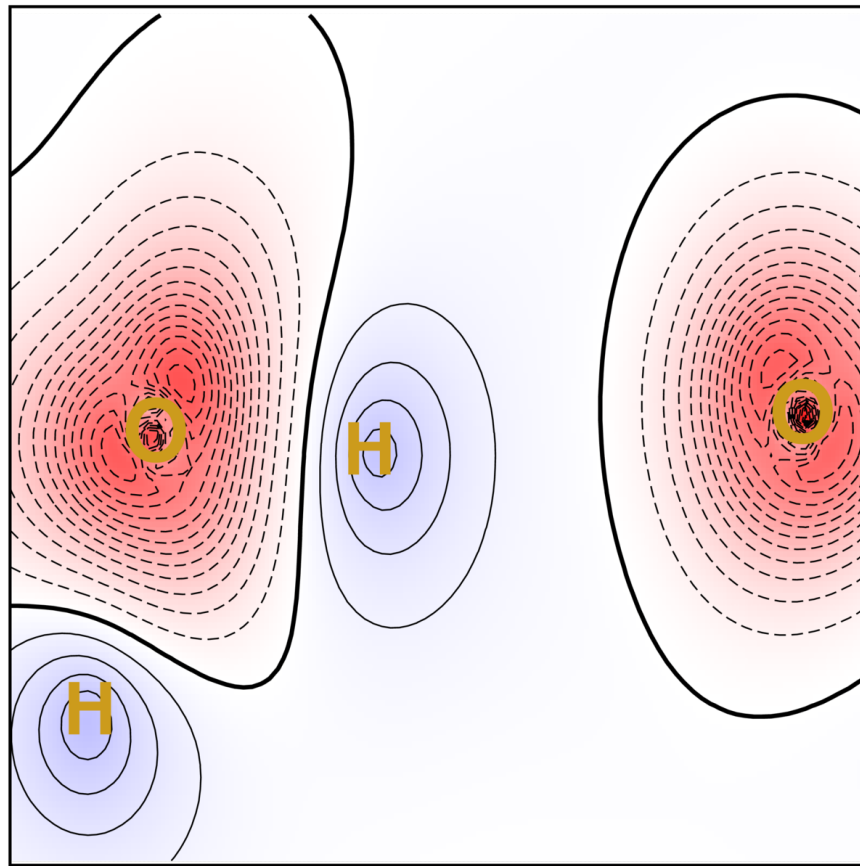


Figure 5. Changes induced by a DCP on calculated electron density of the water dimer (B3LYP-DCP/6-31+G(2d,2p)). The plot shows the contours (in  $5 \times 10^{-5}$  steps, positive contours are full lines, negative contours are dashed lines) as well as a color map (blue is positive, red is negative) resulting from subtracting the non-DCP density from the density obtained in the equivalent calculation using DCPs. The main effect is that the electron density migrates from the oxygen towards the hydrogens and the interstitial space. The thick full line represents the zero-value contour. Colour is available in e-book form only.

DCPs are generally developed for specific atoms by optimizing the exponents and coefficients in equation 93. The values of  $n_{i_i}$  are usually set to 2. In principle, they can take on any integer, although some computational chemistry programs limit these to integer values. The optimizations are performed by minimizing the mean absolute error (MAE) between the binding energies calculated by the DFT method and basis set with the DCPs and those obtained from high-level *ab initio* fitting data. The binding energies for fitting are most often obtained from CCSD(T) calculations with complete-basis-set (CBS) extrapolation and there is a growing body of these data available.<sup>226,242</sup> These fitting data contain one dimensional potential energy surfaces for noncovalently bonded dimers that span the range from just inside the minimum, out to complete dissociation. This is done to ensure that the DCPs are able to reproduce the correct dissociation behavior of noncovalently-bonded systems, though not necessarily the correct  $\frac{1}{r^{-6}}$  behavior in the extremely long-range. Accumulated experience indicates that for most problems of practical interest, obtaining the correct  $\frac{1}{r^{-6}}$  behavior is not required to obtain good performance.



To develop DCPs that perform well for a broad set of systems containing H, C, N, and O atoms, a set of about 16 different noncovalently interacting dimers is required. DCP development follows a bootstrapping approach where the DCPs for carbon and hydrogen are developed together and then used in the generation of DCPs for other atoms such as nitrogen and oxygen. For non-hydrogen atoms, a full set of DCPs will have functions for each angular momentum channel, from s to f. The f-functions operate on all of the electron density in the system and this tends to introduce most of the changes in electron density distribution needed to improve noncovalent properties. Fine adjustments are achieved through the use of the lower angular momentum functions, which affect the distribution associated with s, p, and d electron density. Figure 5 shows the change in electron density upon the application of DCPs to the water dimer.

There are many positive attributes of DCPs. For example, because DCPs have the same expression, they can be employed in the same way as effective core potentials. Many computational chemistry programs allow effective potentials to be specified by the user through the modification of input files and DCPs may also be given in this fashion. Therefore, DCPs can be employed in many computational chemistry packages without the need for reprogramming. Furthermore, since DCPs modify the Hamiltonian associated with the system being modeled, all of the properties are determined self-consistently, meaning that DCPs introduce changes to the energy (or other properties) by altering the electron density. Hence, all of the properties are affected by the presence of the DCPs. Consequently, DCPs can be used with all of the "machinery" of computational chemistry packages, and included in the calculation of properties like solvation energies, NMR chemical shifts, and others.

DCPs can also be used to mitigate, to some extent, the errors associated with basis set incompleteness. The most recently-developed set of DCPs are associated with the B3LYP<sup>234,235</sup> and LC- $\omega$ PBE<sup>243</sup> functionals and 6-31+G(2d,2p) basis sets. DCPs generated from the fitting procedure make up for not only the shortcomings of the underlying functional with respect to noncovalent interactions but also for the errors induced by the reduced size of the basis set. Another positive aspect of DCPs is that they can be designed to incorporate n-body effects simply through the inclusion of the appropriate data in the fitting set. Finally, it is possible to develop DCPs for any DFT method, including those that include other modes of corrections for noncovalent interactions, such as pair-wise schemes or non-local functionals.

One of the most important limitations of the DCP approach is that it is empirical and requires high level *ab initio* and/or experimental data for DCP generation. This means that the development of DCPs for particular atoms may not be possible without first investing heavily in the generation of fitting data. However, unlike pairwise dispersion correction approaches, improvements can be obtained in systems in which only some of the atoms have DCPs applied. Figure 6 demonstrates this feature of DCPs for the potential energy surface of the benzene dimer.

Another drawback of DCPs is that the method is difficult to generalize. Moreover, it is also difficult to understand its mode of action because of the limited theoretical foundation. One possible outcome of this limitation is that DCPs developed to fix one problem may cause another.<sup>235,244</sup> Furthermore, a new set of DCPs is in principle required for every DFT method and basis set combination, just as this is the case for pair-wise dispersion correction techniques. However, in practice, it has been found that the DCPs associated with certain families of density functionals tend to be similar,<sup>233</sup> and the dependence of performance on basis set size is muted for basis sets larger than 6-31+G(d,p). These observations suggest

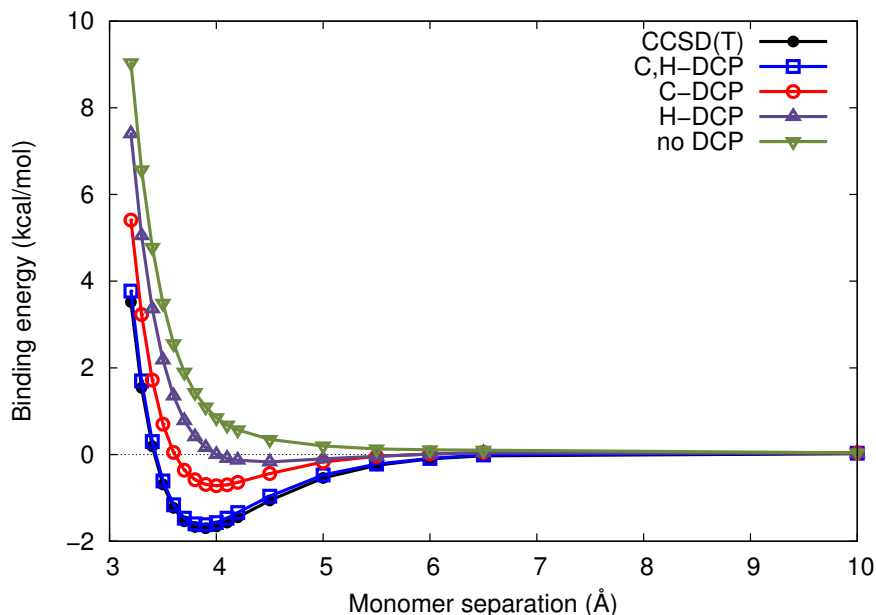


Figure 6. Potential energy curve calculated using LC- $\omega$ PBE/6-31+G(2d,2p) compared to reference data for the stacked benzene dimer. The curves shown include the DCPs for both C and H, only C, only H, and no DCPs. When the DCPs for both atoms are used, the reference curve is accurately reproduced including its long-range behavior.

that some generalizations are possible.

It is also not possible for DCPs to correct for certain underlying deficiencies in particular functionals. For cases in which the underlying DFT method erroneously predicts the energy level of the highest occupied molecular orbital (HOMO) of an electron donor to be too close to the energy level of the lowest unoccupied molecular orbital (LUMO) of an electron acceptor, there will be too much charge transfer and this will result in significant overbinding. This problem stems from the “fractional charge” or “self-interaction”<sup>13,87,245–247</sup> and can occur in molecule-radical complexes<sup>41,248</sup> in addition to molecule-molecule complexes. At this point in time, it appears that DCPs cannot easily correct for self-interaction errors in functionals in which this shortcoming is present. The only reasonable approach is to develop DCPs for DFT methods that are less susceptible to charge transfer problems, i.e. range-separated corrected DFT methods<sup>243</sup> or those with more (ca. 50%) Hartree-Fock exchange.

### *Dispersion-Corrected Atom-Centered Potentials (DCACP)*

The dispersion-corrected atom-centered potential (DCACP) approach is very similar to that for DCPs but was first described several years earlier by von Lilienfeld et al.<sup>249</sup> The corrections are implemented through analytic pseudopotentials of a type similar to those of Goedecker et al.<sup>250,251</sup> DCACPs have the same form as the non-local component of Goedecker pseudopotentials but, like DCPs, do not replace core electrons. Instead, a single high angular momentum function is introduced to existing Goedecker pseudopotentials, and the parameters of this function are optimized to reproduce noncovalent interactions.

The non-local part of the Goedecker pseudopotentials have the form:<sup>249</sup>

$$V_l^{\text{nl}}(\mathbf{r}, \mathbf{r}') = \sum_{m=-l}^{+l} Y_{lm}(\hat{\mathbf{r}}) \sum_{j,h} p_{lh}(r) h_{lhj} p_{lj}(r') Y_{lm}^*(\hat{\mathbf{r}}') \quad [94]$$

where  $Y_{lm}$  are spherical harmonics,  $\hat{\mathbf{r}}$  are unit vectors in the direction of  $\mathbf{r}$ ,  $h_{lhj}$  are adjustable parameters, and

$$p_{lh}(r) \propto r^{l+2(h-1)} \exp^{-r^2/(2r_l^2)} \quad [95]$$

These ECPs have the same form as the effective core potentials described in equation 92. The DCACPs developed in reference 249 and in subsequent work<sup>252</sup> use a single high angular momentum function of this type. This simplifies Eq. 94 to a potential with a proportionality:

$$V_l \propto r^{-2} \sum \sigma_1 \exp -\frac{r^2}{2\sigma_2^2} \quad [96]$$

Again, the form of Eq. 96 is similar to that of equation 93. For the DCACPs, values of the  $\sigma_1$  and  $\sigma_2$  parameters are optimized by minimizing the errors in calculated binding energies and forces in a very small set of reference systems. For example, for hydrogen and carbon, only the parallel  $(\text{H}_2)_2$  and the stacked benzene dimers, respectively, were used as reference systems.<sup>252</sup> Recently, Jordan’s group found that DCACPs containing two functions offer much better performance than the single function approach.<sup>253</sup>

The advantages of DCAPCs are analogous to those of DCPs. For example, DCACPs can be used with plane wave computational packages without the need for reprogramming and are able to take advantage of the full machinery of such packages, including *ab initio* molecular dynamics. They can also be developed for any functional, including those that incorporate other modes of dispersion corrections. However, not all functionals, in particular those that contain Hartree-Fock exchange, are efficiently implemented in all plane wave programs. DCACPs can also be designed to include n-body effects. A unique advantage associated with the use of DCACPs is that is that plane wave basis sets are effectively complete, obviating the problem of basis set deficiency.

The drawbacks to the DCACP approach also mirror those of DCPs. The DCACP approach is empirical and requires high level *ab initio* and/or experimental data in order to generate the potentials. That said, von Lilienfeld et al. used only a very small fitting set (one per atom type) to generate a seemingly highly transferable set of DCACPs.<sup>249,252</sup> This drawback is further mitigated by the fact that it is highly likely that incremental improvements in the treatment of noncovalent interactions can be achieved by applying DCACPs to a subset of atoms in a system of interest, although this has not, to our knowledge, been demonstrated explicitly. In addition, and like DCPs, new DCACPs need to be developed for each density functional.

## Minnesota Functionals

The Minnesota family are a collection of functionals proposed by Truhlar and collaborators. These functionals employ a heavily-parametrized functional form in order to model, on the same footing, diverse types of problems, including barrier heights (chemical kinetics), metal-ligand and metal-metal bond dissociation, main-group thermochemistry and noncovalent interactions. The design procedure of all Minnesota functionals is similar. First,

a functional form with a large number of parameters is adopted, possibly fixing some of the parameters by applying some physical constraints (like the correct uniform electron gas behavior). A training database is then constructed using high-level reference data and, associated to it, a cost function is proposed by mixing the root mean square errors from each of the component subsets of the database. Finally, the parameters in the functional are determined by minimization of the cost function. The functionals are routinely tested on a dataset larger than the training database for consistency.

The Minnesota functional family contains twelve members, that are labeled by the year of publication. In chronological order, they are: M05,<sup>254</sup> M05-2X,<sup>255</sup> M06-L,<sup>97</sup> M06-HF,<sup>256</sup> M06,<sup>257</sup> M08,<sup>258</sup> SOGGA11,<sup>259</sup> M11,<sup>260</sup> M11-L,<sup>261</sup> MN12-L,<sup>71</sup> N12,<sup>72</sup> N12-SX,<sup>73</sup> and MN12-SX.<sup>73</sup> All of these (except M05) contain noncovalent interactions in the training set. Although the performance of some of the functionals for noncovalent interactions is better than that of other base functionals, only M06-2X performs with reasonable accuracy in standard noncovalent interactions tests (see the section below titled “Performance of Dispersion-Corrected Methods”).

The first functional in the Minnesota family is M05,<sup>254</sup> a hybrid with 28% exact exchange. The semilocal exchange functional is a meta-GGA based on PBE exchange:

$$E_x^{\text{semilocal}} = \sum_{\sigma} \int \varepsilon_{x\sigma}^{\text{PBE}} \left( \sum_{i=0}^m a_i w_{\sigma}^i \right) d\mathbf{r} \quad [97]$$

where  $\varepsilon_{x\sigma}^{\text{PBE}}$  is the PBE exchange energy density for spin  $\sigma$ , and  $w_{\sigma}$  is Becke’s measure of the exchange-hole non-locality:<sup>262</sup>

$$w_{\sigma} = \frac{t_{\sigma} - 1}{t_{\sigma} + 1} \quad [98]$$

with  $t_{\sigma} = \tau^{\text{LDA}}/\tau^{\text{exact}}$  being the ratio between the LDA and Kohn-Sham kinetic energy densities. The  $a_i$  are adjustable parameters with  $a_0 = 1$  to recover the correct uniform electron gas limit and  $m = 11$ . The correlation functional is based on the  $\tau\text{HCTH}$ <sup>263</sup> and the BMK<sup>264</sup> functionals but using the self-interaction correlation correction proposed by Becke in the B95 functional.<sup>195,265</sup> The correlation functional contains another 10 adjustable parameters, two of which are independently fitted to atomic reference data for the noble gases. The functional form of M05 (and some of the subsequent functionals) is designed so as to preserve the correct behavior in the uniform electron gas limit.

The key in the performance of the Minnesota functionals is the parameter fitting to an extensive set of reference data. In the case of M05, the data set employed comprises 35 data points including atomization energies, ionization potentials, electron affinities, barrier heights, total energies of atoms, bond dissociation energies and noncovalent binding energies. The 20 parameters (including the fraction of exact exchange) are optimized by minimizing a target function that mixes the root mean square deviations of the different sets using a genetic algorithm. The functional was subsequently tested, with relatively satisfactory results, in a larger set containing 231 data points.

The M05-2X functional,<sup>255</sup> proposed shortly after M05, approximately doubles the amount of exact exchange in M05 (56%), hence the name. The functional form is the same as M05, but the training set used in the determination of the parameters is different, and does not include metallic systems. As a result, M05-2X improves the treatment of thermochemistry, kinetics and noncovalent interactions by sacrificing the good performance in metallic systems. The M05 and M05-2X functionals have also been tested for interactions

in noble gas dimers, group 2 dimers, the Zn dimer and Zn-rare gas dimers.<sup>266</sup> In general, they outperform other non-dispersion-corrected functionals for those systems.

The M06-L functional<sup>97</sup> is a pure meta-GGA functional (no exact exchange). It is the basis of the M06 suite of functionals. The exchange functional is more involved than in the M05 family, and includes a contribution based on the van Voorhis and Scuseria functional.<sup>267</sup>

$$E_x^{\text{semilocal}} = \sum_{\sigma} \int \left[ \varepsilon_{x\sigma}^{\text{PBE}} \left( \sum_{i=0}^m a_i w_{\sigma}^i \right) + \varepsilon_{x\sigma}^{\text{LDA}} h_x(x_{\sigma}, z_{\sigma}) \right] d\mathbf{r} \quad [99]$$

where the additional term not present in M05 (Eq. 97) contains the LDA exchange energy density and a function that depends on the dimensionless density gradient ( $x_{\sigma} = \nabla\rho_{\sigma}/\rho_{\sigma}^{4/3}$ ) and on the variable  $z_{\sigma} = \tau_{\sigma}/\rho_{\sigma}^{5/3} - 3/5(6\pi^2)^{2/3}$ . The expression for  $h_x$  is:

$$h_x(x_{\sigma}, z_{\sigma}) = \left( \frac{d_0}{\gamma(x_{\sigma}, z_{\sigma})} + \frac{d_1 x_{\sigma}^2 + d_2 z_{\sigma}}{\gamma^2(x_{\sigma}, z_{\sigma})} + \frac{d_3 x_{\sigma}^4 + d_4 x_{\sigma}^2 z_{\sigma}}{\gamma^3(x_{\sigma}, z_{\sigma})} \right) \quad [100]$$

with  $\gamma(x, z) = 1 + \alpha(x^2 + z)$ , and  $\alpha$  is a parameter that is different depending on whether  $\gamma$  appears in the exchange or in the correlation functionals. The values for the different  $\alpha$  parameters are taken from previous works.<sup>267</sup> The correlation functional in M06-L is similarly based on M05 but augmented with terms coming from the work of van Voorhis and Scuseria.<sup>267</sup>

In its definition, M06-L contains 32 parameters distributed within different parts of the exchange and correlation functionals. As in M05, the parameters are fitted to a training set by defining a cost function in terms of the weighed root mean square deviations on the different sets. The data sets include atomization energies, ionization potentials, electron affinities, proton affinities, barrier heights, noncovalent interactions, transition metal ligand removal energies, alkyl bond dissociations, isomeric reactions and proton affinities between unsaturated hydrocarbons, excitation energies, bond lengths and bond frequencies. The training set contains 314 data points and the optimization is carried out under constraints to preserve the physical soundness of some parameters and the correct behavior at the uniform gas limit. M06-L performs better than other semilocal functionals or even hybrids in standard thermochemical and kinetics tests (with the possible exception of  $\pi$ -system proton affinities and electron affinities). Being a pure meta-GGA it also presents the advantage of being more computationally efficient than any hybrid functional, and the possibility of implementation in plane wave codes for condensed matter applications.

The closely-related M06-HF functional<sup>256</sup> contains a full (100%) exact exchange contribution plus a term equal to the M06 exchange-correlation energy but with different fitted parameters. The functional is designed for the calculation of excitation energies using TDDFT. The parametrization includes data sets of noncovalently-bound systems, but the results for ground-state properties, including noncovalent binding energies, are, in general, worse than M05-2X.

Zhao and Truhlar subsequently used the same functional form as in M06-L and a greatly enlarged training database to define a hybrid with 27% exact exchange (M06) and a hybrid with double the amount of exact exchange (54%, M06-2X).<sup>257</sup> As in the case of M05 and M05-2X, the former is recommended by the authors for all applications including main-group thermochemistry, kinetics, transition metal chemistry, and noncovalent interactions, whereas the 2X version is not appropriate for organometallic applications.

Because this chapter is about noncovalent interactions, a digression is necessary at this point. All the functionals above have been fitted to noncovalent interactions, but no measure of the applicability of these has been given. For comparison, in ref. 257, the (balanced) mean average errors in the S22 set (see the section titled “Description of Noncovalent Interaction Benchmarks”) using the average of the counterpoise and non-counterpoise-corrected results are 0.47 (M06-2X), 0.71 (M06-HF), 0.75 (M05-2X), 0.77 (M06-2L), 0.85 (M06), and 1.83 (M05) kcal/mol. These results are much better than those obtained using other non-dispersion corrected, less-parametrized density-functionals (see the end of the benchmarks section below), but the performance is not as good as that of other dispersion-corrected functionals using D3, XDM, DCPs or most of the other dispersion corrections (described in the section titled “Performance of Dispersion-Corrected Methods”). Of the Minnesota family, M06-2X, with 0.47 kcal/mol error on average for the S22 set, displays the best performance for noncovalent interactions.

For completeness, the remaining functionals in the Minnesota family are:

- The somewhat less-popular M08-HX and M08-SO functionals.<sup>258</sup> The authors’ motivation was to “improve” the functional expression in the M06 family by increasing its flexibility, resulting in two functionals that depend on 44 parameters each. The M08 functionals are meta-GGA hybrids, where the semilocal exchange is written as:

$$E_x^{\text{semilocal}} = \int \varepsilon_x^{\text{LDA}} (f_1(w)F_x^{\text{PBE}} + f_2(w)F_x^{\text{RPBE}}) d\mathbf{r} \quad [101]$$

with  $\varepsilon_x^{\text{LDA}}$  the LDA exchange energy density,  $F_x^{\text{PBE}}$  the PBE enhancement factor<sup>60</sup> and  $F_x^{\text{RPBE}}$  the RPBE enhancement factor.<sup>268</sup> For the correlation functional,

$$E_c = \int (\varepsilon_c^{\text{LDA}} f_3(w) + H_c^{\text{PBE}} f_4(w)) d\mathbf{r} \quad [102]$$

where  $\varepsilon_c^{\text{LDA}}$  is the LDA correlation energy and  $H_c^{\text{PBE}}$  the gradient correction to correlation from the PBE functional.<sup>60</sup> The  $f_n$  factors are 11-degree polynomials in  $w$ , which depends on the kinetic energy density (Eq. 98).

The difference between M08-HX and M08-SO is in the constraints imposed on the parameters. For the former, the correct behavior in the uniform electron gas limit is imposed, whereas the latter presents the correct behavior to second-order in the reduced-density gradient expansion (proportional to  $s^2$ ) when  $s \rightarrow 0$ . The functionals are fitted using the same procedure as for the other Minnesota functionals, that is, designating a cost function and minimizing it against a very extensive training set. The resulting functionals are hybrids with about 50% exchange (52.23% for M08-HX and 56.79% for M08-SO) that improve slightly on the previous M06 functionals, except for transition metals and systems with multireference character.

- The SOGGA11<sup>259</sup> functional is a semilocal GGA, with parametrized enhancement factors for exchange and correlation (10 parameters each, 20 parameters in total). The SOGGA11 functional is fitted to a training data set and it preserves the correct uniform electron gas limit and the exchange enhancement factor has the correct  $s^2$  behavior in the  $s \rightarrow 0$  limit. However, the enhancement factors for non-zero  $s$  are fluctuating, which is a result of oscillatory parameters coming from the fit (the same effect is observed in the other Minnesota functionals of the pure GGA variety).

- The M11<sup>260</sup> functional is the first range-separated hybrid functional in the Minnesota set. M11 has 42.8% exact-exchange hybrid at short range and 100% at long range, with a range-separation parameter of 0.25 (both the amount of exact exchange and the range-separation parameter are chosen to minimize the mean absolute error in the dataset). The functional form of M11 is similar to M08. The semilocal part of the short-range exchange functional being the same as in M08 (Eq. 101), except in that the range-separation enters the LDA exchange energy density according using the expressions of Chai and Head-Gordon.<sup>90</sup> The correlation functional is exactly the same as in M08. After application of some constraints on the parameter—uniform electron gas limit, quadratic coefficient of the reduced-density gradient expansion, and independence of the kinetic energy density in the bond saddle points and density tails—the resulting functional has 38 coefficients that are obtained by the usual minimization procedure employing a large training set.
- The closely-related M11L functional uses the same range-separated approach and the same functional form as M11, but it replaces exact exchange by a different semilocal functional for the long range exchange. M11L is, therefore, also semilocal. The long-range exchange functional has the same expression as short-range M11 exchange, but the short-range LDA exchange energy density is replaced by its long-range counterpart. This functional is intended to be used in solid-state calculations under plane waves and, as a consequence, is parametrized using a collection of lattice constants of simple solids in the training set.
- The N12 functional<sup>72</sup> is the basis for the latest series in the Minnesota family of functionals. N12 drops all previous constraints on the exchange-correlation functional (including the uniform electron gas limit and the spin-scaling relations for exchange) and gives the exchange energy as:

$$E_{\text{nxc}} = \sum_{\sigma} \int \left[ \varepsilon_{x\sigma}^{\text{LDA}} \sum_{i=0}^m \sum_{j=0}^{m'} a_{ij} u_{x\sigma}^i v_{x\sigma}^j \right] \quad [103]$$

where  $a_{ij}$  are adjustable parameters and the  $u$  and  $v$  variables are defined as in the B97<sup>195</sup> and the Liu-Parr functional<sup>269</sup> respectively:

$$u_{x\sigma} = \frac{\gamma_{x\sigma} x_{\sigma}^2}{1 + \gamma_{x\sigma} x_{\sigma}^2} \quad [104]$$

$$v_{x\sigma} = \frac{\omega_{x\sigma} \rho_{\sigma}^{1/3}}{1 + \omega_{x\sigma} \rho_{\sigma}^{1/3}} \quad [105]$$

where  $\gamma$  and  $\omega$  are parameters and  $x_{\sigma} = \nabla \rho_{\sigma} / \rho_{\sigma}^{4/3}$  is the dimensionless density gradient. The exchange functional is labeled “nxc” because, since it does not obey the usual exchange spin-scaling relations, the authors argue that it is also accounting for correlation. The correlation functional in N12 has a functional form similar to exchange, with a Taylor expansion in  $u$  as a factor of the uniform electron gas correlation energy density. The resulting N12 functional is a pure GGA and the intent of the authors is to provide a GGA that gives good structures (lattice constants, bond lengths) and energetics (atomization energies, cohesive energies) in both molecules and periodic solids.

- The exact exchange expression in equation 103 was extended by employing the variable  $w$  that depends on the kinetic energy density (Eq. 98). The resulting functional (MN12-L) is a semilocal meta-GGA with the exchange energy being:

$$E_{\text{nxc}} = \sum_{\sigma} \int \left[ \varepsilon_{x\sigma}^{\text{LDA}} \sum_{i=0}^3 \sum_{j=0}^{3-i} \sum_{k=0}^{5-i-j} a_{ijk} u_{x\sigma}^i v_{x\sigma}^j w_{x\sigma}^k \right] \quad [106]$$

The correlation functional is the same as in N12. This functional provides a small improvement over the older M11-L.

- The two last functionals in the Minnesota family are N12-SX and MN12-SX, proposed recently by Peverati and Truhlar.<sup>73</sup> These functionals are based on N12 and MN12-L respectively, but use a range-separated approach with short-range exact exchange (similar to the HSE functionals<sup>91,92</sup>). At long range, the two functionals have 25% exact exchange and the range separation parameter is  $\omega = 0.11$  in both cases.

Among the advantages of the Minnesota functionals is their widespread implementation in most popular software packages, including Gaussian,<sup>184</sup> GAMESS,<sup>188,189</sup> and NWChem.<sup>190</sup> The M06-L semilocal functional is also implemented in VASP<sup>191,192</sup> and Quantum ESPRESSO<sup>185</sup> for calculations in periodic solids using plane waves. Their popularity is justified by their good performance (relative to other less-parametrized functionals) in dealing with thermochemical and kinetics problems. Regarding noncovalent interactions, however, one should be aware that the only functional in the family that competes with the other methods presented in this chapter is M06-2X and, even then, this functional has particular disadvantages of its own.

Figure 7 illustrates clearly some of the problems with the Minnesota functionals. The figure represents a potential energy surface of the parallel naphthalene dimer. All Minnesota functionals (including M06-2X) are strongly underestimating the binding energy. In addition, the potential energy surface is uneven with multiple spurious minima precluding the use of these functionals anywhere except at the equilibrium geometry. The roughness of the potential is smaller in M06-2X but the functional is underestimating the correct binding energy by 2 kcal/mol (approximately 50% error). Another spurious feature of the Minnesota potential energy curves for the naphthalene dimer is that they display repulsive behaviour at large monomer separations. Not only do the Minnesota functionals have the incorrect long-range behavior, but they are repulsive except at geometries close to equilibrium. The difficulties of the Minnesota functionals away from equilibrium have been noted by other authors.<sup>111,270</sup> Sensitivity to the integration grid has also been reported.<sup>111</sup>

All Minnesota functionals except M06-2X are also extremely sensitive to basis-set incompleteness errors in the calculation of noncovalent interactions (see the section titled “Performance of Dispersion-Corrected Methods” and Table III). The table shows that the sensitivity is lower in M06-2X, N12, and N12SX, for which it is similar to other density functionals but, for the remaining members in the family, the counterpoise correction has a non-negligible effect, even for a basis set as large as aug-cc-pVQZ (or aug-cc-pV5Z in the case of M06-L).

In addition, noncovalent binding in these functionals arises not from a physically-justified model, but from parameter fitting to a database that includes noncovalently bound dimers and also other systems. Dispersion in the Minnesota functionals is partially accounted for by adjusting a semilocal functional (a method that is similar to using dispersion-correcting



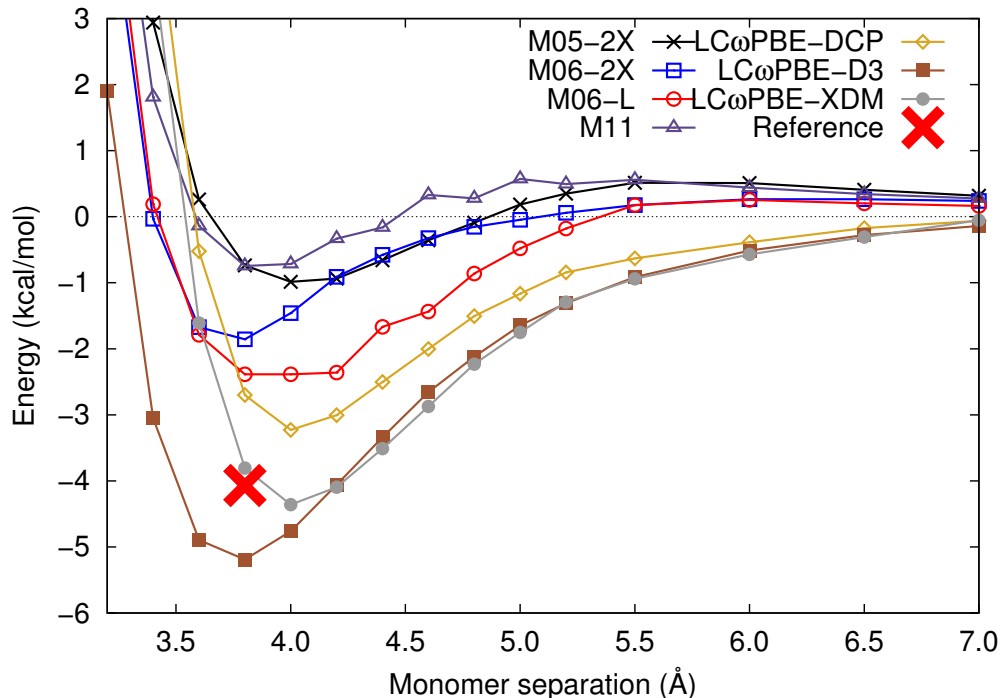


Figure 7. Potential energy curves for the parallel naphthalene dimer, calculated using different dispersion-corrected methods: XDM, one functional corrected with DCPs, DFT-D3 (using Becke-Johnson damping), and four Minnesota functionals, including M06-2X. The calculations were run using aug-cc-pVTZ and a pruned grid with 99 radial and 590 angular (Lebedev) points (the “ultrafine” setting in Gaussian09<sup>184</sup>). The reference value comes from ref. 176.

TABLE III. Mean Absolute Errors (MAE) with (CP) and without (no CP) Counterpoise Corrections for Different Minnesota Functionals and Basis Sets (aNZ = aug-cc-pVNZ).

Functional	Basis set	MAE (CP)	MAE (no CP)	Factor <sup>a</sup>
M06	aQZ	0.79	0.44	1.79
M06-2X	aQZ	0.28	0.23	1.23
M06-HF	aQZ	0.83	0.49	1.70
M06-L	aTZ	0.73	0.28	2.62
M06-L <sup>b</sup>	aQZ	0.90	0.51	1.77
M06-L <sup>b</sup>	a5Z	0.84	0.49	1.73
M11	aQZ	0.79	0.44	1.79
M11L	aQZ	1.37	0.67	2.05
MN12SX	aQZ	1.18	0.67	1.75
N12	aQZ	3.87	3.72	1.04
N12SX	aQZ	2.10	1.97	1.07

<sup>a</sup> Quotient between both MAEs.

<sup>b</sup> SCF convergence problems were found for 2 dimers in M06-L/aug-cc-pVQZ and for 21 dimers in M06-L/aug-cc-pV5Z. The MAEs for those have been calculated using a reduced set.

potentials, described earlier), which is by design unable to describe long-range intermolecular interactions such as dispersion. As a consequence, and in contrast to other dispersion-including methods, dispersion-related binding arises from a semilocal description of the electron density in the intermolecular region. Molecules behave as if they are “sticking” to each other, but the interaction decays quickly when separating the molecules as the electron density becomes the same as in the non-interacting monomers. These observations may explain the sensitivity of the Minnesota functionals to the grid and the basis set, since the representation of the intermolecular regions is done by atom-centered Gaussians.

## Non-Local Functionals

The use of non-local dispersion functionals is an approach that is better rooted in traditional density functional theory development than the functionals described earlier. Non-local functionals model the dispersion energy contribution arising from electron density fluctuations in distant parts of a system by explicitly taking into account the effects those distant regions have on one another. The non-local correlation contribution is:

$$E_c^{\text{nl}} = \frac{1}{2} \int \int \phi(\mathbf{r}, \mathbf{r}') \rho(\mathbf{r}) \rho(\mathbf{r}') d\mathbf{r} d\mathbf{r}' \quad [107]$$

where  $\phi(\mathbf{r}, \mathbf{r}')$  is the correlation kernel. Conceptually, non-local functionals calculate the same dispersion attraction as the simpler pairwise approaches, but they do so without using an asymptotic expression. Non-local functionals are “seamless”, meaning that the correlation energy defined in Eq. 107 is added to the rest of the functional without the need of specifying fragments or using an atomic partition, as is the case in the pairwise approach. In addition, and unlike similar approaches like RPA, all non-local functionals depend only on the density and its derivatives and not on the orbitals (neither occupied nor virtual). Non-local functionals are usually designed with little or no empiricism.

Early studies that were fundamental in the development of non-local functionals for dispersion are those of Zaremba and Kohn<sup>271</sup> and of Rapcewicz and Ashcroft.<sup>272</sup> In the limit of separated (non-overlapping) fragments, the second-order perturbation theory expression for the dispersion interaction is:<sup>271</sup>

$$E_{\text{disp}} = -\frac{1}{2\pi} \int \frac{\chi(\mathbf{r}_1, \mathbf{r}'_1, i\omega) \chi(\mathbf{r}_2, \mathbf{r}'_2, i\omega)}{r_{12} r'_{12}} d\mathbf{r}_1 d\mathbf{r}_2 d\mathbf{r}'_1 d\mathbf{r}'_2 d\omega \quad [108]$$

where the integration over  $\mathbf{r}_1$  is restricted to the first fragment and  $\mathbf{r}_2$  to the second. The  $\chi$  functions are the density-density response functions<sup>273</sup> (usually simply response functions or electric susceptibilities) defined as the linear response of the electron density with respect to a perturbation in the external potential with frequency  $\omega$ :

$$\delta\rho(\mathbf{r}, \omega) = \int \chi(\mathbf{r}, \mathbf{r}', i\omega) \delta V^{\text{ext}}(\mathbf{r}', \omega) d\mathbf{r}' \quad [109]$$

These quantities are central to the current section and are related to the dynamic polarizabilities (see “Pairwise Dispersion Corrections” above) by:<sup>152,273</sup>

$$\alpha_{ij}(i\omega) = \int \mathbf{r}_i \mathbf{r}'_j \chi(\mathbf{r}, \mathbf{r}', i\omega) d\mathbf{r} d\mathbf{r}' \quad [110]$$

where  $i$  and  $j$  are the components of the polarizability tensor. Likewise, they can be used to rewrite the adiabatic connection formula (Eq. 17):

$$E_c = \frac{-1}{2\pi} \int_0^1 d\lambda \int d\mathbf{r} d\mathbf{r}' \frac{1}{|\mathbf{r} - \mathbf{r}'|} \int_0^\infty d\omega \left[ \chi_\lambda(\mathbf{r}, \mathbf{r}', i\omega) - \chi_0(\mathbf{r}, \mathbf{r}', i\omega) \right] \quad [111]$$

where  $\chi_0$  is the response function for the non-interacting system that has an analytical expression in the Kohn-Sham scheme:

$$\chi_0(\mathbf{r}, \mathbf{r}', i\omega) = -4 \sum_i^{\text{occ}} \sum_a^{\text{unocc}} \frac{\varepsilon_{ai}}{\varepsilon_{ai}^2 + \omega^2} \psi_i(\mathbf{r}) \psi_a(\mathbf{r}) \psi_a(\mathbf{r}') \psi_i(\mathbf{r}') \quad [112]$$

with  $i$  running over occupied and  $a$  over unoccupied orbitals, and  $\varepsilon$  represents the orbital energy differences.

The seminal works upon which non-local dispersion functionals rest are the original functionals of Dobson and Dinte (DD)<sup>221</sup> and Andersson, Langreth and Lundqvist (ALL),<sup>274</sup> which have the same expression and were published independently in 1996. The DD/ALL functional is a variant of the Rapcewicz-Ashcroft functional that uses the density response function of the uniform electron gas:

$$\chi(\omega) = \frac{1}{4\pi} \left[ 1 - \frac{1}{\varepsilon(\omega)} \right] = \frac{1}{4\pi} \frac{\omega_p^2}{\omega_p^2 - \omega^2} \quad [113]$$

where  $\varepsilon(\omega) = 1 - \omega_p^2/\omega^2$  is the dielectric function and  $\omega_p = \sqrt{4\pi\rho}$  is the plasma frequency of the uniform electron gas with density  $\rho$ . By using the local approximation to the plasma frequency ( $\omega_p(\mathbf{r}) = \sqrt{4\pi\rho(\mathbf{r})}$ ), the resulting dispersion energy is:

$$E_{\text{disp}} = -\frac{3}{32\pi^2} \int \frac{1}{r_{12}^6} \frac{\omega_p(\mathbf{r})\omega_p(\mathbf{r}')}{\omega_p(\mathbf{r}) + \omega_p(\mathbf{r}')} d\mathbf{r} d\mathbf{r}' \quad [114]$$

where  $\omega_p$  is the local plasma frequency. This functional requires that the interacting systems are non-overlapping. The dynamical polarizabilities and the dispersion interaction coefficients can be calculated in the same fashion.<sup>274</sup> Note the resemblance between equation 114 and London's formula (Eq. 22).

Langreth's group subsequently proposed variations of this functional for different systems, including the study of the interaction between parallel infinite jellium surfaces,<sup>275</sup> a non-overlapping formulation with a cutoff to account for overlaps,<sup>276</sup> and a functional for layered structures.<sup>277</sup> However, the first truly geometry-independent functional is vdw-DF, proposed in 2004 by Dion et al.<sup>278,279</sup>

In vdw-DF, the correlation energy is written as the sum of a semilocal part, represented by LDA correlation, and a long-range non-local energy according to equation 107.

$$E_c = E_c^{\text{sr}} + E_c^{\text{nl}} \quad [115]$$

The key to a "seamless" functional is that the non-local part of the correlation energy vanishes for the uniform electron gas, therefore allowing the treatment of long-range and short-range interactions on the same footing and preventing double counting of correlation effects. The vdw-DF functional makes approximations to the adiabatic connection formula (equation 111) based on a second-order expansion of the  $S = 1 - \varepsilon^{-1}$  variable ( $\varepsilon$  being the

dielectric function) and a plasmon pole approximation to the plane wave representation of  $S$ . By virtue of those approximations, the adiabatic connection formula can be integrated in the coupling constant. After some algebra the kernel in equation 107 is written as a function of two variables  $d$  and  $d'$  that depend only on the distance between  $\mathbf{r}$  and  $\mathbf{r}'$  and on the electron density and its gradient at those points. Their expressions are:

$$d = |\mathbf{r} - \mathbf{r}'|q_0(\mathbf{r}) \quad [116]$$

$$d' = |\mathbf{r} - \mathbf{r}'|q_0(\mathbf{r}') \quad [117]$$

with:

$$q_0(\mathbf{r}) = -\frac{4\pi}{3} (\varepsilon_c^{\text{LDA}}(\mathbf{r}) + \varepsilon_x^{\text{LDA}}(\mathbf{r})[1 + \lambda s(\mathbf{r})^2]) \quad [118]$$

involving the LDA exchange and correlation energy densities, the reduced density gradient:

$$s = \frac{\nabla\rho}{2(3\pi^2)^{1/3}\rho^{4/3}} \quad [119]$$

and the parameter  $\lambda = 0.8491/9$  that controls the relative importance of the gradient correction. The expression of the kernel  $\phi(d, d')$  is complicated, involving a double integral, but the existence of the intermediate  $d$  variables allow a pre-computation of a lookup table for  $\phi$ , which is used to interpolate its values and derivatives in the actual SCF calculation.

The vdw-DF functional has been implemented self-consistently in the plane wave approach by Thonhauser et al.<sup>156</sup> and for Gaussian basis sets by Vydrov et al.<sup>280</sup> Likewise, the analytic energy gradients that are required for geometry optimizations have been implemented in both cases. The computational cost of evaluating the non-local correlation energy is the bottleneck if a semilocal exchange functional is chosen, but it is not more expensive than calculating the exact exchange energy contribution in a hybrid or range-separated hybrid.<sup>270,280</sup> Efficient implementations in the particular case of plane wave basis sets have been proposed as well.<sup>281</sup>

The primary target for the vdw-DF functional are systems with extensive electron-electron delocalization such as metal surfaces, physisorption, interactions with graphene, etc. A review of some applications has been published by Langreth et al.<sup>282</sup> In the case of molecular interactions at equilibrium, however, the functional is plagued by problems coming from spurious binding caused by the semilocal exchange and correlation components.<sup>223</sup> In the original implementation, the authors used the revPBE functional.<sup>61</sup> Several other options for the exchange functional have been explored by other authors.<sup>283</sup> For comparison, the mean average error of vdw-DF on the S22 is 1.44 kcal/mol with revPBE,<sup>284</sup> 1.03 kcal/mol with revised PW86,<sup>284</sup> and 0.23 kcal/mol with a specifically-adapted version of the B88 functional called opt-B88.<sup>283</sup> In addition, vdw-DF has a tendency to overestimate molecular separations and to underestimate the strength of hydrogen bonds.<sup>223,285</sup>

To address some of the problems in vdw-DF, and with an eye on molecular interactions in the overlapping regime, Lee et al. proposed an improved functional, vdw-DF2.<sup>285</sup> The authors replaced the over-repulsive revPBE functional with a revised version of the PW86 functional.<sup>285,286</sup> In addition, the coefficient in the internal coefficient controlling the gradient correction to LDA in equation 118 was modified using the known behavior in the limit of large number of electrons.<sup>287</sup> Lee et al. report an improvement in the mean average error obtained in the S22 using vdw-DF2: 0.51 kcal/mol. The improvement is also evident in the calculation of lattice energies and geometries of molecular crystals.<sup>178</sup> The vdw-DF family of functionals,

and particularly vdw-DF2, are in widespread use today in the physics community and are implemented in popular solid-state codes like Quantum ESPRESSO<sup>185</sup> and VASP.<sup>191,192</sup> To our knowledge, only Q-Chem<sup>186</sup> implements these functionals for gas-phase calculations. The vdw-DF can also be evaluated using the external program noloco.<sup>288</sup>

Based on the poor performance of the original vdw-DF for noncovalently bound molecular systems in gas phase, Vydrov and van Voorhis (VV) proposed a series of modifications, including the VV09<sup>289-291</sup> and the VV10 functionals.<sup>292</sup> VV noted the aforementioned problems in the vdw-DF functional and its inability to couple with either Hartree-Fock exchange or with long-range corrected functionals. The VV family of functionals introduces a reduced number of adjustable parameters (one or two) and violates some conservation laws enforced in the functionals by Langreth et al.<sup>290,291</sup> but the results are greatly improved for molecular systems thanks to the additional flexibility. In particular, VV09 includes one adjustable parameter that is fitted to reproduce atomic  $C_6$  values, which are known to be in severe error when calculated using the vdw-DF functionals (particularly vdw-DF2 with errors slightly over 60%).<sup>293</sup> In addition, VV is formulated for spin-polarized (open-shell) systems and the kernel in equation 107 is analytic rather than numerical. For the S22, rPW86-VV09 gives a MAE of 1.20 kcal/mol<sup>284</sup> with LDA correlation contributing appreciably to the binding.<sup>284</sup>

VV10 is the simplest and most accurate functional<sup>292</sup> in the family. In VV10, the exchange functional can either be revised PW86 (rPW86)<sup>285,286</sup> or LC- $\omega$ PBE with  $\omega = 0.45$ . The former is termed simply VV10 (parameters  $C = 0.0093$  and  $b = 5.9$ , see below) and the second is LC-VV10 ( $C = 0.0089$  and  $b = 6.3$ ). The semilocal correlation functional is PBE correlation in both of them. The non-local correlation energy in VV10 is written as in equation 107. The correlation kernel is proposed *ad hoc* based on the authors' experience:

$$\phi(\mathbf{r}, \mathbf{r}') = -\frac{3}{2gg'(g+g')} \quad [120]$$

with

$$g = \omega_0(\mathbf{r})|\mathbf{r} - \mathbf{r}'|^2 + \kappa(\mathbf{r}) \quad ; \quad g' = \omega_0(\mathbf{r}')|\mathbf{r} - \mathbf{r}'|^2 + \kappa(\mathbf{r}') \quad [121]$$

The related quantities are:

$$\omega_0(\mathbf{r}) = \sqrt{\omega_g^2(\mathbf{r}) + \frac{\omega_p^2(\mathbf{r})}{3}} \quad [122]$$

with  $\omega_p$  the local plasma frequency defined above and  $\omega_g$  the local band gap:<sup>293</sup>

$$\omega_g(\mathbf{r})^2 = C \left| \frac{\nabla \rho(\mathbf{r})}{\rho(\mathbf{r})} \right| \quad [123]$$

where  $C$  is an adjustable parameter. The other component in  $g$  is:

$$\kappa(\mathbf{r}) = b \frac{3\pi\rho(\mathbf{r})^{1/3}}{\omega_p(\mathbf{r})} \quad [124]$$

with  $b$  another adjustable parameter (VV10 introduces this new parameter in addition to the  $C$  already present in VV09). The long-range correlation energy is defined as the non-local part plus a constant times the number of electrons in the system so that it vanishes in the uniform electron gas limit. The functional provides correct asymptotics in the infinite separation limit, is easier to implement, and provides improved statistics thanks to the flexibility provided by its adjustable parameters.

The results for the S66 database are reported in ref.<sup>270</sup> and can be compared with the results in table VI (described later). Vdw-DF2 tends to show a systematic underbinding of all molecular dimers, in particular those involving  $\pi$  systems. Semilocal VV10 overbinds hydrogen-bonds but these effects are fixed when using the long-range corrected version, LC-VV10, which achieves an outstanding 0.15 kcal/mol error on average. Both VV functionals have been implemented self-consistently,<sup>284</sup> including the analytic gradients for geometry optimizations, in Q-Chem.<sup>186</sup>

## PERFORMANCE OF DENSITY-FUNCTIONALS FOR NON-COVALENT INTERACTIONS

### Description of Non-Covalent Interactions Benchmarks

Developers of new DFT methods for noncovalent interactions have focussed largely on the prediction of accurate binding energies. To achieve this end, researchers make use of sets of benchmark data containing structures and binding energies calculated using reliable *ab initio* wavefunction theory methods. A number of benchmark data sets for a wide range of small, noncovalently-bonded dimer systems have been developed. The availability of accurate benchmark data for larger systems is less common. These benchmarks provide the first steps toward the development of comprehensive DFT methods that are capable of accurately including noncovalent interactions into the simulation of materials of all kinds, from small molecular dimers in vacuum to larger molecules immersed in solvents and solids.

A preponderance of benchmark data exists for the binding energies and corresponding structures of noncovalently-interacting dimers in vacuum owing to the ease with which reference data can be calculated. One of the most commonly accessed sources for benchmark data for these systems is the “Benchmark Energy and Geometry Database” of Řezáč et al.<sup>294,295</sup> This on-line resource contains several sets of benchmarks, including the A24 set of small molecule dimers,<sup>226</sup> water clusters containing up to 10 monomers obtained from the work of Shields’s group,<sup>296</sup> the X-40 set of halogen-containing molecular dimers, the S66 set of molecular dimers containing interactions found in organic and biomolecular interactions,<sup>226,297</sup> the S22 set<sup>203,298</sup> which is similar to but smaller than the S66 set, and a few other benchmark sets. Other groups have generated or compiled benchmark data sets, including those of Sherrill,<sup>298</sup> Johnson,<sup>177</sup> Truhlar,<sup>257,299</sup> and Grimme.<sup>187</sup>

The S22 set contains the atomic coordinates for dimer structures whose geometry was optimized using an *ab initio* wavefunction method, mostly MP2/cc-pVTZ with counterpoise (CP) corrections.<sup>300</sup> Amongst the dimers are seven complexes predominantly interacting via hydrogen bonding (dimers of ammonia, water, formic acid, formamide, uracil, and complexes of 2-pyroxidine with 2-aminopyridine and adenine with thymine), eight complexes bound mostly by dispersion (dimers of methane, ethene, benzene, pyrazine, stacked uracil, and complexes of methane-benzene, stacked indole-benzene and stacked adenine-thymine), and seven complexes interacting via mixed forces (ethene-ethyne, benzene-water, benzene-ammonia, benzene-hydrogen cyanide, T-shaped benzene dimer, T-shaped indole-benzene and the phenol dimer). The structures of these complexes are illustrated in Figure 8. The S66 benchmark set is modeled after the S22 set to some degree. It contains the structures and binding energies of 66 molecular dimers in vacuum: 23 dimers interacting predominately by hydrogen bonding, 23 dimers in which the dominant interaction can be considered to be dispersion, and 20 dimers in which the interactions are mixed. The benchmark binding ener-

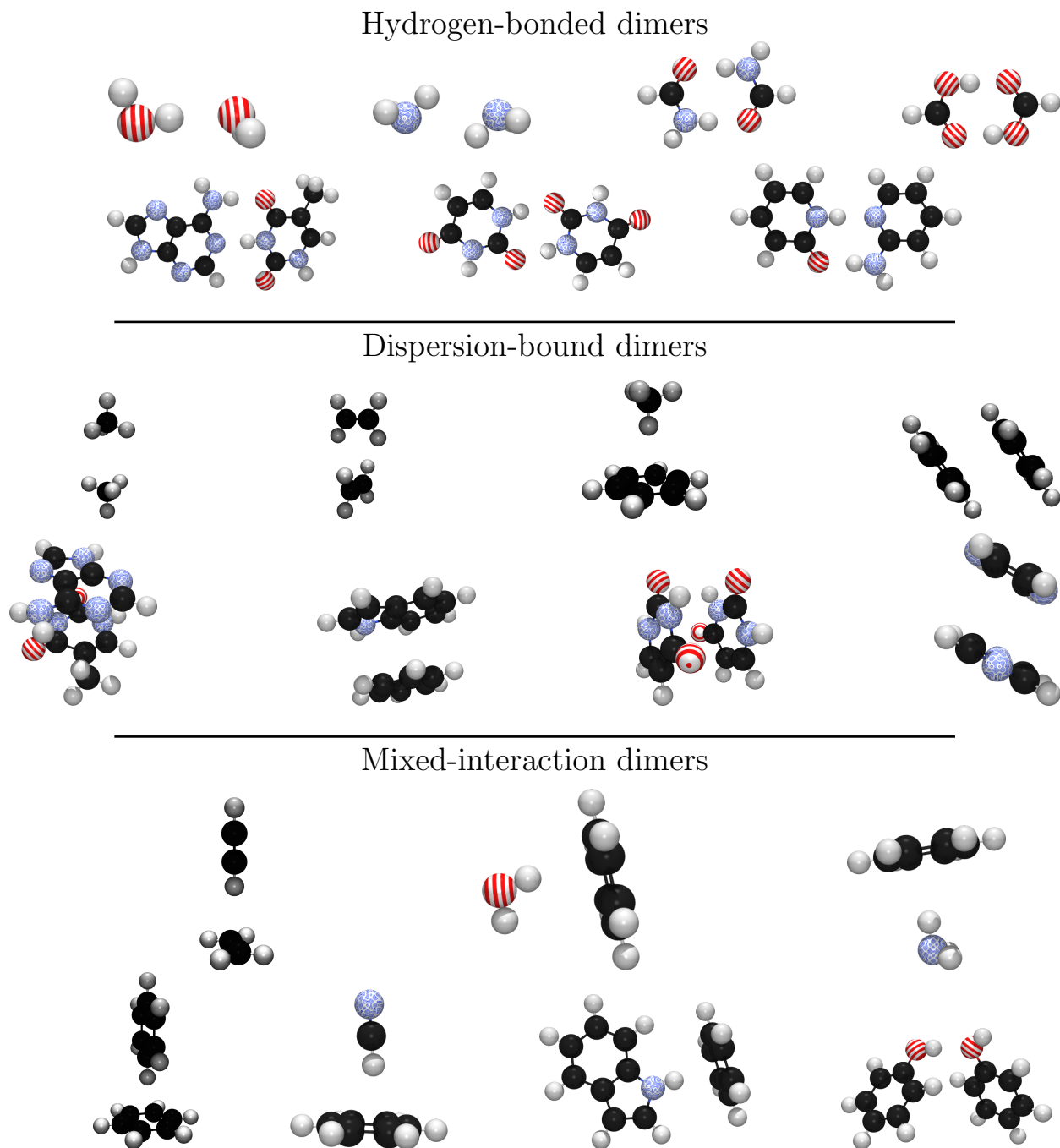


Figure 8. The dimers in the S22 set, grouped by dominant interaction type. The atoms are C (black), hydrogen (light gray), oxygen (red stripes), and nitrogen (blue dots).

gies were computed using CCSD(T) with complete-basis-set extrapolation (CCSD(T)/CBS), which is an approach capable of providing high-quality reference data for noncovalent interactions. Recently, Marshall et al.<sup>298</sup> revised the binding energies of the S22 set using a higher level of theory than was originally used for the S22.<sup>203</sup> The revised S22 set is often referred to as the S22B set.

As an aside, it is important to keep in mind that the term “CBS” is generic and could apply to any procedure involving basis set extrapolations regardless of the quality of the

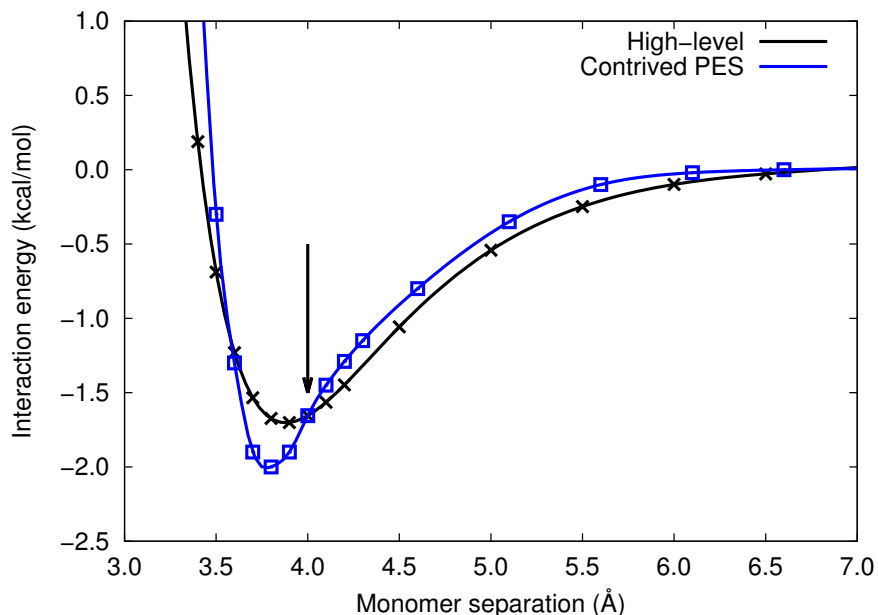


Figure 9. Contrived potential energy surfaces representing the stretching of a noncovalently-interacting dimer. The arrow represents the point at which the high-quality reference energy is provided, and which is used in the training of the hypothetical dispersion-corrected functional.

basis sets employed as part of the extrapolation. It is generally understood that certain extrapolations that make use of energies obtained from double- $\zeta$  basis sets (e.g. aug-cc-pVDZ) are not always able to provide accurate results when it comes to the binding energies in noncovalently bonded systems.<sup>301,302</sup>

When making use of the databases to assess the predictions made by a particular method, the structures are employed as presented with no adjustments or optimizations. The binding energies are then computed simply by calculating the electronic energy of the dimer system and subtracting from that the energy of the two monomers. Users of the structures in the S22 and S66 sets (as well as many other benchmark sets available) should be aware that the binding energies do not include monomer deformation. When the monomers are brought together to form the dimer, they undergo a small amount of structural distortion in order to accommodate their new environment. The degree of the structural distortion depends on the strength of the interaction, and is particularly important in hydrogen-bonded dimers. The reference binding energies reported for the S22 and S66 benchmark sets were calculated as the difference in binding energy of the dimer structure and the monomers in their distorted forms. There is nothing wrong with using these structures to obtain the benchmark binding energies, so long as users of the data are aware of their origin and use the database accordingly. Later in this section, we describe the performance of many dispersion-corrected DFT methods using the S22B and S66 benchmark sets.

The S22 and S66 databases described above, along with a number of the other generally-accessible small-molecule databases, focus exclusively on the binding energies of noncovalently interacting dimer systems at a single dimer structure. This dimer geometry is close to the minimum of the potential energy surface (PES) associated with the dimer. However, it is important to keep in mind that achieving agreement with the database value of a single binding energy near the dimer minimum is no guarantee that the DFT method will repro-



duce the features of the whole potential energy surface accurately. To illustrate this point, consider the two contrived one dimensional PESs shown in Figure 9. The PES defined by the squares represents the benchmark data associated with a particular dimer structure. The minimum of this PES occurs around 4.0Å and is highlighted by an arrow. The structure and binding energy at this geometry is representative of an entry in a database like the S66 set. It is possible for a dispersion-corrected DFT method applied to the minimum energy structure at 4Å to reproduce the binding energy exactly, thus giving the impression that the DFT method performs well in that particular structure. However, it is also possible that the very same DFT method actually produces a PES that looks like the one defined by the squares in Figure 9, rather than reproducing the entire high-level PES. Taking this wider view of the PES, even in one dimension, reveals that the DFT method has some serious deficiencies and performs much worse than is indicated by the results obtained at the minimum.

To a significant extent, the risks of being misled by an approximate computational methodology in the fashion suggested in Figure 9 is quite high if only a small number of dimers are used for performance tests. However, using a large benchmark database like the S66 significantly mitigates these risks because the set contains a small number of distinct atoms that have a large number of different spatial arrangements. In this sense, large benchmark sets offer a means of broadly sampling the different bonding environments of the atoms contained in the set.

In any case, the shortcomings associated with databases that contain information only about noncovalently-interacting dimers at their minima is beginning to be recognized and efforts are being made to create databases that contain more PES information about these dimers. Two prominent examples are the S22x5<sup>303</sup> and S66x8<sup>297</sup> databases, and it seems to be a trend that new databases are developed containing detailed PES information (see, for example, reference 304). One small difficulty, in particular with the S66x8 database, is that the level of theory applied to obtain its reference values is slightly lower than that used for the S66 database. This makes the simultaneous use of the S66x8 and S66 databases for benchmarking approximate methods somewhat confusing and there has not yet been the widespread application of these extended databases to assess dispersion-corrected DFT methods. Our expectation is that databases that contain more information about the potential energy surfaces will become more important in the future. As demonstrated by the generally good performance of most dispersion-corrected DFT methods (Tables V and VI) in the next section, more stringent and detailed tests will be needed in order to differentiate them.

One of the important practical strengths of dispersion-corrected DFT is that it can be used to model large systems containing up to several hundred atoms, depending on the implementation (plane wave or gas-phase), the complexity of the DFT method and the basis set sizes. However, benchmark sets containing large molecular systems were, until very recently, rare. One set containing 7 large systems is available online<sup>295</sup> but is not yet commonly used. A more popular set due to Grimme is the S12L set.<sup>305</sup> The entries in this benchmark set are displayed in Figure 10. The set includes two “tweezer” complexes with tetracyanoquinone (TCNQ) and 1,4-dicyanobenzene, two “pincer” species complexed with heteroatom-substituted  $\pi$ -delocalized molecules, a “buckycatcher” complexed with C<sub>60</sub> and C<sub>70</sub> fullerenes, an amide macrocycle coupled with benzoquinone and glycine glycine anhydride, complexes of cucurbit[6]uril cation with butylammonium and propylammonium, and finally complexes of cucurbit[7]uril bis(trimethylammoniomethyl) ferrocene with neutral

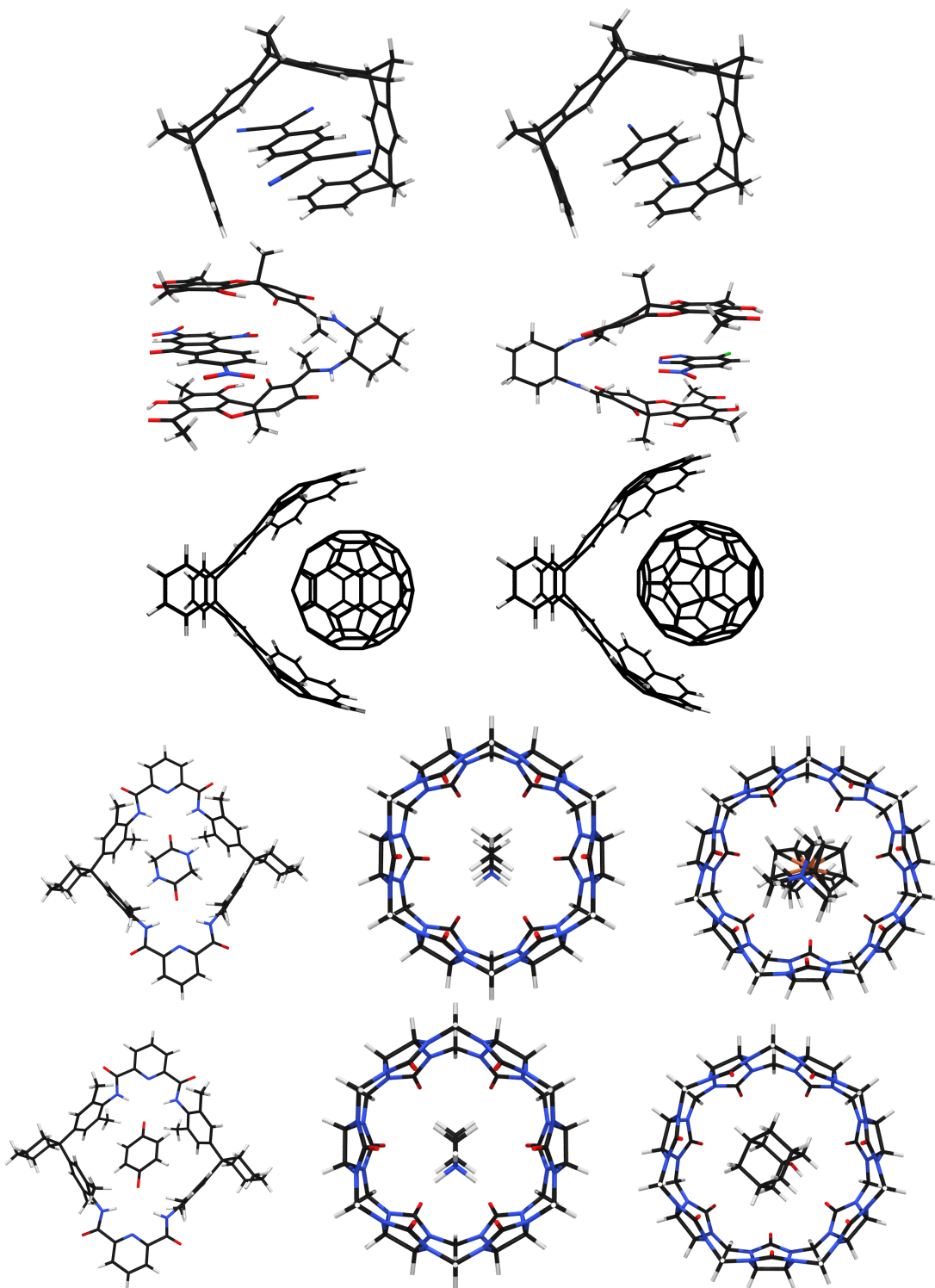


Figure 10. The molecular complexes in the S12L benchmark set.<sup>305</sup>

1-hydroxyadamantane. The binding energies of the dimers in the set range from ca. 20 to 132 kcal/mol and arise from a variety of noncovalent forces. Like the S22 and S66 sets, the binding energies of the entries in the S12L set are determined by computing the differences between the single-point energies of the dimers and their constituent monomers without modifications to the structures. Grimme used experimental association data, back-corrected for the effects of solvent and molecular vibration in order to compute the noncovalent binding energies. Most recently, Tkachenko’s group computed the noncovalent binding energies of a subset of S12L using a quantum Monte Carlo (QMC) technique in order to update the reference binding energies presented by Grimme.<sup>306</sup> QMC methods can, in principle, provide CCSD(T)/CBS quality binding energy but results will be dependent upon the nodal structure of the wavefunction on which the QMC simulations are based.

Our discussion thus far has focussed largely on molecule-molecule interactions and on the problems associated with modeling these systems using modern DFT methods. In condensed matter systems, noncovalent interactions play a central role in determining solvent-solute interactions, physisorption at gas/solid interfaces, and the properties of molecular crystals. Needless to say, in the development of dispersion-corrected DFT methods, there must be a convergence between the properties of the molecular and the bulk regimes.

In terms of benchmarking DFT based methods, few reference sets exist for condensed matter systems. Like the S12L benchmark set described above, computing high-level wavefunction properties like structures and binding energies are out of the question for most condensed matter systems. As such, the development of benchmarking data necessitates the use of experimental data, and this should be viewed positively because it offers a direct comparison between theory and reality. However, it does mean that care must be taken to ensure that all of the effects that are present in the experiment are properly accounted for. These may include the effects of solvent, zero-point/lattice vibration and thermal and entropic effects that come into play at non-zero temperatures, to offer just a few examples.

One of the first convenient benchmark sets described for solids is the C21 set of Otero-de-la-Roza and Johnson.<sup>178</sup> It contains 21 crystals of small molecules, mostly of organic and biomolecular origin, and includes: 1,4-cyclohexanedione, acetic acid, adamantane, ammonia, anthracene, benzene, CO<sub>2</sub>, cyanamide, cytosine, ethylcarbamate, formamide, imidazole, naphthalene,  $\alpha$ -oxalic acid,  $\beta$ -oxalic acid, pyrazine, pyrazole, triazine, trioxane, uracil, and urea. For these molecular crystals, the experimental sublimation enthalpies,  $\Delta H_{sub}^0$ , are available<sup>307</sup> and are back-corrected for zero-point vibration and thermal effects to give values for  $\Delta E_{el}^{exp}$ . Examples of the entries in the set include CO<sub>2</sub>, having the smallest  $\Delta H_{sub}^0$  of 5.9 kcal/mol, to cytosine, which has the largest  $\Delta H_{sub}^0$  of 39.1 kcal/mol. The C21 set also comprises a set for the molecular geometries determined experimentally using X-ray and neutron diffraction, and back-corrected to remove the effects of the crystal vibrations. The C21 set provides a good bridge from the molecular to the condensed regime and offers a convenient and somewhat more comprehensive way of assessing dispersion-corrected DFT methods. That is, while many of the dimer test sets like the S22 and S66 sets include the binding energy of only a single geometry for each dimer, and the S22x5 and S66x8 benchmark sets include one-dimensional PESs, the sublimation enthalpy data of the C21 set reflect the three-dimensional environment experienced by a molecule within a solid. In other words, this environment includes the many-body interactions and the long-range forces that arise from the crystal field.

Being able to assess the interactions amongst molecules in very different orientations accurately will ultimately allow for accurate crystal structure prediction, and this will lead

TABLE IV. Mean Absolute Errors (MAE) of the Binding Energies in the S22B Benchmark Set<sup>203,298</sup> Predicted by Various DFT Methods using def2-QZVP Basis Sets (in kcal/mol).

Functional MAE		Functional MAE		Functional MAE		Functional MAE	
Semilocal		OPBE	7.73	BHLYP	2.85	MPWB1K	1.81
B97	5.25	BPBE	5.19	PBE0	2.36	B1B95	3.26
B986	4.00	rPW86PBE	2.82	PBE38	2.27	BMK	2.61
BOP	6.67	SSB	2.98	revPBE0	4.30	Range-separated	
BLYP	4.77	revSSB	2.45	revPBE38	3.83	CAM-B3LYP	2.52
MPWLYP	3.37	TPSS	3.45	TPSSh	3.28	LC- $\omega$ PBE	2.81
OLYP	7.33	oTPSS	4.48	TPSS0	3.04		
PBE	2.57	Hybrid		PW6B95	1.95		
PBEsol	1.81	B3LYP	3.77	MPW1B95	2.12		
revPBE	5.21	B3PW91	4.13	PWB6K	1.20		

The functionals are grouped by classes, indicated by horizontal labels on the table (semilocal functionals, hybrids, and range-separated hybrids).

to the ability of engaging in meaningful materials design work. However, it should be kept in mind that there is more to structure prediction than calculating accurate interaction energies: Other challenges are associated with the development of algorithms for seeking the local and global minima associated with the arrangement of atoms within a crystal and, for example, differentiating crystal polymorphs.<sup>308</sup> The ability to predict *a priori* molecular crystal structure has implications in the pharmaceutical industry from the standpoint of drug bioavailability and stability.<sup>309</sup> Also important are the legal consequences associated with the protection of intellectual property related to pharmaceuticals and the possibility of the existence of multiple drug polymorphs. The interesting case of polymorphism in the antibiotic Cefdinir is described in reference 309 and points to the potential benefit of molecular crystal structure prediction to this industry.

Before proceeding to the next section where the performance of various dispersion-corrected DFT techniques are compared, we underscore that conventional DFT methods do, in general, a poor job in predicting the binding energies of noncovalently-bonded systems by using one of the benchmark sets described above. Table IV compiles the mean absolute errors in binding energies for a variety of DFT methods that cover the range of GGA, hybrid GGA, meta-GGA and range-separated functionals, as reported by Goerigk and Grimme.<sup>187</sup> Although there are distinct differences in the predictions made by various base functionals for the binding energies of the S22B set, there can be no doubt upon examination of Table IV that conventional DFT methods fail to model noncovalent systems accurately.

## Performance of Dispersion-Corrected Methods

The popularity of the S22 and S66 sets is fortuitous because it makes it somewhat straightforward to compare the performance of different DFT methods for noncovalent interactions. Table V contains the mean absolute errors (MAEs) of calculated binding energies (in kcal/mol) obtained using a variety of density-functional theory methods and dispersion correction schemes, along with the reference to the work from which the quoted results were

taken. The Table is arranged so that GGA, hybrid-GGA, meta-hybrid GGA and range-separated DFT methods are presented from top-to-bottom, left-to-right. It is important to point out that some groups use the term mean absolute deviation (MAD) in reference to MAE. However, these two quantities are very different according to their definitions in statistics. Generally speaking, when groups report data for the S22 benchmark set as MADs, they are really referring to MAEs.

The variety of basis sets employed in the benchmarking studies makes the direct comparison of the results challenging at first sight. However, most works utilize very large and nearly complete basis sets (e.g. def2-QZVP, aug-cc-pVTZ, or plane wave), which permits a nearly direct comparison. The dispersion-correcting potential approach was designed with the goal being efficiently applied to large systems and so it makes use of smaller 6-31+G(2d,2p) basis sets. Recall that DCPs mitigate to some extent the effects of basis set incompleteness and so the expectation is that the performance of DFT-DCP/6-31+G(2d,2p) can be compared to other approaches that use very large basis sets.

In some cases it is useful to compare the results obtained with smaller basis sets in order to understand how performance can vary with basis set size. However, users should be aware of the methods (DFT approach, basis sets, etc.) under which the dispersion correction approach of choice was developed and are advised to apply the same parameters in their calculations, or study the variations caused by basis set incompleteness in their chosen calculation method appropriately.

For the S22B set, the method demonstrating the best performance is TPSS-TS, with an MAE value of only 0.2 kcal/mol. Ten other approaches give MAE values between 0.2 and 0.3 kcal/mol, namely, BLYP-D3, BLYP-XDM, MPW1B95-D3, M06-D3, LC- $\omega$ PBE-D3, PBE-TS, B3LYP-TS, B3LYP-DCP, LC- $\omega$ PBE-DCP, and  $\omega$ B97X-D. It is interesting to note that all of the dispersion-correcting methods are capable of predicting noncovalent binding energies for the S22B set with very low average errors but not necessarily when used in combination with the same functionals. This suggests that each of the dispersion-correcting techniques is best suited to correct for the underlying deficiencies of certain bare functionals, although the broader development and application of methods besides the D3 approach will be required before making definitive statements in this connection. It is also interesting to note that the best performing methods represent various “rungs” of the DFT ladder,<sup>67</sup> with dispersion-corrected GGAs, hybrids, and range-separated functionals making an appearance.

Of the remaining of the methods listed in Table V, 21 give MAE values in the 0.3–0.4 kcal/mol range, 12 fall into the 0.4–0.5 kcal/mol range, and the other 23 methods predict MAE values between 0.5 and 2.1 kcal/mol. The non-local functionals are not amongst the top performers for this benchmark set. All of the methods, except for the Minnesota functionals for which there is not a non-dispersion-corrected version to compare against, represent significant improvements over the results obtained with the bare functionals, as provided in Table IV. However, the fact that so many methods still perform poorly when dispersion corrections are incorporated implies that these functionals have underlying deficiencies beyond just dispersion.

The successful application of D3 and TS corrections to the Minnesota functionals demonstrates that dispersion-correction approaches do not mutually exclude each other. In the particular case of the Minnesota DFT methods, the parameters of the functionals were optimized to minimize the errors associated with a number of molecular properties and not just noncovalent interactions. It follows that Minnesota functionals are, in general, systematically underbinding, and that there is potential to improve them through the use of other

TABLE V. Mean absolute errors (MAEs) in the Binding Energies for the S22B Benchmark Set<sup>203,298</sup> of Noncovalently-Bonded Dimers Predicted by Different Dispersion-Correcting Approaches and Functionals, in kcal/mol.

Func.	Disp.	MAE	Func.	Disp.	MAE	Func.	Disp.	MAE	Func.	Disp.	MAE
B97	D3	0.38	SSB	D3	0.63	PBE0	XDM	0.53	M05-2X	MN	0.79
B986	D3	0.66	revSSB	D3	0.49	PBE38	D3	0.63	M06	D3	0.26
BOP	D3	0.52	TPSS	D3	0.32	PBEh	TS	0.30	M06	TS	0.42
BLYP	D3	0.24	TPSS	TS	0.2	HSE	TS	0.39	M06	MN	1.06
BLYP	XDM	0.22	oTPSS	D3	0.31	revPBE0	D3	0.32	M06-2X	D3	0.36
BLYP	DCACP	0.33 <sup>a</sup>	M06-L	D3	0.44	revPBE38	D3	0.39	M06-2X	MN	0.40 <sup>b</sup>
MPWLYP	D3	0.55	M06-L	TS	0.37	TPSSh	D3	0.38	M06-HF	D3	0.84
OLYP	D3	0.71	B97-1	D3	0.36	TPSS0	D3	0.44	M06-HF	MN	0.62
PBE	D3	0.48	B97-1	XDM	0.62	PW6B95	D3	0.34	CAM-B3LYP	D3	0.67
PBE	TS	0.28	B3LYP	D3	0.36	MPW1B95	D3	0.29	CAM-B3LYP	XDM	0.50
PBE	XDM	0.57	B3LYP	TS	0.23	PWB6K	D3	0.44	LC- $\omega$ PBE	D3	0.28
PBEsol	D3	1.01	B3LYP	XDM	0.31	MPwB1K	D3	0.32	LC- $\omega$ PBE	XDM	0.31
revPBE	D3	0.41	B3LYP	DCP	0.27	B1B95	D3	0.43	LC- $\omega$ PBE	DCP	0.27
OPBE	D3	0.83	B3PW91	D3	0.45	BMK	D3	0.98	$\omega$ B97X-D <sup>c</sup>	D2	0.23 <sup>d</sup>
BPBE	D3	0.49	BHandHLYP	D3	0.66	M05	D3	0.52	VV10	NL	0.31
rPW86PBE	D3	0.35	BHandHLYP	XDM	0.47	M05	MN	2.07	vdW-DF2	NL	0.94
PW86PBE	XDM	0.35	PBE0	D3	0.57	M05-2X	D3	0.35			

D3: DFT-D3/def2 using the original damping function.<sup>187</sup> TS: DFT-TS using “tier2” numerical atom-centered orbital bases.<sup>310</sup> XDM: DFT-XDM/aug-cc-pVTZ.<sup>99</sup> DCACP: DFT-DCACP2/plane wave.<sup>253</sup> DCP: B3LYP-DCP/6-31+G(2d,2p)<sup>234</sup> and LC- $\omega$ PBE/6-31+G(2d,2p).<sup>243</sup> MN: Minnesota/def2-QZVP.<sup>187</sup> VV10: VV10/aug-cc-pVTZ.<sup>292</sup> vdW-DF2: vdW-DF2/aug-cc-pVTZ.<sup>292</sup> The S22 benchmark was used as the fitting set for TS, and as component of the fitting set for D3 and XDM.

<sup>a</sup> The DFT-DCACP/plane wave approach of reference 249 gave a MAE of 0.65 kcal/mol.<sup>253</sup>

<sup>b</sup> M06-2X/6-31+G(2d,2p) produces a MAE of 0.43 kcal/mol.

<sup>c</sup> Employing the original “D” correction for dispersion.

<sup>d</sup>  $\omega$ B97X-D/6-31+G(2d,2p) produces a MAE of 0.58 kcal/mol.

dispersion-correction techniques. This is demonstrated in Table V most dramatically for M05, M05-2X, and M06 where the MAEs are reduced by factors of 2–4 through the use of these functionals with the D3 dispersion correction. However, better results are not always achieved in this way: The combination of M06-HF and D3 increases the MAE from 0.62 to 0.84 kcal/mol.

It is worth mentioning the relative computational costs (i.e. run time) associated with the different dispersion-correction methods. The costs are not very relevant for the S22 set because most of the dimers contained therein are fairly small. However, computational cost becomes a concern when large systems, or a large number of systems, are simulated. The dispersion-correction method with lowest cost of those listed in Table V is the DCP approach owing to the fact that it is designed for use with small basis sets. Despite the small basis sets, the DCP method produces small MAEs for the S22B set of 0.27 and 0.23 kcal/mol, depending on the underlying DFT method.

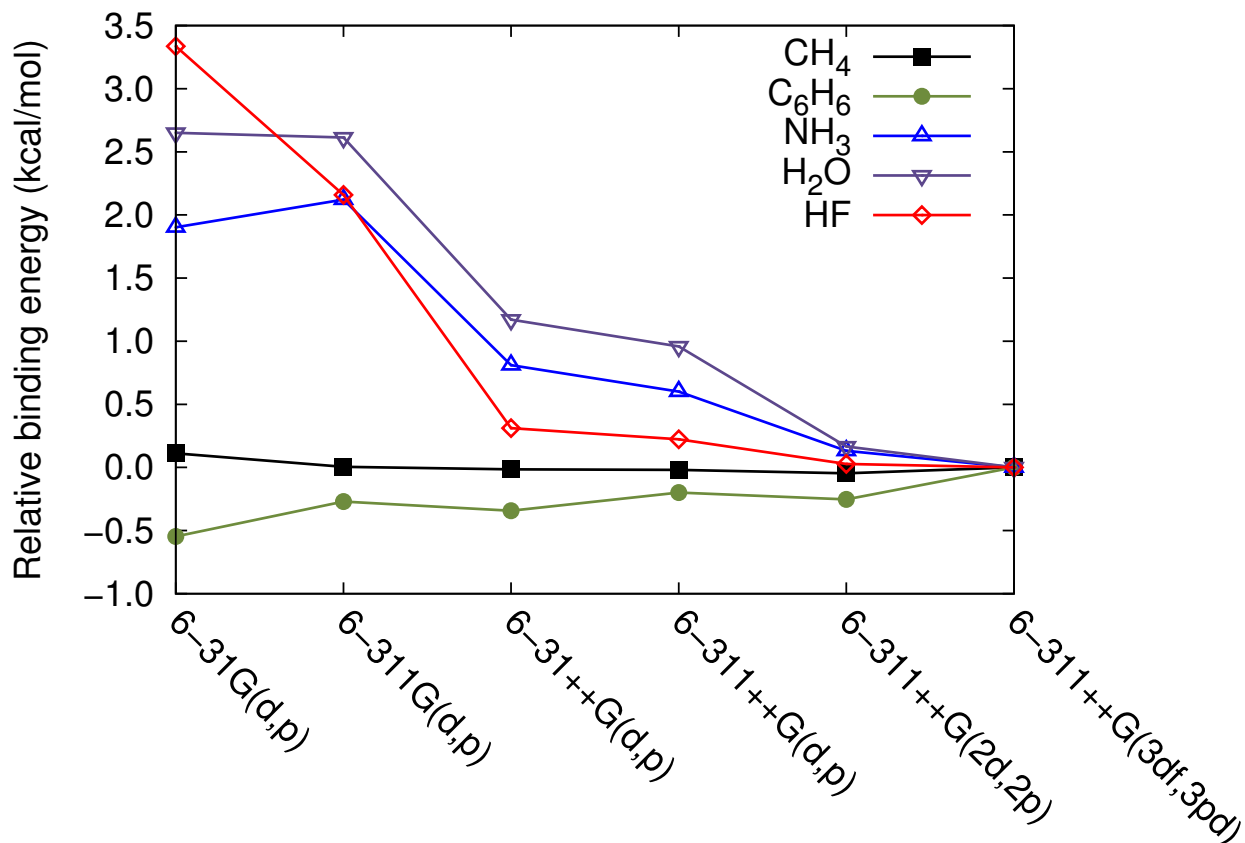


Figure 11. Basis set dependence of the LC- $\omega$ -PBE-XDM binding energies of various noncovalent interacting dimers (from reference 176).

On the point of the basis set dependence of dispersion-corrected methods, the M06-2X functional demonstrates remarkably consistent MAEs for the S22 set as obtained using def2-QZVP and 6-31+G(2d,2p) bases. The differences in the MAEs so calculated is only 0.03 kcal/mol, or about 8%. Conversely, the  $\omega$ B97X-D method display significantly greater basis set dependence, giving differences in the def2-QZVP and 6-31+G(2d,2p) MAEs of 0.35 kcal/mol, which represents a more than two-fold increase in average error. This underscores an important issue that should not be overlooked by users of these methods: There may be significant basis-set dependencies associated with a particular dispersion correction approach that should be determined if basis sets other than the recommended ones are utilized. For DFT methods that are coupled with pair-wise dispersion-correction (D3 and XDM) methods, users can expect basis sets dependencies similar or identical to those of the underlying functional. DFT approaches that are coupled with DCPs are expected to have smaller basis set dependencies than the bare functional.

Figure 11 demonstrates the basis-set dependence of the LC- $\omega$ -PBE functional with XDM. Because XDM is a post-SCF energy correction, the basis set dependence for the bare functional is roughly the same as that illustrated in the Figure. The plot shows that the performance of LC- $\omega$ -PBE-XDM degrades substantially when basis sets smaller than 6-311++G(2d,2p) are used. Interestingly, the basis set dependence increases with the strength of the interaction type. That is, dispersion-dominated dimers present a weak basis set dependence whereas hydrogen-bonded systems are much more affected by basis-set incomplete-

TABLE VI. Mean Absolute Errors (MAE) in the Binding Energies for the S66 Benchmark Set of Noncovalently-Bonded Dimers Predicted by DFT Methods Employing Various Dispersion-Correcting Approaches in kcal/mol.

Func.	Disp.	MAE	Func.	Disp.	MAE	Func.	Disp.	MAE
B97	D3	0.29	M06-L	D3	0.34 <sup>†</sup>	M06-2X	D3	0.24 <sup>†</sup>
BLYP	D3	0.19	M06-L	MN	0.60	M06-2X	MN	0.28 <sup>a</sup>
BLYP	XDM	0.19	B3LYP	D3	0.28	CAM-B3LYP	XDM	0.35
PBE	D3	0.40	B3LYP	XDM	0.22	LC- $\omega$ PBE	D3	0.19
PBE	TS	0.44	B3LYP	DCP	0.19	LC- $\omega$ PBE	XDM	0.21
PBE	XDM	0.39	B97-1	XDM	0.38	LC- $\omega$ PBE	DCP	0.21
PBEh	TS	0.39	BHandHLYP	XDM	0.31	$\omega$ B97X-D <sup>b</sup>	D2	0.29 <sup>c</sup>
PW86PBE	TS	0.39	PBE0	XDM	0.36	VV10	VV10	0.35
PW86PBE	XDM	0.26	PW6B95	D3	0.18	LC-VV10	VV10	0.15
revPBE	D3	0.29	MPW1B95	D3	0.20	vdW-DF2 <sup>k</sup>	vdw-DF2	0.48
TPSS	D3	0.30	M05-2X	D3	0.30 <sup>†</sup>			
oTPSS	D3	0.30	M05-2X	MN	0.58			

D3: DFT-D3/def2-QZVP<sup>311</sup> using the Becke-Johnson damping function<sup>160</sup>

except where indicated by <sup>†</sup>. TS: DFT-TS using “tier2” numerical atom-centered orbital bases.<sup>310</sup> XDM: DFT-XDM/aug-cc-pVTZ.<sup>99</sup> DCP:

B3LYP-DCP/6-31+G(2d,2p)<sup>234</sup> and LC- $\omega$ PBE/6-31+G(2d,2p).<sup>243</sup> MN:

Minnesota/def2-QZVP.<sup>187</sup> VV10: VV10/aug-cc-pVTZ.<sup>292</sup> vdW-DF2:

vdW-DF2/aug-cc-pVTZ.<sup>292</sup>

<sup>a</sup> M06-2X/6-31+G(2d,2p) produces a MAE of 0.25 kcal/mol.

<sup>b</sup> Employing the original “D” correction for dispersion.

<sup>c</sup>  $\omega$ B97X-D/6-31+G(2d,2p) produces a MAE of 0.30 kcal/mol.<sup>234</sup>

ness errors. This makes sense in view that hydrogen bonds involve significant intramolecular charge transfer and orbital interactions, whereas the former does not.

With respect to DCACPs, it is noted that the BLYP-DCACP approach of von Lilienfeld et al.<sup>249</sup> produces rather poor results (see footnote a in Table V). However, keeping in mind that only one DCACP function was used for each atom and that the fitting data used to generate the functions were very small, the performance is reasonable. The recent work of Karalti et al.<sup>253</sup> convincingly demonstrates that using two functions per atom can offer much improved performance in the treatment of noncovalent interactions, with the MAE reduced by almost a factor of 2 over that obtained with the single function DCACPs.

Table VI summarizes the performance of various dispersion-corrected DFT methods on the larger S66 set. As a point of reference, B3LYP without corrections for dispersion gives an MAE of 3.8 kcal/mol for this set. Inclusion of dispersion corrections by any means is expected to reduce the MAE and this is realized in the data provided in Table VI. The best performing method in the table is the long-range corrected, non-local version of the VV10 functional, giving an MAE of only 0.15 kcal/mol. D3, XDM and DCP-corrected functionals round-out the top ten list giving MAEs of 0.18–0.21 kcal/mol, with all classes of functionals represented.

As happened in the S22 set, the combination of dispersion-corrections with different functionals are capable of performing very well for the prediction of noncovalent binding energies



of the S66 set. This offers potential users of these methods some choice in terms of balancing the desired accuracy in noncovalent properties with those of other properties (see, for example, Table I). Alternatively, users may wish to consider the use of more computationally efficient methods, such as DCP-based approaches or functionals that allow for the use of smaller basis sets owing to the small impact of basis set incompleteness in their performance. With respect to molecular properties, it should also be understood that the application of dispersion corrections may also alter the performance of the DFT method for properties other than simple noncovalent interactions. This issue is discussed to some extent in the final section of this chapter.

Other results of note presented in Table VI are those of the M06-2X and M05-2X functionals, which give MAEs of 0.28 and 0.58 kcal/mol, respectively. Both functionals perform better on the S66 set than they do on the S22 set, but the performance of M05-2X may be considered by most to be too poor to be useful for noncovalent interactions. The inclusion of D3 corrections to these two functionals improves their performance - marginally for M06-2X but by almost a factor of 2 for M05-2X. Again this underscores the notion that different dispersion approaches can be combined in order improve their performance for noncovalent interactions.

As described in previous sections, the power of DFT becomes very clear when it is applied to very large systems that are well outside of the range of accurate wavefunction theory methods. The S12L set allows these limits to be explored. The results presented in Table VII show the MAEs predicted by a relatively small number of dispersion-corrected DFT methods. To put the data into some context, the LC- $\omega$ PBE functional with 6-31+G(2d,2p) basis sets predicts an MAE of 17.9 kcal/mol for the set. The binding energies predicted using this approach are consistently underbinding despite benefiting from some stabilization through basis set incompleteness effects. The MAE of 25.4 kcal/mol (underbinding) obtained for the bare PBE functional used with def2-QZVP (without g functions)<sup>312</sup> confirms the expectation that underbinding by bare functionals will become more pronounced as the size of the basis set increases.

The MAEs listed in Table VII obtained by dispersion-corrected DFT methods are much larger than those found for the S22 and S66 sets. This in part relates to the fact that the underlying DFT methods perform very poorly on the S12L set and also because the binding energies of some members of the set are very large.

Risthaus and Grimme’s recent work explored the utility of some dispersion-corrected DFT methods in treating the large systems of the S12L set. In several cases, they found it important to include corrections to the binding energies for 3-body terms, and estimated the magnitude of this contribution using  $C_9$  coefficients estimated from  $C_6$  coefficients. The 3-body corrections range from about 0.7 to 4.6 kcal/mol and reduce the strength with which the complexes are bound. The authors paired the D2 and D3 dispersion corrections with the PBE functional and basis sets of QZ quality and found MAEs of 2.3 and 2.4 kcal/mol, respectively. PBE-NL provided a slightly smaller MAE while M06-L gave an MAE that was nearly twice as large.

Recognizing that the large QZ basis sets (with which the D3 corrections were developed and are normally used) are impractical for very big systems, Risthaus and Grimme also explored the use of smaller, def2-TZVP basis sets and counterpoise corrections on the S12L set. These smaller basis sets with the PBE-D2 approach gave the lowest MAE in binding energy for the set—only 1.6 kcal/mol—whereas the performance of PBE-NL and PBE-D3 were unchanged. The MAEs for M06-2X and M06-L are factors of ca. 2 and 3 larger than

TABLE VII. Mean Absolute Error (MAE) in the Binding Energies Predicted by Selected Density Functionals, Basis Sets and Dispersion Correction Schemes on the S12L set of Noncovalently Bonded Dimers<sup>312</sup> (in kcal/mol).

Density functional	Basis set	Disp. Correction	MAE	Ref.
PBE	def2-QZVP	NL + $\Delta E^{ABC}$	2.1	312
PBE	def2-QZVP <sup>a</sup>	D2 + $\Delta E^{ABC}$	2.3	312
PBE	def2-QZVP <sup>a</sup>	D3 + $\Delta E^{ABC}$	2.4	312
M06-L	def2-QZVP	MN + $\Delta E^{ABC}$	4.1	312
PBE	def2-TZVP <sup>b</sup>	D2 + $\Delta E^{ABC}$	1.6	312
PBE	def2-TZVP <sup>b</sup>	NL + $\Delta E^{ABC}$	2.3	312
PBE	def2-TZVP <sup>b</sup>	D3 + $\Delta E^{ABC}$	2.3	312
M06-2X	def2-TZVP <sup>b</sup>	MN + $\Delta E^{ABC}$	3.3	312
M06-L	def2-TZVP <sup>b</sup>	— + $\Delta E^{ABC}$	4.6	312
PBE	pc-2(spdc)	XDM	2.3 <sup>d</sup>	313
BLYP	pc-2(spdc)	XDM	3.9 <sup>d</sup>	313
B3LYP	pc-2(spdc)	XDM	3.7 <sup>d</sup>	313
LC- $\omega$ PBE	pc-2(spdc)	XDM	6.5 <sup>d</sup>	313
B3LYP	6-31+G(2d,2p)	DCP	2.6	235
LC- $\omega$ PBE	6-31+G(2d,2p)	DCP	3.4	243

NL: Hujo et al. tweak<sup>314</sup> to the original VV10 by Vydrov and van Voorhis.<sup>292</sup>

D2: DFT-D2. D3: DFT-D3.  $\Delta E^{ABC}$ : a three-body Axilrod-Teller-Muto term has been added (Eq. 53).

<sup>a</sup>These basis sets were employed without g-functions.

<sup>b</sup>With counterpoise corrections.<sup>300</sup>

<sup>c</sup>Using the pc-2 basis set of Jensen,<sup>315-317</sup> with the heavy atom f-basis functions removed, as described in reference 176. The pc-2(spdc) basis set has the same number of contracted functions as the 6-31+G(2d,2p) basis set.

<sup>d</sup>These MAEs decrease by 0.2 to 0.3 kcal/mol when the Quantum Monte-Carlo (QMC) reference data of Ambrosetti et al.<sup>306</sup> are used.

the best performing method in the Table.

Considering both low MAEs and basis set size, some of the best performing methods on the S12L set appear to be those based on the XDM approach. These used pc-2(spdc) basis sets, the polarization-consistent-2 set of Jensen<sup>315-317</sup> with the heavy atom f-functions removed. The pc-2(spdc) basis sets were found to offer an excellent compromise between quality of results for noncovalent interactions and computational cost.<sup>176</sup> The PBE approach coupled with XDM gives an MAE for the S12L set of 2.3 kcal/mol. If the QMC reference binding energies are used, the MAE drops to 2.1 kcal/mol. The average of the 3-body correction terms computed by Grimme for the S12L set is 2.2 kcal/mol, and so the good agreement provided by the PBE-XDM approach raises some interesting questions about the role that 3-body corrections actually play in dispersion-corrected DFT. The BLYP and B3LYP were also coupled with XDM and the small pc-2(spdc) basis sets and these approaches gave MAEs that are on par with the M06-2X results.

The DCP approach also produces reasonable results for the S12L set. B3LYP-DCP/6-31+G(2d,2p) gives an MAE of 2.6 kcal/mol, which is competitive with many of the other

TABLE VIII. Mean Absolute Errors (MAE, kcal/mol) and Mean Absolute Percent Errors (MAPE) in the Experimental Lattice Energies Predicted by Selected Functionals and Dispersion Corrections on the C21 Set of Molecular Crystals.<sup>178</sup>

Functional	Disp. Correction	MAE	MAPE
PBE	—	8.6	47.2
PBE	D2	2.2	11.9
PBE	TS	4.1	22.1
PBE	XDM	1.3	6.7
vdw-DF1	NL	2.4	13.5
vdw-DF2	NL	2.4	13.1
B86b	XDM	1.1	6.2
PBE0	MBD	0.9	5.7

D2: DFT-D2 as implemented by Barone et al.<sup>153</sup> TS: Tkatchenko-Scheffler.<sup>150</sup>  
 vdw-DF1: Dion et al. version of the vdw-DF functional.<sup>278</sup> vdw-DF2: Lee et al. version of vdw-DF.<sup>285</sup> PBE0-MBD: TS functional with many-body dispersion corrections.<sup>318</sup> All calculations were carried out in a plane wave/pseudopotentials approach.

methods listed in Table VII. The MAE for LC- $\omega$ PBE-DCP is 3.6 kcal/mol, fairly close to that of M06-2X/def2-TZVP with counterpoise corrections.

The last benchmark set for which we discuss the performance of dispersion-corrected DFT method is the heats of sublimation molecular crystal database (C21) of Otero-de-la-Roza and Johnson.<sup>178</sup> Table VIII summarizes the performance of XDM and TS pair-wise dispersion corrections along with non-local DFT methods, applied with plane wave basis sets. As an aside, DCACPs could be applied to this set because they were designed for use with plane wave codes but, to our knowledge, this has not been done yet. DCPs cannot be applied easily to the C21 set as they are readily applicable only in quantum chemistry (“cluster”) codes. The C21 set also contains a test set using the same crystals in which the X-ray or neutron diffraction structures are compared against the calculated crystal geometries after relaxation under a “thermal pressure”, that encapsulates the effects of crystal vibrations.

For comparison, the PBE functional without corrections for dispersion does poorly in predicting the experimental lattice energies for the set giving a MAE of 8.6 kcal/mol, or nearly 50% average error. Including dispersion corrections improves the predictions greatly. The “TS” parameters for pair-wise dispersion perform the most poorly, giving an MAPE of about 22%; however, recent modifications to the “TS” treatment that include of a many-body correction and incorporate Hartree-Fock exchange via the PBE0 functional, reduce the MAE to below 1 kcal/mol<sup>318</sup> (5.7%). Nevertheless, the PBE0-MBD results are only slightly better than those derived from the PBE-XDM approach, which has neither an explicit correction for many body terms nor does the functional have Hartree-Fock exchange.

The results that are achieved by PBE-XDM and PBE0-MBD point to an important aspect of calculations that should be considered by users who are interested in applying these methods to their own problems. In periodic calculations, the inclusion of Hartree-Fock exchange is far more computationally expensive (up to two orders of magnitude longer running times) than the cost of doing so in cluster calculations (usually less than a factor of two). With any computational approach, users must balance the costs associated with a

given approach against the accuracy of the methods. In the case of the C21 set, for example, users should assess whether they are willing to wait 10 to 100 times longer to achieve an average improvement in performance of 0.4 kcal/mol (or 1%). In addition, the cost of the MBD calculation has, to our knowledge, not been reported.

The results of Table VIII show that dispersion-corrected DFT methods are becoming advanced enough such that accurate relative stability of molecular crystals (particularly in the context of *a priori* molecular crystal structure prediction) should be possible.

## NON-COVALENT INTERACTIONS IN PERSPECTIVE

In this chapter, we demonstrated that dispersion-corrected DFT methods are now capable of providing excellent agreement with benchmark binding energies for a variety of dimer systems. There is no doubt that the methods have advanced to the point where many of them are robust and can be generally applied beyond noncovalently-bonded systems to good effect. Coupled with the demonstration that the XDM and TS approaches are capable of predicting heats of sublimation, dispersion-corrected DFT methods are now promising tools for the *a priori* design of new molecular materials.

It is worthwhile at this point to consider dispersion-corrected DFT from a broader chemical perspective. Thus, we may ask: Does the inclusion of dispersion corrections in DFT methods influence properties other than binding energies? The answer to this question is partially answered by recognizing that many implementations of pair-wise dispersion correction schemes are not self-consistent, which means that the electron density is not affected by them. It follows that, for a given molecular structure, properties not directly taken from the molecular energy will be exactly the same with and without the pair-wise dispersion correction. From this perspective, pair-wise dispersion corrections cannot *directly* influence properties that depend on the electronic structure. The same is not true for the non-local and Minnesota functionals that are formulated self-consistently, although examining “with and without” dispersion scenarios with these families of functionals is not possible. DCPs also operate self-consistently in that they are incorporated into the Hamiltonian of the system and thereby alter electron distributions and thus have the potential to alter properties, which may include among others NMR chemical shifts, dipole moments, and hyperfine coupling constants.

All dispersion corrections, regardless of the type, have the potential to *indirectly* affect molecular properties by altering molecular structure. The relationship between structure and properties is well known in chemistry. As a simple example, the catalytic properties of an enzyme depend crucially on its structure<sup>319</sup> and denaturing the enzyme (i.e. changing its structure through, for instance, heating) reduces or destroys its catalytic properties. In general, by providing a realistic description of the energy landscape that determines the structure by introducing dispersion corrections into DFT methods, the properties depending on that structure will also be better described.

Understanding the ability of dispersion-corrected DFT methods to predict accurate structures can be important for making decisions about how such methods should be used for solving problems in chemistry and physics. A simple and effective example of the impact of noncovalent interactions in the area of organic electronic materials was recently published.<sup>320</sup> In cases where electron transport within these materials is dominated by a hopping mechanism, the process can be modeled as an electron transfer reaction between adjacent molecules in a molecular film. The rate constant for the electron transfer process between

molecules can be approximated using Marcus theory according to:

$$k_{\text{ET}} = \frac{1}{\sqrt{4\pi\lambda k_{\text{B}}T}} V^2 \exp\left(-\frac{\lambda}{4k_{\text{B}}T}\right) \quad [125]$$

where  $k_{\text{B}}$  is the Boltzmann’s constant, and  $\lambda$  is the reorganization energy associated with the geometry change that occurs during the electron transfer process (atomic units are used).

The variable  $V$  is the electron coupling matrix element that relates orbital overlap between adjacent molecules; that ultimately dictates the carrier transport efficacy of a material. Thus, the structure-activity relationship is defined: the spatial arrangement of adjacent molecules in a material dictates the ability of the material to transport charge. In the context of modeling charge transport in organic electronic materials, the ability to predict reasonably accurate structures may be considered to be more important than the ability to predict accurate binding energies. We refer back to Figure 9 to illustrate this point: although the fictitious approximate method predicts the correct binding energy at the accepted dimer minimum indicated at 4 Å, a full structure optimization would result in a intermonomer minimum that is too short by 0.2 Å and this would give an overly-large electron transfer rate constant if applied to organic electronic material.

Structure is also a critical aspect in all problems related to reaction chemistry and covalent bonding. However, the deficiencies with respect to dispersion treatment in many DFT methods become overwhelmed by other shortcomings in the base functionals. This becomes clear when modeling simple thermochemistry, like the C-H bond dissociation enthalpy (BDE) in methane. Here, base DFT methods may predict BDEs that are in error by 3 or 4 kcal/mol. These errors are more than an order of magnitude larger than those obtained without dispersion. Always keep in mind that including accurate dispersion-corrections into a chosen method is usually insufficient for alleviating all of the problems of a DFT method.

In some cases, including dispersion-corrections in a DFT treatment can produce much worse results than might be achieved without them. This is illustrated by considering one of the early studies on the ability of some common DFT based methods to predict accurate barrier heights in simple hydrogen atom exchange reactions. Lynch and Truhlar<sup>102</sup> presented results for a benchmark set of 21 simple forward and reverse bimolecular hydrogen atom transfer reactions (e.g.  $\text{OH} + \text{H}_2 \rightarrow \text{H} + \text{H}_2\text{O}$ ,  $\text{C}_2\text{H}_6 + \text{NH}_2 \rightarrow \text{C}_2\text{H}_5 + \text{NH}_3$ ) and one intramolecular hydrogen atom transfer (namely, *s-trans cis*- $\text{C}_5\text{H}_8 \rightarrow$  *s-trans cis*- $\text{C}_5\text{H}_8$ ) for a total of 43 barrier heights. B3LYP with reasonably large basis sets predicts all but two of the 43 reaction barriers to be too low. How would the results be affected if pair-wise dispersion corrections were applied with B3LYP to these barrier heights? Consider that the transition state for any bimolecular reaction is composed of more atoms than the reactant and product states. Because the energy contribution of any pair-wise dispersion scheme is always stabilizing, it follows that the energy stabilization of the larger transition states will be preferentially stabilized relative to the smaller reactants and products. In this case, applying of pair-wise dispersion schemes will result in predicted barrier heights that are in worse agreement with the benchmark values as compared to the results for the base functional. Of course, in cases where a DFT method predicts barrier heights to be too high, pair-wise dispersion corrections will improve the results.

Recent work by Schreiner’s team provides an interesting counter example to the barrier height problem described above. This group prepared and studied (experimentally and computationally) sterically-crowded molecules based on coupled diamondoid species.<sup>321,322</sup> Diamondoids are small, hydrogen-terminated three-dimensional carbon clusters consisting

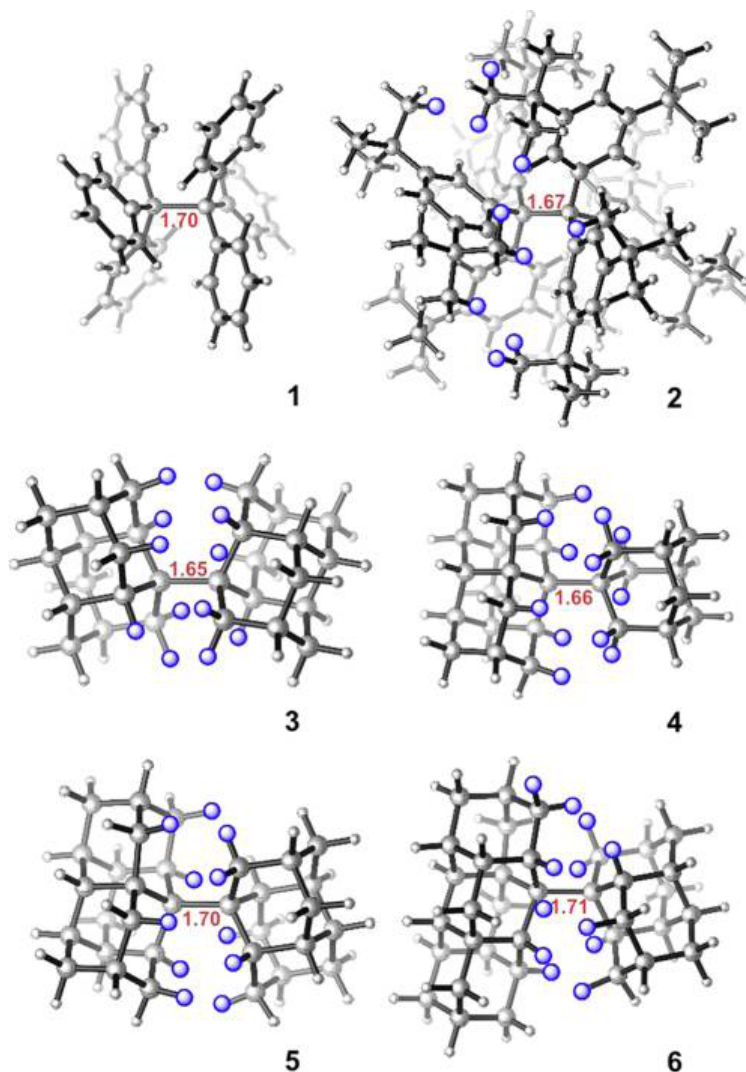


Figure 12. Structures of coupled diamondoid molecules showing unusually long C-C bonds (taken with permission from reference 321).

of adamantane subunits. The coupled diamondoid species, a sampling of which are shown in Figure 12, have one or more very long C-C bonds as a result of the steric strain between juxtaposed diamondoid groups. Some of the C-C bonds are elongated by up to 0.17 Å compared to a "normal" C-C bond. These structures provide a harsh test of dispersion-corrected DFT methods by probing their ability to capture the effects of very close contacts on covalent bonding. Schreiner et al. found that dispersion-corrections were required in order for DFT methods to attain reasonable agreement with the experimentally determined, long C-C bond lengths in the coupled diamondoid systems. Interestingly, most of the DFT methods applied to the rotation barrier about the elongated C-C bond, including those without dispersion-corrections, predicted values in reasonable agreement with the experimentally derived values, most likely because of error cancellation.

The foregoing discussion reminds us that dispersion-corrections are important in the modeling of some, but not all, physical systems. Until underlying functionals themselves are improved, the value derived from dispersion-correction DFT methods will be limited.

In this connection, we remind the reader that the Minnesota functionals considers this by fitting a highly parameterized functional to a broad set of benchmark data that includes thermochemical and kinetic information in addition to noncovalent binding energies. There also seems to be some promise for the application of potential-based correction methods to offer improvements to underlying problems with functionals beyond noncovalent interactions. Since the DCP and DCACP approaches alter electron distributions, it follows that they may be utilized to provide better descriptions of more than just noncovalent binding energies. von Lilienfeld recently demonstrated how DCACPs can be used with the BLYP functional to give molecular vibrational frequencies that are of B3LYP quality, and closer to experimental values.<sup>323</sup> DiLabio and Koleini developed DCPs for use with LC- $\omega$ PBE that, in addition to very good binding energies in noncovalently bonded systems (see Tables V, VI, and VII), are capable of providing excellent bond dissociation enthalpies for X-H and X-Y covalent bonds (X,Y = C, N, O).<sup>243</sup>

We expect that the future development of approximate DFT methods will continue to include the accurate treatment of noncovalent interactions, with near-term focus on many-body effects and on regions intermediate to the covalent and noncovalent bonding regimes. Furthermore, we expect the development of less-empirical and more efficient approaches to dispersion-corrected DFT with the evolution of more detailed understanding of how exchange and correlation functionals interplay in the treatment of noncovalent interactions. Ultimately, considerations of the broader performance of DFT methods for thermochemical, kinetics and other properties should remain the priority.

## REFERENCES

- <sup>1</sup>P. Hohenberg and W. Kohn, *Phys. Rev.*, **136**, B864 (1964). Inhomogeneous Electron Gas.
- <sup>2</sup>W. Kohn and L. J. Sham, *Phys. Rev.*, **140**, 1133 (1965). Self-Consistent Equations Including Exchange and Correlation Effects.
- <sup>3</sup>R. G. Parr and W. Yang, *Density Functional Theory of Atoms and Molecules*, Oxford University Press, New York, 1989.
- <sup>4</sup>R. M. Dreizler and E. K. V. Gross, *Density Functional Theory*, Springer, Berlin, 1990.
- <sup>5</sup>W. Koch and M. C. Holthausen, *A Chemist's Guide to Density Functional Theory*, Wiley-VCH, Weinheim, 2001.
- <sup>6</sup>K. Burke et al., *The ABC of DFT*, Published online at [dft.uci.edu](http://dft.uci.edu), 2007.
- <sup>7</sup>S. Cottenier, *Density Functional Theory and the Family of (L)APW-Methods: a Step-by-Step Introduction*, to be found at <http://www.wien2k.at/reguser/textbooks>, Instituut voor Kern- en Stralingsfysica, K.U.Leuven, Belgium, 2002.
- <sup>8</sup>C. Fiolhais, F. Nogueira, and M. A. Marques, *A Primer in Density Functional Theory*, Springer, 2003.
- <sup>9</sup>D. Sholl and J. Steckel, *Density Functional Theory: A Practical Introduction*, Wiley-Interscience, 2009.
- <sup>10</sup>R. Martin, *Electronic Structure: Basic Theory and Practical Methods*, Cambridge University Press, 2004.
- <sup>11</sup>In the context of the this chapter, we will refer to DFT methods that do not explicitly incorporate corrections for dispersion forces as “conventional” functionals or methods. Other authors use the descriptor “standard” [S. Grimme, *WIREs Comput. Mol. Sci.* **1**, 211 (2011)] in this connection.

- <sup>12</sup>A. J. Cohen, P. Mori-Sánchez, and W. Yang, *Science*, **321**, 792 (2008). Insights into Current Limitations of Density Functional Theory.
- <sup>13</sup>A. J. Cohen, P. Mori-Sánchez, and W. Yang, *Chem. Rev.*, **112**, 289 (2011). Challenges for Density Functional Theory.
- <sup>14</sup>K. Burke, *J. Chem. Phys.*, **136**, 150901 (2012). Perspective on Density Functional Theory.
- <sup>15</sup>D. J. Lacks and R. G. Gordon, *Phys. Rev. A*, **47**, 4681 (1993). Pair Interactions of Rare-Gas Atoms as a Test of Exchange-Energy-Density Functionals in Regions of Large Density Gradients.
- <sup>16</sup>S. Kristyán and P. Pulay, *Chem. Phys. Lett.*, **229**, 175 (1994). Can (Semi) Local Density Functional Theory Account for the London Dispersion Forces?
- <sup>17</sup>P. Hobza, J. Šponer, and T. Reschel, *J. Comput. Chem.*, **16**, 1315 (1995). Density Functional Theory and Molecular Clusters.
- <sup>18</sup>J. Šponer, J. Leszczynski, and P. Hobza, *J. Comput. Chem.*, **17**, 841 (1996). Base Stacking in Cytosine Dimer. A Comparison of Correlated Ab Initio Calculations with Three Empirical Potential Models and Density Functional Theory Calculations.
- <sup>19</sup>J. Pérez-Jordá and A. D. Becke, *Chem. Phys. Lett.*, **233**, 134 (1995). A Density-Functional Study of van der Waals Forces: Rare Gas Diatomics.
- <sup>20</sup>J. M. Pérez-Jordá, E. San-Fabián, and A. J. Pérez-Jiménez, *J. Chem. Phys.*, **110**, 1916 (1999). Density-Functional Study of van der Waals Forces on Rare-Gas Diatomics: Hartree-Fock Exchange.
- <sup>21</sup>O. Couronne and Y. Ellinger, *Chem. Phys. Lett.*, **306**, 71 (1999). An Ab Initio and DFT Study of (N<sub>2</sub>)<sub>2</sub> Dimers.
- <sup>22</sup>E. A. Johnson and G. A. DiLabio, *Chem. Phys. Lett.*, **419**, 333 (2006). Structure and Binding Energies in van der Waals Dimers: Comparison between Density Functional Theory and Correlated ab initio Methods.
- <sup>23</sup>R. A. DiStasio Jr., V. V. Gobre, and A. Tkatchenko, *Psi-k Newsletter*, **114**, 47 (2012). Many-body van der Waals Interactions in Biology, Chemistry, and Physics.
- <sup>24</sup>X. Xu and W. A. Goddard III, *J. Phys. Chem. A*, **108**, 2305 (2004). Bonding Properties of the Water Dimer: A Comparative Study of Density Functional Theories.
- <sup>25</sup>H. B. G. Casimir and D. Polder, *Phys. Rev.*, **73**, 360 (1948). The Influence of Retardation on the London-van der Waals Forces.
- <sup>26</sup>S. Grimme, *WIREs Comput. Mol. Sci.*, **1**, 211 (2011). Density Functional Theory with London Dispersion Corrections.
- <sup>27</sup>K. S. W. Sing, D. H. Everett, R. A. W. Haul, L. Moscou, R. A. Pierotti, J. Rouquérol, and T. Siemieniowska, *Pure Appl. Chem.*, **57**, 603 (1985). Reporting Physisorption Data for Gas/Solid Systems with Special Reference to the Determination of Surface Area and Porosity.
- <sup>28</sup>G. P. Lopinski, D. D. M. Wayner, and R. A. Wolkow, *Nature*, **6**, 48 (2000). Self-Directed Growth of Molecular Nanostructures on Silicon.
- <sup>29</sup>G. A. DiLabio, P. G. Piva, P. Kruse, and R. A. Wolkow, *J. Am. Chem. Soc.*, **126**, 16048 (2004). Dispersion Interactions Enable the Self-Directed Growth of Linear Alkane Nanostructures Covalently Bound to Silicon.
- <sup>30</sup>K. Autumn, M. Sitti, Y. A. Liang, A. M. Peattie, W. R. Hansen, S. Sponberg, T. W. Kenny, R. Fearing, J. N. Israelachvili, and R. J. Full, *Proc. Natl. Acad. Sci. U.S.A.*, **99**, 12252 (2002). Evidence for van der Waals Adhesion in Gecko Setae.
- <sup>31</sup>J. N. Munday, F. Capasso, and V. A. Parsegian, *Nature*, **457**, 170 (2009). Measured Long-Range Repulsive Casimir-Lifshitz Forces.



- <sup>32</sup>P. Muller, *Pure Appl. Chem.*, **66**, 1077 (1994). Glossary of Terms Used in Physical Organic Chemistry.
- <sup>33</sup>L. Pauling, R. B. Corey, and H. R. Branson, *Proc. Natl. Acad. Sci. U.S.A.*, **37**, 205 (1952). The Structure of Proteins: Two Hydrogen-Bonded Helical Configurations of the Polypeptide Chain.
- <sup>34</sup>J. D. Watson and F. H. C. Crick, *Nature*, **171**, 737 (1953). A Structure for Deoxyribose Nucleic Acid.
- <sup>35</sup>G. Litwinienko, G. A. DiLabio, P. Mulder, H.-G. Korth, and K. U. Ingold, *J. Phys. Chem. A*, **113**, 6275 (2009). Intramolecular and Intermolecular Hydrogen Bond Formation by Some Ortho-Substituted Phenols: Some Surprising Results from an Experimental and Theoretical Investigation.
- <sup>36</sup>R. M. Badger and S. H. Bauer, *J. Chem. Phys.*, **5**, 839 (1937). Spectroscopic Studies of the Hydrogen Bond. II. The Shift of the O-H Vibrational Frequency in the Formation of the Hydrogen Bond.
- <sup>37</sup>G. A. Jeffrey, *An Introduction to Hydrogen Bonding.*, Oxford University Press, 1997.
- <sup>38</sup>S. Scheiner, *Hydrogen Bonding: A Theoretical Perspective*, Oxford University Press, 1997.
- <sup>39</sup>M. C. Etter, *Acc. Chem. Res.*, **23**, 120 (1990). Encoding and Decoding Hydrogen-Bond Patterns of Organic Compounds.
- <sup>40</sup>M. Salamone, G. A. DiLabio, and M. Bietti, *J. Am. Chem. Soc.*, **133**, 16625 (2011). Hydrogen Atom Abstraction Selectivity in the Reactions of Alkylamines with the Benzoyloxy and Cumyloxy Radicals. The Importance of Structure and of Substrate Radical Hydrogen Bonding.
- <sup>41</sup>E. R. Johnson, M. Salamone, M. Bietti, and G. A. DiLabio, *J. Phys. Chem. A*, **117**, 947 (2013). Modeling Noncovalent Radical-Molecule Interactions Using Conventional Density-Functional Theory: Beware Erroneous Charge Transfer.
- <sup>42</sup>C. R. Patrick and G. S. Prosser, *Nature*, **187**, 1021 (1960). A Molecular Complex of Benzene and Hexafluorobenzene.
- <sup>43</sup>D. Dougherty, *Science*, **271**, 163 (1996). Cation- $\pi$  Interactions in Chemistry and Biology: a new View of Benzene, Phe, Tyr, and Trp.
- <sup>44</sup>D. Quiñero, C. Garau, C. Rotger, P. Frontera, A. Ballester, A. Costa, and P. M. Deyá, *Angew. Chem. Int. Ed.*, **41**, 3389 (2002). Anion- $\pi$  Interactions: Do They Exist?
- <sup>45</sup>B. L. Schottel, H. T. Chifotides, and K. R. Dunbar, *Chem. Soc. Rev.*, **37**, 68 (2008). Anion- $\pi$  Interactions.
- <sup>46</sup>B. L. Schottel, H. T. Chifotides, and K. R. Dunbar, *Angew. Chem. Int. Ed.*, **43**, 4650 (2004). Halide Recognition through Diagnostic “Anion- $\pi$ ” Interactions: Molecular Complexes of Cl<sup>-</sup>, Br<sup>-</sup>, and I<sup>-</sup> with Olefinic and Aromatic  $\pi$  Receptors.
- <sup>47</sup>P. Metrangola, H. Neukirch, T. Pilati, and G. Resnati, *Acc. Chem. Res.*, **38**, 386 (2005). Halogen Bonding Based Recognition Processes: A World Parallel to Hydrogen Bonding.
- <sup>48</sup>S. Kozuch and J. M. L. Martin, *J. Chem. Theory Comput.*, **9**, 1918 (2013). Halogen Bonds: Benchmark and Theoretical Analysis.
- <sup>49</sup>B. Pinter, N. Nagels, W. A. Herrebout, and F. De Proft, *Chem. Phys. Phys. Chem.*, **19**, 519 (2013). Halogen Bonding from a Hard and Soft Acids and Bases Perspective: Investigation by Using Density Functional Theory Reactivity Indices.
- <sup>50</sup>R. S. Mulliken, C. A. Rieke, and W. G. Brown, *J. Am. Chem. Soc.*, **63**, 41 (1941). Hyperconjugation.
- <sup>51</sup>A. Szabo and N. S. Ostlund, *Modern Quantum Chemistry*, Dover Publications, 1996.
- <sup>52</sup>T. Helgaker, P. Jorgensen, and J. Olsen, *Molecular Electronic-Structure Theory*, Wiley,

- 2013.
- <sup>53</sup>L. H. Thomas, *Proc. Cambridge Phil. Soc.*, **23**, 542 (1927). The Calculation of Atomic Fields.
- <sup>54</sup>E. Fermi, *Rend. Accad. Naz. Lincei*, **6**, 602 (1927). Un Metodo Statistico per la Determinazione di Alcune Proprietà dell'Atomo.
- <sup>55</sup>E. Teller, *Rev. Mod. Phys.*, **34**, 627 (1962). On the Stability of Molecules in the Thomas-Fermi Theory.
- <sup>56</sup>E. H. Lieb and B. Simon, *Adv. Math.*, **23**, 22 (1977). The Thomas-Fermi Theory of Atoms, Molecules and Solids.
- <sup>57</sup>D. M. Ceperley and B. J. Alder, *Phys. Rev. Lett.*, **45**, 566 (1980). Ground State of the Electron Gas by a Stochastic Method.
- <sup>58</sup>S. H. Vosko, L. Wilk, and M. Nusair, *Can. J. Phys.*, **58**, 1200 (1980). Accurate Spin-Dependent Electron Liquid Correlation Energies for Local Spin Density Calculations: a Critical Analysis.
- <sup>59</sup>J. P. Perdew and A. Zunger, *Phys. Rev. B*, **23**, 5048 (1981). Self-Interaction Correction to Density-Functional Approximations for Many-Electron Systems.
- <sup>60</sup>J. Perdew, K. Burke, and M. Ernzerhof, *Phys. Rev. Lett.*, **77**, 3865 (1996). Generalized Gradient Approximation Made Simple.
- <sup>61</sup>Y. Zhang and W. Yang, *Phys. Rev. Lett.*, **80**, 890 (1998). Comment on "Generalized Gradient Approximation Made Simple".
- <sup>62</sup>J. Perdew, A. Ruzsinszky, G. Csonka, O. Vydrov, G. Scuseria, L. Constantin, X. Zhou, and K. Burke, *Phys. Rev. Lett.*, **100**, 136406 (2008). Restoring the Density-Gradient Expansion for Exchange in Solids and Surfaces.
- <sup>63</sup>J. Perdew and W. Yue, *Phys. Rev. B*, **33**, 8800 (1986). Accurate and Simple Density Functional for the Electronic Exchange Energy: Generalized Gradient Approximation.
- <sup>64</sup>A. Becke, *J. Chem. Phys.*, **85**, 7184 (1986). On the Large-Gradient Behavior of the Density Functional Exchange Energy.
- <sup>65</sup>A. D. Becke, *Phys. Rev. A*, **38**, 3098 (1988). Density-Functional Exchange-Energy Approximation with Correct Asymptotic Behavior.
- <sup>66</sup>C. Lee, W. Yang, and R. G. Parr, *Phys. Rev. B*, **37**, 785 (1988). Development of the Colle-Salvetti Correlation-Energy Formula into a Functional of the Electron Density.
- <sup>67</sup>J. Tao, J. P. Perdew, V. N. Staroverov, and G. E. Scuseria, *Phys. Rev. Lett.*, **91**, 146401 (2003). Climbing the Density Functional Ladder: Nonempirical Meta-Generalized Gradient Approximation Designed for Molecules and Solids.
- <sup>68</sup>J. P. Perdew, A. Ruzsinszky, G. I. Csonka, L. A. Constantin, and J. Sun, *Phys. Rev. Lett.*, **103**, 026403 (2009). Workhorse Semilocal Density Functional for Condensed Matter Physics and Quantum Chemistry.
- <sup>69</sup>J. Sun, B. Xiao, Y. Fang, R. Haunschild, P. Hao, A. Ruzsinszky, G. I. Csonka, G. E. Scuseria, and J. P. Perdew, *Phys. Rev. Lett.*, **111**, 106401 (2013). Density Functionals that Recognize Covalent, Metallic, and Weak Bonds.
- <sup>70</sup>J. P. Perdew, *MRS bull.*, **38**, 743 (2013). Climbing the Ladder of Density Functional Approximations.
- <sup>71</sup>R. Peverati and D. G. Truhlar, *Phys. Chem. Chem. Phys.*, **14**, 13171 (2012). An Improved and Broadly Accurate Local Approximation to the Exchange-Correlation Density Functional: The MN12-L Functional for Electronic Structure Calculations in Chemistry and Physics.
- <sup>72</sup>R. Peverati and D. G. Truhlar, *J. Chem. Theory Comput.*, **8**, 2310 (2012). Exchange-

Correlation Functional with Good Accuracy for Both Structural and Energetic Properties while Depending Only on the Density and Its Gradient.

- <sup>73</sup>R. Peverati and D. G. Truhlar, *Phys. Chem. Chem. Phys.*, **14**, 16187 (2012). Screened-Exchange Density Functionals with Broad Accuracy for Chemistry and Solid-State Physics.
- <sup>74</sup>A. D. Becke, *J. Chem. Phys.*, **98**, 1372 (1993). A New Mixing of Hartree-Fock and Local Density-Functional Theories.
- <sup>75</sup>J. Harris and R. Jones, *J. Phys. F: Met. Phys.*, **4**, 1170 (1974). The Surface Energy of a Bounded Electron Gas.
- <sup>76</sup>O. Gunnarsson and B. I. Lundqvist, *Phys. Rev. B*, **13**, 4274 (1976). Exchange and Correlation in Atoms, Molecules, and Solids by the Spin-Density-Functional Formalism.
- <sup>77</sup>D. C. Langreth and J. P. Perdew, *Phys. Rev. B*, **15**, 2884 (1977). Exchange-Correlation Energy of a Metallic Surface: Wave-Vector Analysis.
- <sup>78</sup>A. D. Becke, *J. Chem. Phys.*, **98**, 5648 (1993). Density-Functional Thermochemistry. III. The Role of Exact Exchange.
- <sup>79</sup>J. P. Perdew, M. Ernzerhof, and K. Burke, *J. Chem. Phys.*, **105**, 9982 (1996). Rationale for Mixing Exact Exchange with Density Functional Approximations.
- <sup>80</sup>C. Adamo and V. Barone, *J. Chem. Phys.*, **110**, 6158 (1999). Toward Reliable Density Functional Methods without Adjustable Parameters: The PBE0 Model.
- <sup>81</sup>J. P. Perdew, *Phys. Rev. B*, **33**, 8822 (1986). Density-Functional Approximation for the Correlation Energy of the Inhomogeneous Electron Gas.
- <sup>82</sup>H. J. Monkhorst, *Phys. Rev. B*, **20**, 1504 (1979). Hartree-Fock Density of States for Extended Systems.
- <sup>83</sup>B. G. Janesko, T. M. Henderson, and G. E. Scuseria, *Phys. Chem. Chem. Phys.*, **11**, 443 (2009). Screened Hybrid Density Functionals for Solid-State Chemistry and Physics.
- <sup>84</sup>A. Savin, *Beyond the Kohn-Sham Determinant*, Recent Advances in Density Functional Methods, Part I (ed. D. P. Chong), World Scientific, 1995.
- <sup>85</sup>A. Savin, *On Degeneracy, Near-Degeneracy and Density Functional Theory*, Recent Developments and Applications of Modern Density Functional Theory (ed. J. M. Seminario), Elsevier, 1996.
- <sup>86</sup>P. M. Gill, R. D. Adamson, and J. A. Pople, *Mol. Phys.*, **88**, 1005 (1996). Coulomb-Attenuated Exchange Energy Density Functionals.
- <sup>87</sup>O. A. Vydrov and G. E. Scuseria, *J. Chem. Phys.*, **125**, 234109 (2006). Assessment of a Long-Range Corrected Hybrid Functional.
- <sup>88</sup>O. A. Vydrov, J. Heyd, A. V. Krukau, and G. E. Scuseria, *J. Chem. Phys.*, **125**, 074106 (2006). Importance of Short-Range versus Long-Range Hartree-Fock Exchange for the Performance of Hybrid Density Functionals.
- <sup>89</sup>T. Yanai, D. P. Tew, and N. C. Handy, *Chem. Phys. Lett.*, **393**, 51 (2004). A New Hybrid Exchange-Correlation Functional Using the Coulomb-Attenuating Method (CAM-B3LYP).
- <sup>90</sup>J.-D. Chai and M. Head-Gordon, *J. Chem. Phys.*, **128**, 084106 (2008). Systematic Optimization of Long-Range Corrected Hybrid Density Functionals.
- <sup>91</sup>J. Heyd, G. E. Scuseria, and M. Ernzerhof, *J. Chem. Phys.*, **118**, 8207 (2003). Hybrid Functionals Based on a Screened Coulomb Potential.
- <sup>92</sup>A. V. Krukau, O. A. Vydrov, A. F. Izmaylov, and G. E. Scuseria, *J. Chem. Phys.*, **125**, 224106 (2006). Influence of the Exchange Screening Parameter on the Performance of Screened Hybrid Functionals.

- <sup>93</sup>J. Heyd and G. E. Scuseria, *J. Chem. Phys.*, **121**, 1187 (2004). Efficient Hybrid Density Functional Calculations in Solids: Assessment of the Heyd–Scuseria–Ernzerhof Screened Coulomb Hybrid Functional.
- <sup>94</sup>M. A. L. Marques, C. A. Ullrich, F. Nogueira, A. Rubio, K. Burke, and E. K. U. Gross, Eds., *Time-Dependent Density Functional Theory*, Springer, 2006.
- <sup>95</sup>E. Runge and E. K. Gross, *Phys. Rev. Lett.*, **52**, 997 (1984). Density-Functional Theory for Time-Dependent Systems.
- <sup>96</sup>J. Slater, *The Self-Consistent Field for Molecules and Solids*, number v. 4 in Quantum theory of molecules and solids, McGraw-Hill, 1974.
- <sup>97</sup>Y. Zhao and D. G. Truhlar, *J. Chem. Phys.*, **125**, 194101 (2006). A New Local Density Functional for Main-Group Thermochemistry, Transition Metal Bonding, Thermochemical Kinetics, and Noncovalent Interactions.
- <sup>98</sup>F. Hamprecht, A. Cohen, D. Tozer, and N. Handy, *J. Chem. Phys.*, **109**, 6264 (1998). Development and Assessment of New Exchange–Correlation Functionals.
- <sup>99</sup>A. Otero-de-la Roza and E. R. Johnson, *J. Chem. Phys.*, **138**, 204109 (2013). Non-Covalent Interactions and Thermochemistry Using XDM-Corrected Hybrid and Range-Separated Hybrid Density Functionals.
- <sup>100</sup>L. A. Curtiss, K. Raghavachari, P. C. Redfern, and J. A. Pople, *J. Chem. Phys.*, **112**, 7374 (2000). Assessment of Gaussian-3 and Density Functional Theories for a Larger Experimental Test Set.
- <sup>101</sup>E. R. Johnson, O. J. Clarkin, and G. A. DiLabio, *J. Phys. Chem. A*, **107**, 9953 (2003). Density Functional Theory Based Model Calculations for Accurate Bond Dissociation Enthalpies. 3. A Single Approach for XH, XX, and XY (X, Y= C, N, O, S, Halogen) Bonds.
- <sup>102</sup>B. J. Lynch and D. G. Truhlar, *J. Phys. Chem. A*, **105**, 2936 (2001). How Well Can Hybrid Density Functional Methods Predict Transition State Geometries and Barrier Heights?
- <sup>103</sup>M. D. Wodrich, C. Corminboeuf, and P. v. R. Schleyer, *Org. Lett.*, **8**, 3631 (2006). Systematic Errors in Computed Alkane Energies Using B3LYP and Other Popular DFT Functionals.
- <sup>104</sup>L. A. Curtiss, P. C. Redfern, K. Raghavachari, and J. A. Pople, *J. Chem. Phys.*, **114**, 108 (2001). Gaussian-3X (G3X) Theory: Use of Improved Geometries, Zero-Point Energies, and Hartree-Fock Basis Sets.
- <sup>105</sup>S. Grimme, M. Steinmetz, and M. Korth, *J. Org. Chem.*, **72**, 2118 (2007). How to Compute Isomerization Energies of Organic Molecules with Quantum Chemical Methods.
- <sup>106</sup>Y. Zhao and D. Truhlar, *J. Chem. Theory Comput.*, **1**, 415 (2005). Benchmark Databases for Nonbonded Interactions and their Use to Test Density Functional Theory.
- <sup>107</sup>E. R. Johnson and A. D. Becke, *Can. J. Chem.*, **87**, 1369 (2009). Tests of an Exact-Exchange-Based Density-Functional Theory on Transition-Metal Complexes.
- <sup>108</sup>J. Hepburn, G. Scoles, and R. Penco, *Chem. Phys. Lett.*, **36**, 451 (1975). A Simple but Reliable Method for the Prediction of Intermolecular Potentials.
- <sup>109</sup>C. D. Sherrill, T. Takatani, and E. G. Hohenstein, *J. Phys. Chem. A*, **113**, 10146 (2009). An Assessment of Theoretical Methods for Nonbonded Interactions: Comparison to Complete Basis Set Limit Coupled-Cluster Potential Energy Curves for the Benzene Dimer, the Methane Dimer, Benzene-Methane, and Benzene-H<sub>2</sub>S.
- <sup>110</sup>C. Kittel, *Introduction to Solid State Physics*, John Wiley & Sons, New York, 8th ed., 1996.
- <sup>111</sup>E. R. Johnson, I. D. Mackie, and G. A. DiLabio, *J. Phys. Org. Chem.*, **22**, 1127 (2009).

- Dispersion Interactions in Density-Functional Theory.
- <sup>112</sup>F. Ortmann, F. Bechstedt, and W. G. Schmidt, *Phys. Rev. B*, **73**, 205101 (2006). Semiempirical van der Waals Correction to the Density Functional Description of Solids and Molecular Structures.
- <sup>113</sup>S. M. Cybulski and M. L. Lytle, *J. Chem. Phys.*, **127**, 141102 (2007). The Origin of Deficiency of the Supermolecule Second-Order Møller-Plesset Approach for Evaluating Interaction Energies.
- <sup>114</sup>A. Tkatchenko, R. A. DiStasio Jr., M. Head-Gordon, and M. Scheffler, *J. Chem. Phys.*, **131**, 094106 (2009). Dispersion-Corrected Møller-Plesset Second-Order Perturbation Theory.
- <sup>115</sup>J. C. Grossman, E. Schwegler, E. W. Draeger, F. Gygi, and G. Galli, *J. Chem. Phys.*, **120**, 300 (2004). Towards an Assessment of the Accuracy of Density Functional Theory for First Principles Simulations of Water.
- <sup>116</sup>B. Santra, J. c. v. Klimeš, D. Alfè, A. Tkatchenko, B. Slater, A. Michaelides, R. Car, and M. Scheffler, *Phys. Rev. Lett.*, **107**, 185701 (2011). Hydrogen Bonds and van der Waals Forces in Ice at Ambient and High Pressures.
- <sup>117</sup>B. Santra, A. Michaelides, and M. Scheffler, *J. Chem. Phys.*, **127**, 184104 (2007). On the Accuracy of Density-Functional Theory Exchange-Correlation Functionals for H-Bonds in Small Water Clusters: Benchmarks Approaching the Complete Basis Set Limit.
- <sup>118</sup>P. W. Atkins and R. S. Friedman, *Molecular Quantum Mechanics*, Oxford University Press, New York, 4th ed., 2005.
- <sup>119</sup>J. Tao, J. P. Perdew, and A. Ruzsinszky, *Proc. Natl. Acad. Sci. U.S.A.*, **109**, 18 (2012). Accurate van der Waals Coefficients from Density Functional Theory.
- <sup>120</sup>M. Zgarbová, M. Otyepka, J. Šponer, P. Hobza, and P. Jurečka, *Phys. Chem. Chem. Phys.*, **12**, 10476 (2010). Large-Scale Compensation of Errors in Pairwise-Additive Empirical Force Fields: Comparison of AMBER Intermolecular Terms with Rigorous DFT-SAPT Calculations.
- <sup>121</sup>E. R. Johnson and A. D. Becke, *J. Chem. Phys.*, **124**, 174104 (2006). A Post-Hartree-Fock Model of Intermolecular Interactions: Inclusion of Higher-Order Corrections.
- <sup>122</sup>R. Ahlrichs, R. Penco, and G. Scoles, *Chem. Phys.*, **19**, 119 (1977). Intermolecular Forces in Simple Systems.
- <sup>123</sup>R. G. Gordon and Y. S. Kim, *J. Chem. Phys.*, **56**, 3122 (1972). Theory for the Forces between Closed-Shell Atoms and Molecules.
- <sup>124</sup>A. Rae, *Chem. Phys. Lett.*, **18**, 574 (1973). A Theory for the Interactions between Closed Shell Systems.
- <sup>125</sup>J. S. Cohen and R. T. Pack, *J. Chem. Phys.*, **61**, 2372 (1974). Modified Statistical Method for Intermolecular Potentials. Combining Rules for Higher van der Waals Coefficients.
- <sup>126</sup>T. A. Halgren, *J. Am. Chem. Soc.*, **114**, 7827 (1992). The Representation of van der Waals (vdW) Interactions in Molecular Mechanics Force Fields: Potential Form, Combination Rules, and vdW Parameters.
- <sup>127</sup>B. R. Brooks, C. L. Brooks, III, A. D. Mackerell, Jr., L. Nilsson, R. J. Petrella, B. Roux, Y. Won, G. Archontis, C. Bartels, S. Boresch, A. Caffisch, L. Caves, Q. Cui, A. R. Dinner, M. Feig, S. Fischer, J. Gao, M. Hodoscek, W. Im, K. Kuczera, T. Lazaridis, J. Ma, V. Ovchinnikov, E. Paci, R. W. Pastor, C. B. Post, J. Z. Pu, M. Schaefer, B. Tidor, R. M. Venable, H. L. Woodcock, X. Wu, W. Yang, D. M. York, and M. Karplus, *J. Comput. Chem.*, **30**, 1545 (2009). CHARMM: the Biomolecular Simulation Program.
- <sup>128</sup>D. A. Pearlman, D. A. Case, J. W. Caldwell, W. S. Ross, T. E. Cheatham III, S. DeBolt,

- D. Ferguson, G. Seibel, and P. Kollman, *Comput. Phys. Commun.*, **91**, 1 (1995). AMBER, a Package of Computer Programs for Applying Molecular Mechanics, Normal Mode Analysis, Molecular Dynamics and Free Energy Calculations to Simulate the Structural and Energetic Properties of Molecules.
- <sup>129</sup>F. Gianturco, F. Paesani, M. Laranjeira, V. Vassilenko, and M. Cunha, *J. Chem. Phys.*, **110**, 7832 (1999). Intermolecular Forces from Density Functional Theory. III. A Multi-property Analysis for the Ar ( $^1S$ )–CO ( $^1\Sigma$ ) Interaction.
- <sup>130</sup>M. Elstner, P. Hobza, T. Frauenheim, S. Suhai, and E. Kaxiras, *J. Chem. Phys.*, **114**, 5149 (2001). Hydrogen Bonding and Stacking Interactions of Nucleic Acid Base Pairs: A Density-Functional-Theory Based Treatment.
- <sup>131</sup>Q. Wu and W. Yang, *J. Chem. Phys.*, **116**, 515 (2002). Empirical Correction to Density Functional Theory for van der Waals Interactions.
- <sup>132</sup>X. Wu, M. Vargas, S. Nayak, V. Lotrich, and G. Scoles, *J. Chem. Phys.*, **115**, 8748 (2001). Towards Extending the Applicability of Density Functional Theory to Weakly Bound Systems.
- <sup>133</sup>J. C. Slater and J. G. Kirkwood, *Phys. Rev.*, **37**, 682 (1931). The van der Waals Forces in Gases.
- <sup>134</sup>G. Zeiss, W. J. Meath, J. MacDonald, and D. Dawson, *Can. J. Phys.*, **55**, 2080 (1977). Dipole Oscillator Strength Distributions, Sums, and Some Related Properties for Li, N, O, H<sub>2</sub>, N<sub>2</sub>, O<sub>2</sub>, NH<sub>3</sub>, H<sub>2</sub>O, NO, and N<sub>2</sub>O.
- <sup>135</sup>D. J. Margoliash and W. J. Meath, *J. Chem. Phys.*, **68**, 1426 (1978). Pseudospectral Dipole Oscillator Strength Distributions and Some Related Two Body Interaction Coefficients for H, He, Li, N, O, H<sub>2</sub>, N<sub>2</sub>, O<sub>2</sub>, NO, N<sub>2</sub>O, H<sub>2</sub>O, NH<sub>3</sub>, and CH<sub>4</sub>.
- <sup>136</sup>B. Jhanwar and W. J. Meath, *Mol. Phys.*, **41**, 1061 (1980). Pseudo-Spectral Dipole Oscillator Strength Distributions for the Normal Alkanes through Octane and the Evaluation of Some Related Dipole-Dipole and Triple-Dipole Dispersion Interaction Energy Coefficients.
- <sup>137</sup>B. Jhanwar and W. J. Meath, *Chem. Phys.*, **67**, 185 (1982). Dipole Oscillator Strength Distributions, Sums, and Dispersion Energy Coefficients for CO and CO<sub>2</sub>.
- <sup>138</sup>A. Kumar and W. J. Meath, *Mol. Phys.*, **54**, 823 (1985). Pseudo-Spectral Dipole Oscillator Strengths and Dipole-Dipole and Triple-Dipole Dispersion Energy Coefficients for HF, HCl, HBr, He, Ne, Ar, Kr and Xe.
- <sup>139</sup>A. Kumar and W. J. Meath, *Can. J. Chem.*, **63**, 1616 (1985). Integrated Dipole Oscillator Strengths and Dipole Properties for Ne, Ar, Kr, Xe, HF, HCl, and HBr.
- <sup>140</sup>A. Kumar and W. J. Meath, *Mol. Phys.*, **75**, 311 (1992). Dipole Oscillator Strength Properties and Dispersion Energies for Acetylene and Benzene.
- <sup>141</sup>A. Kumar, W. J. Meath, P. Bündgen, and A. J. Thakkar, *J. Chem. Phys.*, **105**, 4927 (1996). Reliable Anisotropic Dipole Properties, and Dispersion Energy Coefficients, for O<sub>2</sub> Evaluated Using Constrained Dipole Oscillator Strength Techniques.
- <sup>142</sup>A. Kumar and W. Meath, *Mol. Phys.*, **90**, 389 (1997). Isotropic Dipole Properties for Acetone, Acetaldehyde and Formaldehyde.
- <sup>143</sup>A. Kumar, *J. Mol. Struct. (THEOCHEM)*, **591**, 91 (2002). Reliable Isotropic Dipole Properties and Dispersion Energy Coefficients for CCl<sub>4</sub>.
- <sup>144</sup>M. Kumar, A. Kumar, and W. J. Meath, *Mol. Phys.*, **100**, 3271 (2002). Dipole Oscillator Strength Properties and Dispersion Energies for Cl<sub>2</sub>.
- <sup>145</sup>A. Kumar, M. Kumar, and W. J. Meath, *Chem. Phys.*, **286**, 227 (2003). Dipole Oscillator Strength Properties and Dispersion Energies for SiH<sub>4</sub>.

- <sup>146</sup>A. Kumar, M. Kumar, and W. J. Meath, *Mol. Phys.*, **101**, 1535 (2003). Dipole Oscillator Strengths, Dipole Properties and Dispersion Energies for SiF<sub>4</sub>.
- <sup>147</sup>S. Grimme, *J. Comput. Chem.*, **25**, 1463 (2004). Accurate Description of van der Waals Complexes by Density Functional Theory Including Empirical Corrections.
- <sup>148</sup>S. Grimme, *J. Comput. Chem.*, **27**, 1787 (2006). Semiempirical GGA-Type Density Functional Constructed with a Long-Range Dispersion Correction.
- <sup>149</sup>S. Grimme, J. Antony, S. Ehrlich, and H. Krieg, *J. Chem. Phys.*, **132**, 154104 (2010). A Consistent and Accurate ab initio Parametrization of Density Functional Dispersion Correction (DFT-D) for the 94 Elements H-Pu.
- <sup>150</sup>A. Tkatchenko and M. Scheffler, *Phys. Rev. Lett.*, **102**, 73005 (2009). Accurate Molecular van der Waals Interactions from Ground-State Electron Density and Free-Atom Reference Data.
- <sup>151</sup>J.-D. Chai and M. Head-Gordon, *Phys. Chem. Chem. Phys.*, **10**, 6615 (2008). Long-Range Corrected Hybrid Density Functionals with Damped Atom-Atom Dispersion Corrections.
- <sup>152</sup>J. F. Dobson and T. Gould, *J. Phys.: Condens. Matter*, **24**, 073201 (2012). Calculation of Dispersion Energies.
- <sup>153</sup>V. Barone, M. Casarin, D. Forrer, M. Pavone, M. Sambi, and A. Vittadini, *J. Comput. Chem.*, **30**, 934 (2009). Role and Effective Treatment of Dispersive Forces in Materials: Polyethylene and Graphite Crystals as Test Cases.
- <sup>154</sup>A. Otero-de-la Roza and E. R. Johnson, *J. Chem. Phys.*, **136**, 174109 (2012). Van der Waals Interactions in Solids Using the Exchange-Hole Dipole Moment Model.
- <sup>155</sup>E. R. Johnson, *J. Chem. Phys.*, **135**, 234109 (2011). Dependence of Dispersion Coefficients on Atomic Environment.
- <sup>156</sup>T. Thonhauser, V. Cooper, S. Li, A. Puzder, P. Hyldgaard, and D. Langreth, *Phys. Rev. B*, **76**, 125112 (2007). Van der Waals Density Functional: Self-Consistent Potential and the Nature of the Van der Waals Bond.
- <sup>157</sup>J. Kong, Z. Gan, E. Proynov, M. Freindorf, and T. Furlani, *Phys. Rev. A*, **79**, 042510 (2009). Efficient Computation of the Dispersion Interaction with Density-Functional Theory.
- <sup>158</sup>Y. Ikabata, T. Sato, and H. Nakai, *Int. J. Quantum Chem.*, **113**, 257 (2013). Self-Consistent Field Treatment and Analytical Energy Gradient of Local Response Dispersion Method.
- <sup>159</sup>É. Brémond, N. Golubev, S. N. Steinmann, and C. Corminboeuf, *J. Chem. Phys.*, **140**, 18A516 (2014). How Important is Self-Consistency for the dDsC Density Dependent Dispersion Correction?
- <sup>160</sup>A. D. Becke and E. R. Johnson, *J. Chem. Phys.*, **122**, 154104 (2005). Exchange-Hole Dipole Moment and the Dispersion Interaction.
- <sup>161</sup>A. D. Becke and E. R. Johnson, *J. Chem. Phys.*, **123**, 154101 (2005). A Density-Functional Model of the Dispersion Interaction.
- <sup>162</sup>E. R. Johnson and A. D. Becke, *J. Chem. Phys.*, **123**, 024101 (2005). A Post-Hartree-Fock Model of Intermolecular Interactions.
- <sup>163</sup>A. D. Becke and E. R. Johnson, *J. Chem. Phys.*, **124**, 014104 (2006). Exchange-Hole Dipole Moment and the Dispersion Interaction: High-Order Dispersion Coefficients.
- <sup>164</sup>E. R. Johnson and A. D. Becke, *Chem. Phys. Lett.*, **432**, 600 (2006). Van der Waals Interactions from the Exchange Hole Dipole Moment: Application to Bio-Organic Benchmark Systems.
- <sup>165</sup>A. D. Becke and E. R. Johnson, *J. Chem. Phys.*, **127**, 124108 (2007). A Unified Density-

- Functional Treatment of Dynamical, Nondynamical, and Dispersion Correlations.
- <sup>166</sup>A. D. Becke and E. R. Johnson, *J. Chem. Phys.*, **127**, 154108 (2007). Exchange-Hole Dipole Moment and the Dispersion Interaction Revisited.
- <sup>167</sup>F. O. Kannemann and A. D. Becke, *J. Chem. Theory Comput.*, **5**, 719 (2009). Van Der Waals Interactions in Density-Functional Theory: Rare-Gas Diatomics.
- <sup>168</sup>F. O. Kannemann and A. D. Becke, *J. Chem. Theory Comput.*, **6**, 1081 (2010). Van der Waals Interactions in Density-Functional Theory: Intermolecular Complexes.
- <sup>169</sup>A. Otero-de-la Roza and E. R. Johnson, *J. Chem. Phys.*, **138**, 054103 (2013). Many-Body Dispersion Interactions from the Exchange-Hole Dipole Moment Model.
- <sup>170</sup>F. L. Hirshfeld, *Theor. Chim. Acta*, **44**, 129 (1977). Bonded-Atom Fragments for Describing Molecular Charge Densities.
- <sup>171</sup>F. O. Kannemann and A. D. Becke, *J. Chem. Phys.*, **136**, 34109 (2012). Atomic Volumes and Polarizabilities in Density-Functional Theory.
- <sup>172</sup>A. D. Becke and M. R. Roussel, *Phys. Rev. A*, **39**, 3761 (1989). Exchange Holes in Inhomogeneous Systems: A Coordinate-Space Model.
- <sup>173</sup>B. M. Axilrod and E. Teller, *J. Chem. Phys.*, **11**, 299 (1943). Interaction of the van der Waals Type Between Three Atoms.
- <sup>174</sup>Y. Muto, *J. Phys. Math. Soc. Japan*, **17**, 629 (1943).
- <sup>175</sup>R. J. Bell, *J. Phys. B: At. Mol. Phys.*, **3**, 751 (1970). Multipolar Expansion for the Non-Additive Third-Order Interaction Energy of Three Atoms.
- <sup>176</sup>E. R. Johnson, A. Otero-de-la Roza, S. G. Dale, and G. A. DiLabio, *J. Chem. Phys.*, **139**, 214109 (2013). Efficient Basis Sets for Non-Covalent Interactions in XDM-Corrected Density-Functional Theory.
- <sup>177</sup>[http://gatsby.ucmerced.edu/wiki/Benchmark\\_data](http://gatsby.ucmerced.edu/wiki/Benchmark_data).
- <sup>178</sup>A. Otero-de-la Roza and E. R. Johnson, *J. Chem. Phys.*, **137**, 054103 (2012). A Benchmark for Non-Covalent Interactions in Solids.
- <sup>179</sup>E. R. Johnson and A. Otero-de-la Roza, *J. Chem. Theory Comput.*, **8**, 5124 (2012). Adsorption of Organic Molecules on Kaolinite from the Exchange-Hole Dipole Moment Dispersion Model.
- <sup>180</sup>G. A. DiLabio, E. R. Johnson, and A. Otero-de-la Roza, *Phys. Chem. Chem. Phys.*, **15**, 12821 (2013). Performance of Conventional and Dispersion-Corrected Density-Functional Theory Methods for Hydrogen Bonding Interaction Energies.
- <sup>181</sup>Z. Ye, A. Otero-de-la Roza, E. R. Johnson, and A. Martini, *Appl. Phys. Lett.*, **103**, 081601 (2013). Effect of Tip Shape on Atomic-Friction at Graphite Step Edges.
- <sup>182</sup>C. Isborn, C. Tang, A. Martini, E. R. Johnson, A. Otero-de-la Roza, and V. Tung, *J. Phys. Chem. Lett.*, **4**, 2914 (2013). Carbon Nanotube Chirality Determines Efficiency of Electron Transfer to Fullerene in All-Carbon Photovoltaics.
- <sup>183</sup>A. Otero-de-la Roza, J. D. Mallory, and E. R. Johnson, *J. Chem. Phys.*, **140**, 18A504 (2014). Metallophilic Interactions from Dispersion-Corrected Density-Functional Theory.
- <sup>184</sup>M. J. Frisch, G. W. Trucks, H. B. Schlegel, G. E. Scuseria, M. A. Robb, J. R. Cheeseman, G. Scalmani, V. Barone, B. Mennucci, G. A. Petersson, H. Nakatsuji, M. Caricato, X. Li, H. P. Hratchian, A. F. Izmaylov, J. Bloino, G. Zheng, J. L. Sonnenberg, M. Hada, M. Ehara, K. Toyota, R. Fukuda, J. Hasegawa, M. Ishida, T. Nakajima, Y. Honda, O. Kitao, H. Nakai, T. Vreven, J. A. Montgomery, Jr., J. E. Peralta, F. Ogliaro, M. Bearpark, J. J. Heyd, E. Brothers, K. N. Kudin, V. N. Staroverov, R. Kobayashi, J. Normand, K. Raghavachari, A. Rendell, J. C. Burant, S. S. Iyengar, J. Tomasi, M. Cossi, N. Rega, J. M. Millam, M. Klene, J. E. Knox, J. B. Cross, V. Bakken, C. Adamo, J. Jaramillo,



- R. Gomperts, R. E. Stratmann, O. Yazyev, A. J. Austin, R. Cammi, C. Pomelli, J. W. Ochterski, R. L. Martin, K. Morokuma, V. G. Zakrzewski, G. A. Voth, P. Salvador, J. J. Dannenberg, S. Dapprich, A. D. Daniels, O. Farkas, J. B. Foresman, J. V. Ortiz, J. Cioslowski, and D. J. Fox, Gaussian 09 Revision A.1x.
- <sup>185</sup>P. Giannozzi, S. Baroni, N. Bonini, M. Calandra, R. Car, C. Cavazzoni, D. Ceresoli, G. L. Chiarotti, M. Cococcioni, I. Dabo, A. Dal Corso, S. de Gironcoli, S. Fabris, G. Fratesi, R. Gebauer, U. Gerstmann, C. Gougoussis, A. Kokalj, M. Lazzeri, L. Martin-Samos, N. Marzari, F. Mauri, R. Mazzarello, S. Paolini, A. Pasquarello, L. Paulatto, C. Sbraccia, S. Scandolo, G. Sclauzero, A. P. Seitsonen, A. Smogunov, P. Umari, and R. M. Wentzcovitch, *J. Phys.: Condens. Matter*, **21**, 395502 (2009). QUANTUM ESPRESSO: a Modular and Open-Source Software Project for Quantum Simulations of Materials.
- <sup>186</sup>Y. Shao, L. F. Molnar, Y. Jung, J. Kussmann, C. Ochsenfeld, S. T. Brown, A. T. Gilbert, L. V. Slipchenko, S. V. Levchenko, D. P. O'Neill, R. A. DiStasio Jr., R. C. Lochan, T. Wang, G. J. Beran, N. A. Besley, J. M. Herbert, C. Yeh Lin, T. Van Voorhis, S. Hung Chien, A. Sodt, R. P. Steele, V. A. Rassolov, P. E. Maslen, P. P. Korambath, R. D. Adamson, B. Austin, J. Baker, E. F. C. Byrd, H. Dachsel, R. J. Doerksen, A. Dreuw, B. D. Dunietz, A. D. Dutoi, T. R. Furlani, S. R. Gwaltney, A. Heyden, S. Hirata, C.-P. Hsu, G. Kedziora, R. Z. Khalliulin, P. Klunzinger, A. M. Lee, M. S. Lee, W. Liang, I. Lotan, N. Nair, B. Peters, E. I. Proynov, P. A. Pieniazek, Y. Min Rhee, J. Ritchie, E. Rosta, C. David Sherrill, A. C. Simmonett, J. E. Subotnik, H. Lee Woodcock III, W. Zhang, A. T. Bell, A. K. Chakraborty, D. M. Chipman, F. J. Keil, A. Warshel, W. J. Hehre, H. F. Schaefer III, J. Kong, A. I. Krylov, P. M. W. Gill, and M. Head-Gordon, *Phys. Chem. Chem. Phys.*, **8**, 3172 (2006). Advances in Methods and Algorithms in a Modern Quantum Chemistry Program Package.
- <sup>187</sup>L. Goerigk and S. Grimme, *Phys. Chem. Chem. Phys.*, **13**, 6670 (2011). A Thorough Benchmark of Density Functional Methods for General Main Group Thermochemistry, Kinetics, and Noncovalent Interactions.
- <sup>188</sup>M. W. Schmidt, K. K. Baldridge, J. A. Boatz, S. T. Elbert, M. S. Gordon, J. H. Jensen, S. Koseki, N. Matsunaga, K. A. Nguyen, S. Su, T. L. Windus, M. Dupuis, and J. A. Montgomery, *J. Comput. Chem.*, **14**, 1347 (1993). General Atomic and Molecular Electronic Structure System.
- <sup>189</sup>M. S. Gordon and M. W. Schmidt, *Advances in Electronic Structure Theory: GAMESS a Decade Later*, Theory and Applications of Computational Chemistry: the First Forty Years (ed. C. E. Dykstra, G. Frenking, K. S. Kim, and G. E. Scuseria), Elsevier, Amsterdam, 2005.
- <sup>190</sup>M. Valiev, E. J. Bylaska, N. Govind, K. Kowalski, T. P. Straatsma, H. J. J. Van Dam, D. Wang, J. Nieplocha, E. Apra, T. L. Windus, and W. A. de Jong, *Comput. Phys. Commun.*, **181**, 1477 (2010). NWChem: A Comprehensive and Scalable Open-Source Solution for Large Scale Molecular Simulations.
- <sup>191</sup>G. Kresse and J. Furthmüller, *Comput. Mater. Sci.*, **6**, 15 (1996). Efficiency of Ab-Initio Total Energy Calculations for Metals and Semiconductors Using a Plane-Wave Basis Set.
- <sup>192</sup>G. Kresse and J. Furthmüller, *Phys. Rev. B*, **54**, 11169 (1996). Efficient Iterative Schemes for Ab Initio Total-Energy Calculations Using a Plane-Wave Basis Set.
- <sup>193</sup>X. Gonze, G.-M. Rignanese, M. Verstraete, J.-M. Beuken, Y. Pouillon, R. Caracas, F. Jollet, M. Torrent, G. Zerah, M. Mikami, P. Ghosez, M. Veithen, J.-Y. Raty, V. Olevano, F. Bruneval, L. Reining, R. Godby, G. Onida, D. R. Hamann, and D. C. Allan, *Z. Kristallogr.*, **220**, 558 (2005). A Brief Introduction to the ABINIT Software Package.

- <sup>194</sup>X. Gonze, J.-M. Beuken, R. Caracas, F. Detraux, M. Fuchs, G.-M. Rignanesi, L. Sindic, M. Verstraete, G. Zerah, F. Jollet, M. Torrent, A. Roy, M. Mikami, P. Ghosez, J.-Y. Raty, and D. C. Allan, *Comput. Mater. Sci.*, **25**, 478 (2002). First-Principles Computation of Material Properties: the ABINIT Software Project.
- <sup>195</sup>A. D. Becke, *J. Chem. Phys.*, **107**, 8554 (1997). Density-Functional Thermochemistry. V. Systematic Optimization of Exchange-Correlation Functionals.
- <sup>196</sup>K. Eichkorn, O. Treutler, H. Öhm, M. Häser, and R. Ahlrichs, *Chem. Phys. Lett.*, **240**, 283 (1995). Auxiliary Basis Sets to Approximate Coulomb Potentials.
- <sup>197</sup>K. Eichkorn, F. Weigend, O. Treutler, and R. Ahlrichs, *Theor. Chem. Acc.*, **97**, 119 (1997). Auxiliary Basis Sets for Main Row Atoms and Transition Metals and Their Use to Approximate Coulomb Potentials.
- <sup>198</sup>TURBOMOLE V6.5 2013, a development of University of Karlsruhe and Forschungszentrum Karlsruhe GmbH, 1989-2007, TURBOMOLE GmbH, since 2007; available from <http://www.turbomole.com>.
- <sup>199</sup>L. A. Curtiss, K. Raghavachari, P. C. Redfern, and J. A. Pople, *J. Chem. Phys.*, **106**, 1063 (1997). Assessment of Gaussian-2 and Density Functional Theories for the Computation of Enthalpies of Formation.
- <sup>200</sup>P. Pykkö and M. Atsumi, *Chem. Eur. J.*, **15**, 186 (2009). Molecular Single-Bond Covalent Radii for Elements 1–118.
- <sup>201</sup>X. Chu and A. Dalgarno, *J. Chem. Phys.*, **121**, 4083 (2004). Linear Response Time-Dependent Density Functional Theory for van der Waals Coefficients.
- <sup>202</sup>A. Bondi, *J. Phys. Chem.*, **68**, 441 (1964). Van der Waals Volumes and Radii.
- <sup>203</sup>P. Jurečka, J. Šponer, J. Černý, and P. Hobza, *Phys. Chem. Chem. Phys.*, **8**, 1985 (2006). Benchmark Database of Accurate (MP2 and CCSD(T) Complete Basis Set Limit) Interaction Energies of Small Model Complexes, DNA Base Pairs, and Amino Acid Pairs.
- <sup>204</sup>A. Tkatchenko, R. DiStasio Jr., R. Car, and M. Scheffler, *Phys. Rev. Lett.*, **108**, 236402 (2012). Accurate and Efficient Method for Many-Body van der Waals Interactions.
- <sup>205</sup>R. A. DiStasio Jr., O. A. von Lilienfeld, and A. Tkatchenko, *Proc. Natl. Acad. Sci. U.S.A.*, **109**, 14791 (2012). Collective Many-Body van der Waals Interactions in Molecular Systems.
- <sup>206</sup>A. Tkatchenko, A. Ambrosetti, and R. A. DiStasio Jr., *J. Chem. Phys.*, **138**, 074106 (2013). Interatomic Methods for the Dispersion Energy Derived from the Adiabatic Connection Fluctuation-Dissipation Theorem.
- <sup>207</sup>J. J. Rehr, E. Zaremba, and W. Kohn, *Phys. Rev. B*, **12**, 2062 (1975). Van der Waals Forces in the Noble Metals.
- <sup>208</sup>V. Blum, R. Gehrke, F. Hanke, P. Havu, V. Havu, X. Ren, K. Reuter, and M. Scheffler, *Comput. Phys. Commun.*, **180**, 2175 (2009). Ab Initio Molecular Simulations with Numeric Atom-Centered Orbitals.
- <sup>209</sup>S. N. Steinmann, G. Csonka, and C. Corminboeuf, *J. Chem. Theory Comput.*, **5**, 2950 (2009). Unified Inter- and Intramolecular Dispersion Correction Formula for Generalized Gradient Approximation Density Functional Theory.
- <sup>210</sup>S. N. Steinmann and C. Corminboeuf, *J. Chem. Theory Comput.*, **6**, 1990 (2010). A System-Dependent Density-Based Dispersion Correction.
- <sup>211</sup>S. N. Steinmann and C. Corminboeuf, *J. Chem. Phys.*, **134**, 044117 (2011). A Generalized-Gradient Approximation Exchange Hole Model for Dispersion Coefficients.
- <sup>212</sup>S. N. Steinmann and C. Corminboeuf, *J. Chem. Theory Comput.*, **7**, 3567 (2011). Comprehensive Benchmarking of a Density-Dependent Dispersion Correction.

- <sup>213</sup>K. Tang and J. P. Toennies, *J. Chem. Phys.*, **80**, 3726 (1984). An Improved Simple Model for the van der Waals Potential Based on Universal Damping Functions for the Dispersion Coefficients.
- <sup>214</sup>G. te Velde, F. M. Bickelhaupt, E. J. Baerends, C. Fonseca Guerra, S. J. van Gisbergen, J. G. Snijders, and T. Ziegler, *J. Comput. Chem.*, **22**, 931 (2001). Chemistry with ADF.
- <sup>215</sup>C. Fonseca Guerra, J. Snijders, G. te Velde, and E. Baerends, *Theor. Chem. Acc.*, **99**, 391 (1998). Towards an Order-N DFT Method.
- <sup>216</sup>E. J. Baerends, T. Ziegler, J. Autschbach, D. Bashford, A. Bérces, F. M. Bickelhaupt, C. Bo, P. M. Boerrigter, L. Cavallo, D. P. Chong, L. Deng, R. M. Dickson, D. E. Ellis, M. van Faassen, L. Fan, T. H. Fischer, C. Fonseca Guerra, M. Franchini, A. Ghysels, A. Giammona, S. J. A. van Gisbergen, A. W. Götz, J. A. Groeneveld, O. V. Gritsenko, M. Grüning, S. Gusarov, F. E. Harris, P. van den Hoek, C. R. Jacob, H. Jacobsen, L. Jensen, J. W. Kaminski, G. van Kessel, F. Kootstra, A. Kovalenko, M. V. Krykunov, E. van Lenthe, D. A. McCormack, A. Michalak, M. Mitoraj, S. M. Morton, J. Neugebauer, V. P. Nicu, L. Noodleman, V. P. Osinga, S. Patchkovskii, M. Pavanello, P. H. T. Philipsen, D. Post, C. C. Pye, W. Ravenek, J. I. Rodriguez, P. Ros, P. R. T. Schipper, G. Schreckenbach, J. S. Seldenthuis, M. Seth, J. G. Snijders, M. Solà, M. Swart, D. Swerhone, G. te Velde, P. Vernooijs, L. Versluis, L. Visscher, O. Visser, F. Wang, T. A. Wesolowski, E. M. van Wezenbeek, G. Wiesenekker, S. K. Wolff, T. K. Woo, and A. L. Yakovlev, ADF2013, SCM, Theoretical Chemistry, Vrije Universiteit, Amsterdam, The Netherlands, <http://www.scm.com>.
- <sup>217</sup><http://lcmd.epfl.ch/page-81952-en.html>.
- <sup>218</sup>T. Sato and H. Nakai, *J. Chem. Phys.*, **131**, 224104 (2009). Density Functional Method Including Weak Interactions: Dispersion Coefficients Based on the Local Response Approximation.
- <sup>219</sup>T. Sato and H. Nakai, *J. Chem. Phys.*, **133**, 194101 (2010). Local Response Dispersion Method. II. Generalized Multicenter Interactions.
- <sup>220</sup>A. Stone, *The Theory of Intermolecular Forces*, International Series of Monographs on Chemistry, Clarendon Press, 1997.
- <sup>221</sup>J. F. Dobson and B. P. Dinte, *Phys. Rev. Lett.*, **76**, 1780 (1996). Constraint Satisfaction in Local and Gradient Susceptibility Approximations: Application to a Van der Waals Density Functional.
- <sup>222</sup>A. D. Becke, *J. Chem. Phys.*, **88**, 2547 (1988). A Multicenter Numerical Integration Scheme for Polyatomic Molecules.
- <sup>223</sup>O. A. Vydrov and T. Van Voorhis, *J. Chem. Phys.*, **130**, 104105 (2009). Improving the Accuracy of the Nonlocal van der Waals Density Functional with Minimal Empiricism.
- <sup>224</sup>T. Tsuneda, T. Suzumura, and K. Hirao, *J. Chem. Phys.*, **110**, 10664 (1999). A New One-Parameter Progressive Colle-Salvetti-Type Correlation Functional.
- <sup>225</sup>R. Kar, J.-W. Song, T. Sato, and K. Hirao, *J. Comput. Chem.*, **34**, 2353 (2013). Long-Range Corrected Density Functionals Combined with Local Response Dispersion: A Promising Method for Weak Interactions.
- <sup>226</sup>J. Rezáč, K. E. Riley, and P. Hobza, *J. Chem. Theory Comput.*, **7**, 2427 (2011). S66: A well-balanced database of benchmark interaction energies relevant to biomolecular structures.
- <sup>227</sup>J. Tao, J. P. Perdew, and A. Ruzsinszky, *Phys. Rev. B*, **81**, 233102 (2010). Long-range van der Waals Attraction and Alkali-Metal Lattice Constants.
- <sup>228</sup>J. Tao, J. P. Perdew, and A. Ruzsinszky, *Int. J. Mod. Phys. B*, **27**, 1330011 (2013).

Long-Range van der Waals Interaction.

- <sup>229</sup>A. Ruzsinszky, J. P. Perdew, J. Tao, G. I. Csonka, and J. Pitarke, *Phys. Rev. Lett.*, **109**, 233203 (2012). Van der Waals Coefficients for Nanostructures: Fullerenes Defy Conventional Wisdom.
- <sup>230</sup>N. Alves de Lima, *J. Chem. Phys.*, **132**, 014110 (2010). Van der Waals Density Functional from Multipole Dispersion Interactions.
- <sup>231</sup>A. Austin, G. A. Petersson, M. J. Frisch, F. J. Dobek, G. Scalmani, and K. Throssell, *J. Chem. Theory Comput.*, **8**, 4989 (2012). A Density Functional with Spherical Atom Dispersion Terms.
- <sup>232</sup>G. A. DiLabio, *Chem. Phys. Lett.*, **455**, 348 (2008). Accurate Treatment of van der Waals Interactions Using Standard Density Functional Theory with Effective Core-Type Potentials: Application to Carbon-Containing Dimers.
- <sup>233</sup>I. D. Mackie and G. A. DiLabio, *J. Phys. Chem. A*, **112**, 10968 (2008). Interactions in Large, Polyaromatic Hydrocarbons Dimers: Application of Density Functional Theory with Dispersion Corrections.
- <sup>234</sup>E. Torres and G. A. DiLabio, *J. Phys. Chem. Lett.*, **3**, 1738 (2012). A (Nearly) Universally Applicable Method for Modeling Noncovalent Interactions Using B3LYP.
- <sup>235</sup>G. A. DiLabio, M. Koleini, and E. Torres, *Theor. Chem. Acc.*, **132**, 1 (2013). Extension of the B3LYP-Dispersion-Correcting Potential Approach to the Accurate Treatment of both Inter- and Intra-Molecular Interactions.
- <sup>236</sup><http://www.ualberta.ca/~gdilabio/>.
- <sup>237</sup>G. A. DiLabio, M. M. Hurley, and P. A. Christiansen, *J. Chem. Phys.*, **116**, 9578 (2002). Simple One-Electron Quantum Capping Potentials for Hybrid QM/MM Studies of Biological Molecules.
- <sup>238</sup>G. A. DiLabio, R. A. Wolkow, and E. R. Johnson, *J. Chem. Phys.*, **122**, 044708 (2005). Efficient Silicon Surface and Cluster Modeling Using Quantum Capping Potentials.
- <sup>239</sup>P. A. Christiansen, Y. S. Lee, and K. S. Pitzer, *J. Chem. Phys.*, **71**, 4445 (1979). Improved ab initio Effective Core Potentials for Molecular Calculations.
- <sup>240</sup>S. A. Wildman, G. A. DiLabio, and P. A. Christiansen, *J. Chem. Phys.*, **107**, 9975 (1997). Accurate Relativistic Effective Potentials for the Sixth-Row Main Group Elements.
- <sup>241</sup>G. A. DiLabio and P. A. Christiansen, *J. Chem. Phys.*, **108**, 7527 (1998). Separability of Spin-Orbit and Correlation Energies for the Sixth-Row Main Group Hydride Ground States.
- <sup>242</sup>L. Goerigk and S. Grimme, *J. Chem. Theory Comput.*, **6**, 107 (2010). A General Database for Main Group Thermochemistry, Kinetics, and Noncovalent Interactions—Assessment of Common and Reparameterized (meta-)GGA Density Functionals.
- <sup>243</sup>G. A. DiLabio and M. Koleini, *J. Chem. Phys.* (in press, 2014). Dispersion-Correcting Potentials can Significantly Improve the Bond Dissociation Enthalpies and Noncovalent Binding Energies Predicted by Density-Functional Theory.
- <sup>244</sup>L. Goerigk, *J. Chem. Theory Comput.*, **10**, 968 (2014). How Do DFT-DCP, DFT-NL, and DFT-D3 Compare for the Description of London-Dispersion Effects in Conformers and General Thermochemistry?
- <sup>245</sup>Y. K. Zhang and W. T. Yang, *J. Chem. Phys.*, **109**, 2604 (1998). A Challenge for Density Functionals: Self-Interaction Error Increases for Systems with a Noninteger Number of Electrons.
- <sup>246</sup>A. Ruzsinszky, J. P. Perdew, G. I. Csonka, O. A. Vydrov, and G. E. Scuseria, *J. Chem. Phys.*, **125**, 194112 (2006). Spurious Fractional Charge on Dissociated Atoms: Pervasive

- and Resilient Self-Interaction Error of Common Density Functionals.
- <sup>247</sup>E. Ruiz, D. R. Salahub, and A. Vela, *J. Chem. Phys.*, **100**, 12265 (1996). Charge-Transfer Complexes: Stringent Tests for Widely Used Density Functionals.
- <sup>248</sup>A. I. Gilson, G. Van Der Rest, J. Chamot-Rooke, W. Kurlancheek, M. Head-Gordon, D. Jacquemin, and G. Frison, *J. Phys. Chem. Lett.*, **2**, 1426 (2011). Ground Electronic State of Peptide Cation Radicals: A Delocalized Unpaired Electron?
- <sup>249</sup>O. A. von Lilienfeld, I. Tavernelli, U. Rothlisberger, and D. Sebastiani, *Phys. Rev. Lett.*, **93**, 153004 (2004). Optimization of Effective Atom Centered Potentials for London Dispersion Forces in Density Functional Theory.
- <sup>250</sup>S. Goedecker, M. Teter, and J. Hutter, *Phys. Rev. B*, **54**, 1703 (1996). Separable Dual-Space Gaussian Pseudopotentials.
- <sup>251</sup>C. Hartwigsen, S. Goedecker, and J. Hutter, *Phys. Rev. B*, **58**, 3641 (1998). Relativistic Separable Dual-Space Gaussian Pseudopotentials from H to Rn.
- <sup>252</sup>I.-C. Lin, M. D. Coutinho-Neto, C. Felsenheimer, O. A. von Lilienfeld, I. Tavernelli, and U. Rothlisberger, *Phys. Rev. B*, **75**, 205131 (2007). Library of Dispersion-Corrected Atom-Centered Potentials for Generalized Gradient Approximation Functionals: Elements H, C, N, O, He, Ne, Ar, and Kr.
- <sup>253</sup>O. Karalti, X. Su, W. A. Al-Saidi, and K. D. Jordan, *Chem. Phys. Lett.*, **591**, 133 (2014). Correcting Density Functionals for Dispersion Interactions Using Pseudopotentials.
- <sup>254</sup>Y. Zhao, N. E. Schultz, and D. Truhlar, *J. Chem. Phys.*, **123**, 161103 (2005). Exchange-Correlation Functional with Broad Accuracy for Metallic and Nonmetallic Compounds, Kinetics, and Noncovalent Interactions.
- <sup>255</sup>Y. Zhao, N. E. Schultz, and D. G. Truhlar, *J. Chem. Theory Comput.*, **2**, 364 (2006). Design of Density Functionals by Combining the Method of Constraint Satisfaction with Parametrization for Thermochemistry, Thermochemical Kinetics, and Noncovalent Interactions.
- <sup>256</sup>Y. Zhao and D. G. Truhlar, *J. Phys. Chem. A*, **110**, 13126 (2006). Density Functional for Spectroscopy: no Long-Range Self-Interaction Error, Good Performance for Rydberg and Charge-Transfer States, and Better Performance on Average than B3LYP for Ground States.
- <sup>257</sup>Y. Zhao and D. G. Truhlar, *Theor. Chem. Acc.*, **120**, 215 (2008). The M06 Suite of Density Functionals for Main Group Thermochemistry, Thermochemical Kinetics, Noncovalent Interactions, Excited States, and Transition Elements: Two New Functionals and Systematic Testing of Four M06-Class Functionals and 12 Other Functionals.
- <sup>258</sup>Y. Zhao and D. G. Truhlar, *J. Chem. Theory Comput.*, **4**, 1849 (2008). Exploring the Limit of Accuracy of the Global Hybrid Meta Density Functional for Main-Group Thermochemistry, Kinetics, and Noncovalent Interactions.
- <sup>259</sup>R. Peverati, Y. Zhao, and D. G. Truhlar, *J. Phys. Chem. Lett.*, **2**, 1991 (2011). Generalized Gradient Approximation That Recovers the Second-Order Density-Gradient Expansion with Optimized Across-the-Board Performance.
- <sup>260</sup>R. Peverati and D. G. Truhlar, *J. Phys. Chem. Lett.*, **2**, 2810 (2011). Improving the Accuracy of Hybrid Meta-GGA Density Functionals by Range Separation.
- <sup>261</sup>R. Peverati and D. G. Truhlar, *J. Phys. Chem. Lett.*, **3**, 117 (2011). M11-L: A Local Density Functional That Provides Improved Accuracy for Electronic Structure Calculations in Chemistry and Physics.
- <sup>262</sup>A. D. Becke, *J. Chem. Phys.*, **112**, 4020 (2000). Simulation of Delocalized Exchange by Local Density Functionals.

- <sup>263</sup>A. D. Boese and N. C. Handy, *J. Chem. Phys.*, **116**, 9559 (2002). New Exchange-Correlation Density Functionals: The Role of the Kinetic-Energy Density.
- <sup>264</sup>A. D. Boese and J. M. Martin, *J. Chem. Phys.*, **121**, 3405 (2004). Development of Density Functionals for Thermochemical Kinetics.
- <sup>265</sup>A. D. Becke, *J. Chem. Phys.*, **104**, 1040 (1996). Density-Functional Thermochemistry. IV. A New Dynamical Correlation Functional and Implications for Exact-Exchange Mixing.
- <sup>266</sup>Y. Zhao and D. G. Truhlar, *J. Phys. Chem. A*, **110**, 5121 (2006). Comparative DFT Study of van der Waals Complexes: Rare-Gas Dimers, Alkaline-Earth Dimers, Zinc Dimer, and Zinc-Rare-Gas Dimers.
- <sup>267</sup>T. Van Voorhis and G. E. Scuseria, *J. Chem. Phys.*, **109**, 400 (1998). A Novel Form for the Exchange-Correlation Energy Functional.
- <sup>268</sup>B. Hammer, L. B. Hansen, and J. K. Nørskov, *Phys. Rev. B*, **59**, 7413 (1999). Improved Adsorption Energetics Within Density-Functional Theory Using Revised Perdew-Burke-Ernzerhof Functionals.
- <sup>269</sup>S. Liu and R. G. Parr, *Phys. Rev. A*, **55**, 1792 (1997). Expansions of Density Functionals in Terms of Homogeneous Functionals: Justification and Nonlocal Representation of the Kinetic Energy, Exchange Energy, and Classical Coulomb Repulsion Energy for Atoms.
- <sup>270</sup>O. A. Vydrov and T. Van Voorhis, *J. Chem. Theory Comput.*, **8**, 1929 (2012). Benchmark Assessment of the Accuracy of Several Van der Waals Density Functionals.
- <sup>271</sup>E. Zaremba and W. Kohn, *Phys. Rev. B*, **13**, 2270 (1976). Van der Waals Interaction Between an Atom and a Solid Surface.
- <sup>272</sup>K. Rapcewicz and N. Ashcroft, *Phys. Rev. B*, **44**, 4032 (1991). Fluctuation Attraction in Condensed Matter: A Nonlocal Functional Approach.
- <sup>273</sup>A. Zangwill and P. Soven, *Phys. Rev. A*, **21**, 1561 (1980). Density-Functional Approach to Local-Field Effects in Finite Systems: Photoabsorption in the Rare Gases.
- <sup>274</sup>Y. Andersson, D. C. Langreth, and B. I. Lundqvist, *Phys. Rev. Lett.*, **76**, 102 (1996). Van der Waals Interactions in Density-Functional Theory.
- <sup>275</sup>H. Rydberg, B. I. Lundqvist, D. C. Langreth, and M. Dion, *Phys. Rev. B*, **62**, 6997 (2000). Tractable Nonlocal Correlation Density Functionals for Flat Surfaces and Slabs.
- <sup>276</sup>E. Hult, H. Rydberg, B. I. Lundqvist, and D. C. Langreth, *Phys. Rev. B*, **59**, 4708 (1999). Unified Treatment of Asymptotic van der Waals Forces.
- <sup>277</sup>H. Rydberg, M. Dion, N. Jacobson, E. Schröder, P. Hyldgaard, S. Simak, D. C. Langreth, and B. I. Lundqvist, *Phys. Rev. Lett.*, **91**, 126402 (2003). Van der Waals Density Functional for Layered Structures.
- <sup>278</sup>M. Dion, H. Rydberg, E. Schröder, D. C. Langreth, and B. I. Lundqvist, *Phys. Rev. Lett.*, **92**, 246401 (2004). Van der Waals Density Functional for General Geometries.
- <sup>279</sup>M. Dion, H. Rydberg, E. Schröder, D. C. Langreth, and B. I. Lundqvist, *Phys. Rev. Lett.*, **95**, 109902 (2005). Erratum: Van Der Waals Density Functional for General Geometries.
- <sup>280</sup>O. A. Vydrov, Q. Wu, and T. Van Voorhis, *J. Chem. Phys.*, **129**, 014106 (2008). Self-Consistent Implementation of a Nonlocal van der Waals Density Functional with a Gaussian Basis Set.
- <sup>281</sup>G. Román-Pérez and J. M. Soler, *Phys. Rev. Lett.*, **103**, 096102 (2009). Efficient Implementation of a Van der Waals Density Functional: Application to Double-Wall Carbon Nanotubes.
- <sup>282</sup>D. C. Langreth, B. I. Lundqvist, S. D. Chakarova-Käck, V. R. Cooper, M. Dion, P. Hyldgaard, A. Kelkkanen, J. Kleis, L. Kong, S. Li, P. G. Moses, E. Murray, A. Puzder, H. Rydberg, E. Schröder, and T. Thonhauser, *J. Phys.: Condens. Matter*, **21**, 084203

- (2009). A Density Functional for Sparse Matter.
- <sup>283</sup>J. Klimeš, D. R. Bowler, and A. Michaelides, *J. Phys.: Condens. Matter*, **22**, 022201 (2010). Chemical Accuracy for the van der Waals Density Functional.
- <sup>284</sup>O. A. Vydrov and T. Van Voorhis, *J. Chem. Phys.*, **132**, 164113 (2010). Implementation and Assessment of a Simple Nonlocal van der Waals Density Functional.
- <sup>285</sup>K. Lee, E. D. Murray, L. Kong, B. I. Lundqvist, and D. C. Langreth, *Phys. Rev. B*, **82**, 081101 (2010). Higher-Accuracy Van der Waals Density Functional.
- <sup>286</sup>E. D. Murray, K. Lee, and D. C. Langreth, *J. Chem. Theory Comput.*, **5**, 2754 (2009). Investigation of Exchange Energy Density Functional Accuracy for Interacting Molecules.
- <sup>287</sup>P. Elliott and K. Burke, *Can. J. Chem.*, **87**, 1485 (2009). Non-Empirical Derivation of the Parameter in the B88 Exchange Functional.
- <sup>288</sup>D. Nabok, P. Puschnig, and C. Ambrosch-Draxl, *Comput. Phys. Commun.*, **182**, 1657 (2011). Noloco: An efficient implementation of van der Waals Density Functionals Based on a Monte-Carlo Integration Technique.
- <sup>289</sup>O. A. Vydrov and T. Van Voorhis, *Phys. Rev. Lett.*, **103**, 063004 (2009). Nonlocal Van der Waals Density Functional Made Simple.
- <sup>290</sup>D. C. Langreth and B. I. Lundqvist, *Phys. Rev. Lett.*, **104**, 099303 (2010). Comment on Nonlocal van der Waals Density Functional Made Simple.
- <sup>291</sup>O. A. Vydrov and T. Van Voorhis, *Phys. Rev. Lett.*, **104**, 099304 (2010). Vydrov and Van Voorhis Reply.
- <sup>292</sup>O. A. Vydrov and T. V. Voorhis, *J. Chem. Phys.*, **133**, 244103 (2010). Nonlocal Van der Waals Density Functional: The Simpler the Better.
- <sup>293</sup>O. A. Vydrov and T. Van Voorhis, *Phys. Rev. A*, **81**, 062708 (2010). Dispersion Interactions from a Local Polarizability Model.
- <sup>294</sup>J. Řezáč, P. Jurečka, K. E. Riley, J. Černý, H. Valdes, K. Pluháčková, K. Berka, T. Řezáč, M. Pitoňák, J. Vondrášek, and P. Hobza, *Collect. Czech. Chem. Commun.*, **73**, 1261 (2008). Quantum Chemical Benchmark Energy and Geometry Database for Molecular Clusters and Complex Molecular Systems ([www.begdb.com](http://www.begdb.com)): A Users Manual and Examples.
- <sup>295</sup>[www.begdb.com](http://www.begdb.com).
- <sup>296</sup>B. Temelso, K. A. Archer, and G. C. Shields, *J. Phys. Chem. A*, **115**, 12034 (2011). Benchmark Structures and Binding Energies of Small Water Clusters with Anharmonicity Corrections.
- <sup>297</sup>J. Řezáč, K. E. Riley, and P. Hobza, *J. Chem. Theory Comput.*, **7**, 3466 (2011). Extensions of the S66 Data Set: More Accurate Interaction Energies and Angular-Displaced Nonequilibrium Geometries.
- <sup>298</sup>M. S. Marshall, L. A. Burns, and C. D. Sherrill, *J. Chem. Phys.*, **135**, 194102 (2011). Basis Set Convergence of the Coupled-Cluster Correction,  $\Delta_{\text{MP2}}^{\text{CCSD}(\text{T})}$ : Best Practices for Benchmarking Non-Covalent Interactions and the Attendant Revision of the S22, NBC10, HBC6, and HSG Databases.
- <sup>299</sup><http://comp.chem.umn.edu/db/>.
- <sup>300</sup>S. F. Boys and F. Bernardi, *Mol. Phys.*, **19**, 553 (1970). The Calculation of Small Molecular Interactions by the Differences of Separate Total Energies. Some Procedures with Reduced Errors.
- <sup>301</sup>I. D. Mackie and G. A. DiLabio, *J. Chem. Phys.*, **135**, 134318 (2011). Approximations to Complete Basis Set-Extrapolated, Highly Correlated Non-Covalent Interaction Energies.
- <sup>302</sup>L. A. Burns, M. S. Marshall, and C. D. Sherrill, *J. Chem. Theory Comput.*, **10**, 49

- (2014). Comparing Counterpoise-Corrected, Uncorrected, and Averaged Binding Energies for Benchmarking Noncovalent Interactions.
- <sup>303</sup>L. Gráfová, M. Pitoňák, J. Řezáč, and P. Hobza, *J. Chem. Theory Comput.*, **6**, 2365 (2010). Comparative Study of Selected Wave Function and Density Functional Methods for Noncovalent Interaction Energy Calculations Using the Extended S22 Data Set.
- <sup>304</sup>J. Řezáč, K. E. Riley, and P. Hobza, *J. Chem. Theory Comput.*, **73**, 4285 (2012). Benchmark Calculations of Noncovalent Interactions of Halogenated Molecules.
- <sup>305</sup>S. Grimme, *Chem. Eur. J.*, **18**, 9955 (2012). Supramolecular Binding Thermodynamics by Dispersion-Corrected Density Functional Theory.
- <sup>306</sup>A. Ambrosetti, D. Alfé, R. A. DiStasio Jr., and A. Tkatchenko, *J. Phys. Chem. Lett.*, **5**, 849 (2014). Hard Numbers for Large Molecules: Toward Exact Energetics for Supramolecular Systems.
- <sup>307</sup>W. Acree Jr and J. S. Chickos, *J. Phys. Chem. Ref. Data*, **39**, 043101 (2010). Phase Transition Enthalpy Measurements of Organic and Organometallic Compounds. Sublimation, Vaporization and Fusion Enthalpies from 1880 to 2010.
- <sup>308</sup>S. M. Woodley and R. Catlow, *Nat. Mater.*, **7**, 937 (2008). Crystal Structure Prediction from First Principles.
- <sup>309</sup>W. Cabri, P. Ghetti, G. Pozzi, and M. Alpegiani, *Org. Proc. Res. Dev.*, **11**, 64 (2007). Polymorphisms and Patent, Market, and Legal Battles: Cefdinir Case Study.
- <sup>310</sup>N. Marom, A. Tkatchenko, M. Rossi, V. V. Gobre, O. Hod, M. Scheffler, and L. Kronik, *J. Chem. Theory Comput.*, **7**, 3944 (2011). Dispersion Interactions with Density-Functional Theory: Benchmarking Semiempirical and Interatomic Pairwise Corrected Density Functionals.
- <sup>311</sup>L. Goerigk, H. Kruse, and S. Grimme, *Chem. Phys. Chem.*, **12**, 3421 (2011). Benchmarking Density Functional Methods against the S66 and S66×8 Datasets for Non-Covalent Interactions.
- <sup>312</sup>T. Risthaus and S. Grimme, *J. Chem. Theory Comput.*, **9**, 1580 (2013). Benchmarking of London Dispersion-Accounting Density Functional Theory Methods on Very Large Molecular Complexes.
- <sup>313</sup>A. Otero-de-la Roza and E. R. Johnson, Unpublished results, 2014.
- <sup>314</sup>W. Hujo and S. Grimme, *J. Chem. Theory Comput.*, **7**, 3866 (2011). Performance of the van der Waals Density Functional VV10 and (Hybrid) GGA Variants for Thermochemistry and Noncovalent Interactions.
- <sup>315</sup>F. Jensen and T. Helgaker, *J. Chem. Phys.*, **121**, 3463 (2004). Polarization Consistent Basis Sets. V. The Elements Si–Cl.
- <sup>316</sup>F. Jensen, *J. Chem. Phys.*, **116**, 7372 (2002). Polarization Consistent Basis Sets. II. Estimating the Kohn-Sham Basis Set Limit.
- <sup>317</sup>F. Jensen, *J. Chem. Phys.*, **115**, 9113 (2001). Polarization Consistent Basis Sets: Principles.
- <sup>318</sup>A. M. Reilly and A. Tkatchenko, *J. Phys. Chem. Lett.*, **4**, 1028 (2013). Seamless and Accurate Modeling of Organic Molecular Materials.
- <sup>319</sup>E. I. Solomon, T. C. Brunold, M. I. Davis, J. N. Kemsley, S.-K. Lee, N. Lehnert, F. Neese, A. J. Skulan, Y.-S. Yang, and J. Zhou, *Chem. Rev.*, **100**, 235 (2000). Geometric and Electronic Structure/Function Correlations in Non-Heme Iron Enzymes.
- <sup>320</sup>S. A. McClure, J. M. Buriak, and G. A. DiLabio, *J. Phys. Chem. C*, **114**, 10952 (2010). Transport Properties of Thiophenes: Insights from Density-Functional Theory Modeling Using Dispersion-Correcting Potentials.



- <sup>321</sup>A. A. Fokin, L. V. Chernish, P. A. Gunchenko, E. Y. Tikhonchuk, H. Hausmann, M. Serafin, J. E. P. Dahl, R. M. K. Carlson, and P. R. Schreiner, *J. Am. Chem. Soc.*, **134**, 13641 (2012). Stable Alkanes Containing Very Long Carbon-Carbon Bonds.
- <sup>322</sup>P. R. Schreiner, L. V. Chernish, P. A. Gunchenko, E. Y. Tikhonchuk, H. Hausmann, M. Serafin, S. Schlecht, J. E. P. Dahl, R. M. K. Carlson, and A. A. Fokin, *Nature*, **477**, 308 (2011). Overcoming Lability of Extremely Long Alkane Carbon-Carbon Bonds through Dispersion Forces.
- <sup>323</sup>O. A. von Lilienfeld, *Mol. Phys.*, **111**, 2147 (2013). Force Correcting Atom Centred potentials for Generalised Gradient Approximated Density Functional Theory: Approaching Hybrid Functional Accuracy for Geometries and Harmonic Frequencies in Small Chlorofluorocarbons.